Effect of Climate and Land Use Changes on Sediment Load for Brahmaputra River Basin Using HEC-HMS

A Thesis Submitted

by

Shammi Haque
1014162012P

In partial fulfilment of the requirements for the Degree of
MASTER OF SCIENCE IN WATER RESOURCES ENGINEERING

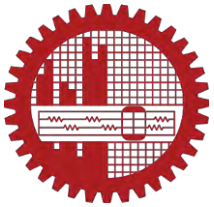

Department of Water Resources Engineering
BANGLADESH UNIVERSITY OF ENGINEERING & TECHNOLOGY (BUET)
DHAKA-1000

April 2018

DEPARTMENT OF WATER RESOURECS ENGINEERING
BANGLADESH UNIVERSITY OF ENGINEERING AND TECHNOLOGY

The thesis titled **'Effect of Climate and Land Use Changes on Sediment Load for Brahmaputra River Basin Using HEC-HMS'** submitted by Shammi Haque, Roll No. 1014162012P, Session October, 2014, has been accepted as satisfactory in partial fulfillment of the requirements for the degree of Master of Science in Water Resources Engineering on 28 April, 2018.

BOARD OF EXAMINERS

.....

Dr. Md. Mostafa Ali
Professor
Department of Water Resources Engineering
BUET, Dhaka.

Chairman
(Supervisor)

.....

Head
Department of Water Resources Engineering
BUET, Dhaka

Member
(Ex-Officio)

.....

Dr. Md. Sabbir Mostafa Khan
Professor
Department of Water Resources Engineering
BUET, Dhaka

Member

.....

Dr. K. M. Ahtesham Hossain
Assistant Professor
Department of Water Resources Engineering
BUET, Dhaka

Member

.....

Dr. A.K.M. Saiful Islam
Professor
Institute of Water and Flood Management
BUET, Dhaka

Member
(External)

CANDIDATE'S DECLARATION

It is hereby declared that this thesis or any part of it has not been submitted elsewhere for the award of any degree or diploma.

Haque .....

Shammi Haque

Dedicated to

My Beloved Parents, the source of all inspirations in my life

ACKNOWLEDGEMENT

The author is grateful to the Almighty ALLAH for successful completion of this thesis work. The author would like to express her sincere gratitude to her supervisor Dr. Md. Mostafa Ali, Professor and Head, Department of Water Resources Engineering, Bangladesh University of Engineering and Technology, without whose constant supervision and endless support this research work would probably reach nowhere. His constant guidance, invaluable suggestions, motivation in difficult times and affectionate encouragement were extremely helpful in accomplishing this study.

The author expresses her sincere appreciation and deep gratitude to Dr. A.K.M. Saiful Islam, Professor, Institute of Water and Flood Management, Bangladesh University of Engineering and Technology, Ms. Shampa, Assistant Professor, Institute of Water and Flood Management, Bangladesh University of Engineering and Technology and Md. Jamal Uddin Khan, PhD Student, Universite Toulouse III - Paul Sabatier, France for their enormous help in data collection and guidance.

The author thanks to Dr. Md. Sabbir Mostafa Khan, Professor, Department of Water Resources Engineering, Bangladesh University of Engineering and Technology, Dr. K. M. Ahtesham Hossain, Assistant Professor, Department of Water Resources Engineering, Bangladesh University of Engineering and Technology and Dr. A.K.M. Saiful Islam, Professor, Institute of Water and Flood Management, Bangladesh University of Engineering and Technology, for their kind review and suggestions, without these suggestions the successful completion of the thesis was quite impossible.

ABSTRACT

Brahmaputra River Basin (BRB), the largest contributor of sediment load in Ganges-Brahmaputra-Meghna (GBM) delta, is highly vulnerable to future climate change. The present to future assessment of sediment load from BRB is challenging due to unavailability of measured data and uncertainty in climatic parameters. The Brahmaputra river and its' nature together with eco-hydrology and livelihood of people surrounding it, are highly dependent on incoming sediment load. Many researchers give assessment of climate changes of BRB on flow, but assessment on sediment load due to future climatic scenarios is unavailable. The present study focuses on developing a hydrological and sediment routing model of BRB using HEC-HMS to estimate present to future sediment load considering climate and land use change.

The catchment and river network of BRB have been delineated using SRTM 90m DEM. Soil Moisture Accounting for computing runoff volume, Snyder unit hydrograph for direct runoff, linear reservoir for baseflow and Muskingum Cunge for routing have been considered for representing hydrological processes of BRB. Land cover map from 0.5 km MODIS-based Global Land Cover analysis and soil map from FAO have been used to estimate impervious area, maximum infiltration rate, surface storage and MUSLE factors. Using climatic data from NASA POWER and sensitivity analysis of SMA algorithm parameters, this hydrological model has been calibrated from 1983 to 1996 and validated for 1997-2010 at Bahadurabad transit (SW 46.9L). The NSE, PBIAS, RSR, R^2 values are 0.65, -20.92, 0.59, 0.76 and 0.54, -23.40, 0.68, 0.71 for calibration and validation period respectively. Using MUSLE and Engelund Hansen equation and obtaining the boundary conditions from calibrated hydrological model and secondary literature, surface erosion and sediment routing model has been calibrated and validated for observed sediment load of 1983-2010 collected from BWDB.

The simulated annual average sediment load at Bahadurabad transit from calibrated and validated HEC-HMS model is about 370.20 Mt/year. For future climate changes, synthetic approach for changing precipitation about -25% to 40% have been performed. The result shows that BRB is almost equally sensitive to a reduction and increase in precipitation for discharge and sediment load. For -25% to 40% changes of baseline precipitation in future, average annual sediment load varies from -31.34% to 41.92% of

climatic base period values. For 40% increase of precipitation in future, annual sediment load from BRB will increase up to 525.38 Mt/year.

The calibrated surface erosion and sediment routing model of BRB then has been used to assess the impact of climate change on sediment load together with water availability of BRB by applying RCP 8.5 scenario of selected RCMs outputs obtained from CORDEX database. HEC-HMS simulated mean annual and seasonal (pre-monsoon, monsoon, post-monsoon and dry) streamflow of BRB for the 2010-2039 (2020s), 2040-2069 (2050s), and 2070-2099 (2080s) of the 21st century was compared with the corresponding climate normal streamflow. A gradual increase in annual average flow is found from 2020s to 2080s which indicates that uncertainty associated with the projected streamflow of BRB increases as we go distant future. For impact analysis on sediment load at Bahadurabad transit of BRB, mean annual and mean seasonal (pre-monsoon, monsoon, post-monsoon and dry) simulated sediment load have been assessed. It reveals that though the uncertainty in percentage change in seasonal sediment load of pre-monsoon is higher than the monsoon season, the contribution of sediment load of pre-monsoon is very much lower than the monsoon season. So, increase in sediment load for monsoon season will have much effect on changes in total sediment load at Bahadurabad transit of BRB. The percentage changes in average annual sediment load from baseline period for 2020s, 2050s and 2080s are 34%, 67% and 115% respectively and it increases gradually. Also, uncertainty associated with the projected sediment load of BRB increases as we go distant future can be stated due to growing nature of range between 75th and 25th percentile from 2020s to 2080s.

An increase in urbanization area, about 5% and 15% for all over BRB, have been done to analyze the changes of sediment load. The average monthly, seasonal and annual sediment load coming from basin area decreases almost linearly with respective increase in urbanization. But, at Bahadurabad transit (SW 46.9L), these values remain almost same as the present condition. It reveals that the decrease amount of sediment load from the basin area has been adjusted with the increased volume of sediment load carried by the increased amount of overland flow due to urbanization.

TABLE OF CONTENTS

LIST OF FIGURES

LIST OF TABLES

LIST OF ABBREVIATION

Acronym	Definition
2020s	2010-2039
2050s	2040-2069
2080s	2070-2099
BMD	Bangladesh Meteorological Department
BRB	Brahmaputra River Basin
BWDB	Bangladesh Water Development Board
CORDEX	Coordinated Regional Climate Downscaling Experiment
DEM	Digital Elevation Model
FAO	Food and Agriculture Organization
GBM	Ganges Brahmaputra Meghna
GCM	General Circulation Model
HEC-HMS	Hydrologic Engineering Center Hydrologic Modeling System
m^3/s	Cubic meter per second
Mt/month	Million tonnes per month
Mt/year	Million tonnes per year
MUSLE	Modified Universal Soil Loss Equation
NASA	National Aeronautics and Space Administration
NASA POWER	NASA Prediction of Power Worldwide Energy Resources
PET	Potential Evapotranspiration
RCM	Regional Climate Model
RCP	Representative Concentration Pathways
SMA	Soil Moisture Accounting
SWAT	Soil Water Assessment Tool
USGS	U.S. Geological Survey

CHAPTER 1
INTRODUCTION

1.1 Background and Present State of the Problem

Ganges-Brahmaputra-Meghna (GBM) river basins is a transboundary river basin that encompasses approximately 1.72 million km^2, distributed between India (64.02%), China (17.69%), Nepal (8.57%), Bangladesh (7%) and Bhutan (2.73%) (JRCB, 2018). Bangladesh is a lower most riparian country of GBM basins. A large amount of discharge and sediment load from upstream countries passes through Bangladesh towards the Bay of Bengal. Among the three major river systems of this country, Jamuna carries the highest discharge and sediment load. The mean annual discharge of Jamuna is about 20000 m^3/s (Sarker et al., 2013). According to Coleman (1969), the sediment load of the Jamuna was 555 Mt/year during the early 1960s. A massive sediment yields from the Jamuna River which is about 590 Mt/year (FAP, 1996) to 792 Mt/year (Islam et al., 1999) estimated in previous studies. Sediments contain essential nutrients and material for ecosystems and agricultural lands and it is vital from environmental, economic, and social perspectives (Apitz, 2012). The quantity and quality of sediments are affected due to natural variability in hydrological conditions, as well as changes in land use, water use, and climate (e.g., Chalov et al. 2015).

Bangladesh being a part of this greatest deltaic plain, is highly vulnerable to climate changes. For control and management of sediment flows in future, responses to changes in ambient conditions therefore need to be predicted, especially in regions where livelihood depends on river systems and their natural processes. Even though basin-wide integrated resource management is fundamental for a sustainable development in this region (Rasul, 2014; Liu, 2015) and management of sediment and erosion has so far mainly been a national concern (Ray et al., 2015). The consideration of larger spatial perspectives and the development of cross-boundary collaboration are thus key challenges for the region, particularly with ongoing climatic changes, causing altered precipitation and temperature patterns that could leave an imprint on riverine sediment transport.

Modeling systems for managing water resources in the GBM Basins were set up by researchers in some previous studies (e.g. Akbor et al., 2014; Nishat and Rahman, 2009). A study by Paul (2014) concluded that QUMP ensemble members of PRECIS shows the higher possibility of increase of the flow in pre-monsoon than monsoon season. But as the volume of monsoon flow will be ten times higher than that of pre-monsoon, therefore, flooding in this basin will be increased in the future was predicted in this study. Considering land use and climate change scenarios, Pervez et al. (2015) assessed the changes on the future freshwater availability in the Brahmaputra river basin. Flood inundation map for Sirajganj district considering upstream flow from Brahmaputra river basin was developed using HEC-HMS by previous researcher (Rouf, 2015). Alam et al. (2016) analyzed the impact of climate change on streamflow of BRB using a physically based semi distributed hydrological model, SWAT. Khaled et al. (2017) stated an increase and decrease in mean monthly discharges during pre-monsoon months and post-monsoon months for BRB. While climate change is predicted to increase monsoon discharges and reduce dry season flows (Yu et al., 2010), little is known regarding its impact on the sediment regime. For different DEM resolutions and land use scenarios, discharge and sediment transport were analyzed by some researchers for other basins (Santos et al., 2010 and Dehvari, 2014). For making the best use of water resources of Brahmaputra river basin (BRB), engineer as well as policy maker need some results of sediment load together with flow prediction which are currently unavailable.

In this regard, Brahmaputra river basin has been selected as the study area. Hydrologic Engineering Center Hydrologic Modeling System, HEC HMS 4.1 (Scharffenberg, 2015) can act as a useful tool for developing a hydrological and sediment yield model at Bahadurabad Transit (SW 46.9L) of BRB.

1.2 Objectives of the Study

The specific objectives of this study are:

- To setup a hydrological model for Brahmaputra River Basin (BRB)
- To setup surface erosion and sediment routing model for Brahmaputra River Basin (BRB)
- To estimate future sediment load at Bahadurabad transit (SW 46.9L) considering future climate and land use changes

1.3 Organization of the Thesis

Chapter 1 is an introduction to the thesis. Here, the background and present state of the study and objective of the thesis have been discussed.

Chapter 2 is literature review and theoretical background. This chapter contains review of hydro-morphological status of the study area, Brahmaputra River Basin. Also, literature of several topics which include- review of previous studies for estimating surface runoff and sediment yield, climate change impact assessment on different basins, impact of climate change on water availability and sediment load of Brahmaputra River Basin have been described. The basic concepts and theories of different hydrological processes in HEC-HMS are also discussed.

Chapter 3 discusses the steps followed in the present thesis to setup, from data collection to calibration/validation of surface runoff and sediment yield models and assess the impact of climate and land use changes on sediment load in Brahmaputra River Basin.

Chapter 4 describes the detail procedure followed to setup surface runoff and sediment yield models of Brahmaputra River Basin. This chapter describes the bias correction done on climate data, parameters used to calibrate the model and evaluate the performance of calibration/validation.

Chapter 5 is results and discussions which contains sensitivity analysis of the calibrated and validated model, selection of RCM models for RCP 8.5 for assessing impact of climate change on water and sediment load availability and discussion on impact of land use changes on sediment load at Bahadurabad transit (SW46.9L).

Chapter 6 is conclusions and recommendations. This chapter gives a summary of the results obtained in this study and also includes recommendations for further study relevant to this topic.

CHAPTER 2
LITERATURE REVIEW AND THEORETICAL BACKGROUND

2.1 Hydro-Morphological Status of Brahmaputra River Basin

The river Brahmaputra-Jamuna is originated in the Himalayas, passing through China, India and entering Bangladesh through the northern boundary. It drains the northern and eastern slopes of the Himalayas and has a catchment area of about 552000 km^2. 50.5% of which lie in China, 33.6% in India, 8.1% in Bangladesh and 7.8% in Bhutan (Figure 2.1). Its basin in India is shared by Arunachal Pradesh (41.88%), Assam (36.33%), Nagaland (5.57%), Meghalaya (6.10%), Sikkim (3.75%) and West Bengal (6.47%) (Singh et al., 2004). Immerzeel (2008) categorized the Brahmaputra basin into three different physiographic zones: Tibetan Plateau (TP), Himalayan Belt (HB), and the floodplain (FP).

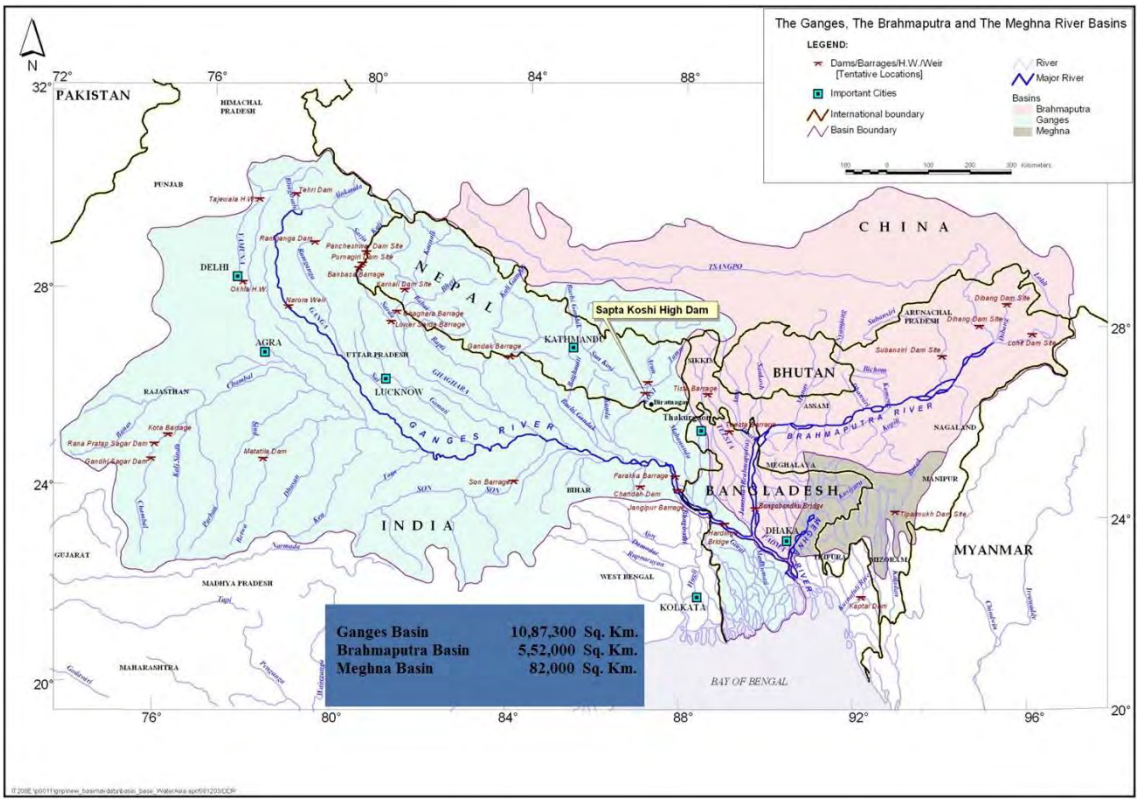

Figure 2.1: Brahmaputra River Basin (BRB) in GBM basins (JCRB, 2018)

2.1.1 Topography

The Brahmaputra drains almost 3000 km of China, India and Bangladesh. The river starts it journey at an altitude of 5100 m from the Chemayungdung glacier of the Himalayas (Figure 2.1). Then it flows for about 1400 km in an easterly direction across the Tibetan plateau, which is bordered by the Himalayas in the south and the Gandis Mountains in the north, while it descends to 3000 m. In this reach the river is known as the Tsangpo or Yarlung Zangbo (Jiang) River. At an altitude of 200 m above sea level it leaves the Himalayan range as the Dihang River (Jagers, 2003). At Assam province in India, the river meets the Lohit and Dibang River and takes its name as the Brahmaputra. Then the river flows to the west and near the international border between India and Bangladesh at the ninety degrees east meridian, it makes a sharp left turn, goes south and enters Bangladesh from where the river is known as the Jamuna.

The main river channel traverses three different countries: China, India and Bangladesh. Originating from the great glacier mass of Chema-Yung-Dung in the Kailas range of southern Tibet at an elevation of 5300 m above sea level, the Brahmaputra river travels a total distance of 2880 km (1625 km in China, 918 km in India and 337 km in Bangladesh) before emptying into the Bay of Bengal through a joint channel with the Ganga (Ganges River). The long profile for the entire river course is shown in Figure 2.2.

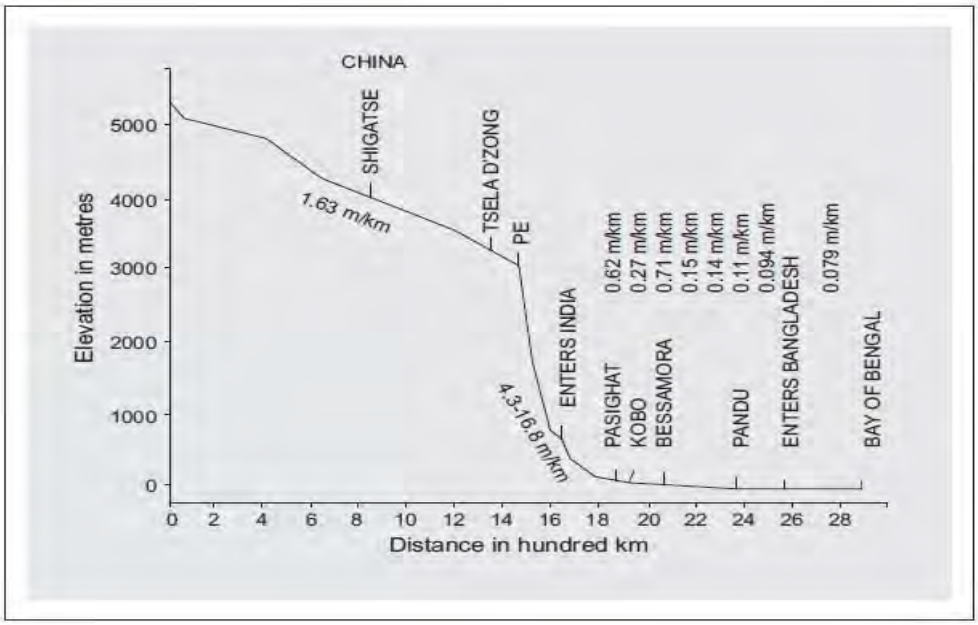

Figure 2.2: Longitudinal profile of Brahmaputra river (Mahanta et al., 2014)

In China, the river is known as the Yarlung Tsangpo and flows east at an average height of 4000 m above sea level. At its easternmost point, it bends around Mt. Namcha Barwa and forms the Yarlung Tsangpo Canyon, which is considered the deepest in the world. As the river enters Arunachal Pradesh (India), it makes a very rapid descend from its original height in Tibet, and finally appears in the plains, where it is called Dihang. It flows for about 35 km and is joined by two other major rivers: Dibang and Lohit. From this confluence, the river becomes very wide and is called Brahmaputra. A few more tributaries join the main course of the river later on namely, BurhiDihing, Dikhou, Dhansiri and Kopili rivers on the left bank and Subansiri, Kameng, Manas, Sankosh, Dudhkumar/ Raidak, Jaldhaka/Dharla, Teesta, and Atrai rivers on the right bank. In Assam, the river is sometimes as wide as 10 km or more. Between Dibrugarh, and Lakhimpur districts, the river divides into two channels-the northern Kherkutia channel and the southern Brahmaputra channel. The two channels join again about 100 km downstream, forming the Majuli island. At Guwahati, near the ancient pilgrimage centre of Hajo, the Brahmaputra cuts through the rocks of the Shillong Plateau and is at its narrowest and is 1 km wide. (Singh et al., 2004).

For different river of Bangladesh, the average bed slope of this river is 7.5 cm/km (CEGIS, 2010). In fact, bed slope varies from the upstream to the downstream reach. The upper section has an 8.5 cm/km slope while at the downstream section the slope is 6.0 cm/km (CEGIS, 2010).

2.1.2 Flow Regime

The basin is characterized by high seasonal variability in flow, sediment transport and channel configuration (Goswami, 1985). The Brahmaputra-Jamuna River is one of the world's greatest rivers, ranking in the top three in terms of both sediment and water discharge (Rajib et al., 2011). On the Bangladesh plains the gradients are small and relatively minor changes in land elevation are sufficient to cause dramatic changes in the river course. Natural causes for such changes can be tectonic movements, severe floods caused by tropical monsoons, and extreme sediment loads (Jagers, 2003).

The Brahmaputra-Jamuna River has a direct and significant influence on the overall water availability of the country (Paul, 2014). The rise in the hydrograph of the Jamuna begins due to Himalayan snowmelt in May, but the hydrograph is dominated by monsoon rainfall

which is concentrated during the period of June to October. Average discharge of the Brahmaputra is approximately 20000 m^3/s (Immerzeel, 2008). The highest recorded daily discharge in the Brahmaputra at Pandu was 72726 m^3/s August 1962 while the lowest was 1757 m^3/s in February 1968. At Bahadurabad, the highest recorded peak flow was 102534 m^3/s in 1998 and the minimum was 3280 m^3/s in 1960 (Mirza, 2003).

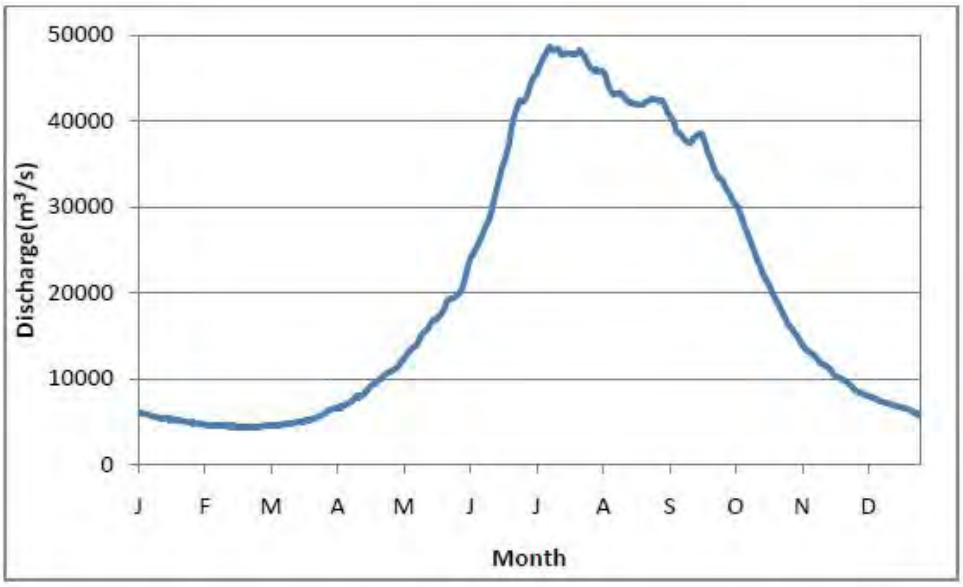

Figure 2.3: Mean daily discharge hydrograph of the river at Bahadurabad transit from 1956 to 2006 (Shampa, 2015)

The Figure 2.3 shows the mean annual hydrograph of the river at Bahadurabad which is prepared from the daily discharge data from 1956 to 2006 (Shampa, 2015). It indicates that in dry period the average flow is about 5000 m^3/s and flood season it goes up to 50000 m^3/s. Such a big variation of the discharge may be one of the causes of heavy dynamicity of the river.

2.1.3 Sediment Regime

The Brahmaputra River Basin (BRB) supplies enormous quantities of sediment from the actively uplifting mountains in the Himalayas, the erosive foothills of the Himalayan foredeep and the great alluvial deposits stored in the Assam Valley. Holeman (1968) estimated the sediment load in the Brahmaputra which was 1.6 billion tonnes/year. But he did not mention the time period and location of measurement. Colman (1969) stated that the total suspended load was 610 Mt/year. BWDB measurements in the late 1960s

showed that the suspended sediment load in both the Jamuna and the Ganges were 1047 Mt/year. Most of this is in the silt size class (suspended load) but around 15 to 25 percent is sand (bed load). The annual average sediment load as measured during 1966-1969 by the BWDB is tabulated in Table 2.1.

Table 2.1: The annual average sediment load measured by the BWDB (Delft Hydraulics and DHI, 1996a)

Period	Types of sediment	Sediment load in Jamuna (Mt/year)
1966-1969	S_{wash} load	335
	$S_{susp.}$ bed	220
	Total S_s	555

The measurements of FAP 24 in the early 1990s shows that suspended bed material load was about 402 Mt/year in this river which is much less than in the 1960s as measured by BWDB. The slight decrease in wash load in the Jamuna might be due to the continuation of the reduction in wash load since the 1950 earthquake, which overrules the assumption of increased sediment due to intensive agricultural practices in the Assam valley (CEGIS, 2010).

The sand size sediment is relatively uniformly graded. The range of d_{50} values vary between 0.21 mm and 0.14 mm (FAP 24). Sarker and Thorne (2006) related the reduction in bed material load in the Jamuna and Padma rivers to the propagation of sediment wave through the Brahmaputra-Jamuna-Padma-Lower Meghna River system due to huge landslides in the Himalayas caused by the 1950 Assam earthquake. Sarker (2009) analyzed the size of bed material (d_{50}) at Bahadurabad and found the value in an average of 0.20 mm.

2.1.4 Climate

In the basin area, the year can be divided into four seasons: the relatively dry, cool winter from December through February; the dry, hot summer from March through May; the southwest monsoon from June through September when the predominating southwest maritime winds bring rains; and the retreating monsoon of October and November (Mahanta et al., 2014) Brahmaputra River Basin receives an average of 1900 mm rainfall

per year. The climate of the basin is monsoon driven with a distinct wet season from June to September, which accounts for 60–70% of the annual rainfall.

2.2 Previous Study for Estimating Surface Runoff and Sediment Yield

Large-scale water resources modeling can provide useful insights on future water availability scenarios for downstream nations in anticipation of proposed upstream water resources projects in large international river basins (IRBs). However, model set up can be challenging due to the large amounts of data requirement on both static states (soils, vegetation, topography, drainage network, etc.) and dynamic variables (rainfall, streamflow, soil moisture, evapotranspiration, etc.) over the basin from multiple nations and data collection agencies. Under such circumstances, satellite remote sensing provides a more pragmatic and convenient alternative because of the vantage of space and easy availability from a single data platform.

In a study by Nishat and Rahman (2009), a water resources management model using MIKE BASIN, over the Ganges, Brahmaputra, and Meghna (GBM) river basins was set up. The objective was to provide Bangladesh, the lowermost riparian nation in the GBM basins, a framework for assessing proposed water diversion scenarios in the upstream transboundary regions of India and deriving quantitative impacts on water availability. Using an array of satellite remote sensing data on topography, vegetation, and rainfall from the transboundary regions, it was possible to calibrate MIKE BASIN to a satisfactory level and predict streamflow in the Ganges and Brahmaputra rivers at the entry points of Bangladesh at relevant scales of water resources management. Simulated runoff for the Ganges and Brahmaputra rivers followed the trends in the rated discharge for the calibration period. However, monthly flow volume differs from the actual rated flow by (-) 8% to (+) 20% in the Ganges basin, by (-) 15 to (+) 12% in the Brahmaputra basin, and by (-) 15 to (+) 19% in the Meghna basin. A large-scale modeling initiative is generic enough for other downstream nations in IRBs to adopt for their own modeling needs.

The WEPP model was used in within Lucknow River basin, Ontario, Canada to estimate surface runoff and sediment yield in different slope and management systems in a 13 year simulation period. Three small watersheds, with areas between 4594 m^2 to 19325 m^2 were delineated using LiDAR DEM. The principal objective of this study was to assess the

effect of using three different DEM resolutions (1, 5 and 10 m) on WEPP model output. The model was tested using Lucknow River daily discharge data. The t-test results showed that there are significant differences between measured and simulated WEPP output in annual basis, while Nash-Sutcliffe coefficient represented low deviation between the daily average measured and predicted data in a longer period (13 years). As the DEM resolution became coarser, the mean values of the prediction of runoff depth and sediment yield changed for each event size. The ANOVA test showed that the WEPP model with 1- m DEM resolution did not predict runoff or sediment yield significantly better than simulation using 5 and 10- m resolutions in this particular landscape. This conclusion is important because it implies that it may not be necessary to extract costly fine–resolution DEM for the application of watershed modeling in undulating topography such as southern Ontario (Dehvari, 2014).

In a study by Singh and Jain (2015), a continuous Soil Moisture Accounting (SMA) algorithm was used in a Hydrologic Engineering Center Hydrologic Modeling System (HEC-HMS) to model stream flow in the Vamsadhara River Basin in India. The spatial domain of the catchment was discretised into smaller sub-basins to account for catchment heterogeneity in terms of topography, land use and soil. The SMA algorithm in HEC-HMS was calibrated using data from 1984 to 1989 and has been validated for the period from 1990 to 1993 on a continuous time scale. Statistical and visual evaluation was conducted to determine the performance of the HEC-HMS model in the Vamsadhara River Basin. For the calibration period, the performance of the model ranges from good to very good with a coefficient of determination R^2=0.71, Nash-Sutcliffe Efficiency EFF=0.701, percentage error in volume PEV=2.64%, percentage error in peak PEP=0.21%, and index of agreement d=0.94. Similarly, the model performance for the validation period ranges from good to very good with R^2=0.78, EFF=0.762, PEV=12.33%, PEP = -15.2%, and d= 0.93. Sensitivity analysis of model parameters has also been conducted and the ranking of different parameters have been assigned based on their sensitivity in terms of percent change in simulated runoff volume. Sensitivity analysis helps to understand the behaviour of the model. Overall, the SMA procedure in the HEC-HMS conceptual model performed satisfactorily and can be used for long-term runoff modeling in the Vamsadhara River Basin.

In Chambal river basin of India Bhattacharya et al. (2013), used Variable Infiltration Capacity (VIC) a macro-scale hydrological model to generate water balance components including runoff, evapotranspiration and baseflow at 0.25*0.25degree grid for the year 2000. Remote Sensing and GIS data were incorporated in this process. The model was used to estimate daily variation of runoff over entire basin. The effect of change of Land cover, slope and soil type on runoff also investigated in this study. Simulation of VIC model showed the annual runoff generation over the basin is 50%. The hydrological processes were influenced by land use/ land cover, soil and slop characteristics in considerable manner. Higher runoff produce correspondent to less vegetative area where as low runoff produced in densely vegetated areas. Higher slopes contribute high runoff where as plain area produces low runoff. Also, runoff changes in considerable manner with respect to soil type and soil characteristics over the area. The sandy soil produces less runoff and clay soil produces high runoff.

2.3 Climate Change Impact Assessment on Different Basins

The Huaihe River, which is one of major rivers in China, is frequently subject to flooding and drought. The Variable Infiltration capacity (VIC) model with a resolution of 0.5°×0.5° was calibrated using data from eleven well gauged sub-basins of the Huaihe River basin by Zhang et al. (2012). The model parameters from the well gauged stations were then transferred to poorly gauged areas, according to similarities in climate conditions, soil texture etc.

A mean monthly water balance (WB) model was developed to show the Hydrologic effects of climate change in the Yukon River Basin**.** The scenarios indicate an increase in annual runoff in the twenty-first century for the YRB with simulated increases in precipitation having the greatest effect on increase in runoff. Simulation of increase in temperature was found to alter the timing of snow accumulation and melt (Hay et al., 2010).

Climate change and the response of hydrologic systems are the main issues of modeling the hydrological impacts of global climate change. In the Dongjiang Basin which is situated at South China, six hydrological models are simulated to compare the hydrological impacts of climate change. Six water balance models are used by Jiang et al. (2007) to show the diversion of the models' result with respect to historical and

alternative climates for the same input data series. It also investigates potential impacts of human-induced climate change on the water availability in the basin.

Variation in future climate pattern is closely related to hydrologic changes including impact on regionally available water. Global atmospheric general circulation models (GCMs) is being used as a tool for the simulation of present climate and to predict future climate scenario. Need of hydrologic model arises from the gap in GCMs ability to represent local subgrid-scale features and dynamics. XU (1999) reviewed the existing gaps between GCMs and hydrological models, the recent research developments, and the challenges for the future studies of the hydrological impacts of climate change.

The impact of climate change on sediment yield in the Nam Ou basin was analyzed by Shrestha et al. (2013). The Soil and Water Assessment Tool (SWAT) is used to assess future changes in sediment flux attributable to climate change. Future climate (temperature and precipitation) from four general circulation models (GCMs) and a regional circulation model (PRECIS) are downscaled using a delta change approach. Results indicate up to 3.0^0C shift in seasonal temperature and 27% (decrease) to 41% (increase) in seasonal precipitation. The simulation results show that the changes in annual stream discharges are likely to range from a 17% decrease to 66% increase in the future, which will lead to predicted changes in annual sediment yield ranging from a 27% decrease to about 160% increase. A higher discharge and sediment flux is expected during the wet seasons, although the highest relative changes are observed during the dry months.

In the Be River Catchment of Vietnam, the impact of climate change on hydrology and sediment load was assessed by using SWAT hydrological model by Khoi et al. (2013). The calibration and validation results indicate that the SWAT model is a reasonable tool to simulate the impact of environmental change on hydrology and sediment yield for this catchment. Based on the calibrated model, the responses of hydrology and sediment yield to climate change were simulated for four GCM simulations (CGCM3.1 (T63), CM2.0, CM2.1, and HadCM3). The simulated results exhibit that the annual streamflow is expected to decrease by 2.4% to 4.4%, and the annual sediment load is projected to change by -1.4% to 4.5% in the future which indicated that changes in sediment yield due to climate change are larger than the corresponding changes in streamflow.

The changes in runoff and sediment load of the Xiliugou basin in the upper Yellow River were investigated by using temperature, wind, precipitation, water discharge, and sediment load data. The contributions of climate change and human activities to these changes were quantitatively estimated in this study. Results show that the runoff and sediment load of the stream declined gradually in 1960–2012. According to the abrupt change point detected, the runoff and sediment series were divided into two periods: 1960–1998 and 1999–2012. The reductions of runoff and sediment load in 1999–2012 were found to be related to climate change and human activities, and the latter played a dominant role with a contribution of about 68% and 75%, respectively (Haifang et al., 2015).

2.4 Impact of Climate Change on Water Availability and Sediment Load of Brahmaputra River Basin

According to IPCC, the mega deltas in South, East and Southeast Asia such as the Ganges-Brahmaputra-Meghna delta in Bangladesh are likely to be most affected by climate changes. Uncertainty remains in prediction of future conditions in these deltas. Changes in future climate will have immense impact on the water resources and flood protection in these densely populated areas. Olesen et al. (2001) discussed in their study about the climate change challenges for adaptation of new technologies and protection against natural disasters.

Mirza et al. (2003) investigated impacts of climate change on the magnitude, extent and depth of flooding in Bangladesh. A sequence of empirical models and the MIKE11-GIS hydrodynamic model were used. Climate scenarios were constructed from the results of four climate models: CSIRO9, UKTR, GFDL and LLNL. Surprisingly, the model results indicate that most changes in the mean flooded areas occur between 0 and 2ºC in relation to the increases in the peak discharges of the Ganges, Brahmaputra and Meghna Rivers rather than at higher temperature increases.

Chowdhury et al. (2008) worked on a grid-based hydrological model called ‘Global Water AVailability Assessment (GWAVA)’. The surface water runoff processes in the basins of Ganges, Brahmaputra and Meghna have been simulated by a coarse scale representation at 0.5ºx0.5ºresolution. Bangladesh is represented by a fine scale resolution of 0.1ºx0.1º. Climate scenarios were constructed from the results of four Global climate

models: HADCM3, R30, CGCM2 and AGCM and two Regional models: HadRM2 and PRECISA2.

In a study by Ghosh et al. (2011), a single projected meteorological scenario (A2 scenario; SRES-98 emission scenarios after IPCC) has been used to evaluate the effect of climate change on Flood Vulnerability of the Brahmaputra River Basin. A physically based macro-scale distributed hydrological model (DHM), which works on the concept of hydrological similarity classes (HSCs), has been calibrated validated and then used to assess the possible future changes in the flood characteristics and flood vulnerability of the Brahmaputra basin, India, due to climate and land use changes. The projected climate change can increase the peak flow of Brahmaputra by about 28%, the same has been found to be increased by a maximum of about 9% for land use/ land cover changes.

Gain et al. (2011) applied a new method to construct a daily discharge time series from using a discharge-weighted ensemble based on inputs from 12 GCMs to a global hydrological model. Weighted discharge time series were subsequently used to analyze future trends in average flow and extreme flow results show that climate change is likely to improve dry season conditions in the LBRB. The authors said that Low flow conditions may even be slightly underestimated as the accelerated glacial melt in the upstream parts of the catchment may, albeit temporarily, further enhance low flow. They also said that there might be a large increase of peak flow and frequency.

Salehin et al. (2011) used grid-based model over the Ganges-Brahmaputra-Meghna for both conditions as coarser and fine model. The coarse grid model has a snowmelt runoff module, which calculates snowmelt and glacial melt runoff in the Ganges and Brahmaputra basins following the temperature index method. The coarse grid model is verified against observed daily discharge at important locations, Bahadurabad on the Brahmaputra and Hardinge Bridge on the Ganges and against available monthly discharge data in the Nepalese part of the Ganges basin. The author used CRU (climate Research units) data as precipitation source for their model. They also recommend the use of meteorological satellite data (Tropical Rainfall Measuring Mission or TRMM data) for this kind of hydrological model.

Most of the predictions based on GCMs indicate decrease in the annual, wet season and dry season flow volumes on the Brahmaputra Basin while those based on RCMs indicate

increase. Ghosh and Datta (2011) found that the impact of climate change is likely to be greater compared to changes in land use/land cover in the basin. Another study by IWM and CCC (2008) found that the frequency of flood flows in the Brahmaputra River at Bahadurabad has already increased compared to earlier flow records.

Ghosh and Dutta (2012) analyzed the impact of climate change on the Tezpur, Guwahati and Dhubri stations of Brahmaputra Basin using macro-scaled distributed hydrology model. The author said that there are very likely to increase of peak flow, flow duration during pre-monsoon and monsoon for future climate change. But the chance of time of peak during pre-monsoon might be increase whereas the chance of time of peak during monsoon might be same. The authors also said that the no of flood wave for pre-monsoon will be chance to increase in 2070s but the no of flood wave for monsoon will be decrease in 2070s. Almost all the tributaries of the Brahmaputra river system are likely to carry an increased peak discharge with greater variation in annual peak discharge series.

Paul (2014) used SWAT to setup a semi-distributed hydrological model of Brahmaputra river basin for assessing future flow on BRB using QUMP ensembles experiments of PRECIS for the early century (2011-2040), mid-century (2041-2071) and end century (2071- 2099). In this study, the chance of change of monthly flow for August might increase 4% for 2020s was found. It might increase to 5% and 8% for 2050s and 2080s, respectively. However, the inter-quartiles of mean flow in March simulated by the RCM ensemble members are very high. This shows the level of uncertainties of future predictions is high. On the other hand, results obtained by the simulation of SWAT model using multi-ensemble members agree that the possibility of increase of the flow in June and July will be high. Although the percentages of increase of flow in the pre-monsoon season are higher than that of monsoon flow, the volume of monsoon flow will be ten times higher than that of pre-monsoon. Therefore, flooding in this basin will be increased in the future was predicted in this study.

Alam (2015) found maximum projected increase in mean annual streamflow found about 15.019%, 32.457% and 47.436% for MIROC-ESM-CHEM RCP8.5 (warmest), GISS-E2-H RCP4.5 (moderate warm) and BCC-CSM1.1 RCP8.5 (wettest) in 2020s, 2050s and 2080s respectively for Brahmaputra river basin. The minimum projected change in streamflow found are -3.290%, 1.800% and -0.908% for HadGEM2-ES RCP8.5 (driest),

GISS-E2-R RCP2.6 (coolest) and GISS-E2-R RCP2.6 (coolest) in 2020s, 2050s and 2080s respectively from this basin. On average, at the end of 21st century (2080s), the mean dry and wet period streamflow of BRB is projected to increase by about 177.93% and 11% of their mean dry and wet period discharge in climate normal period, respectively. In 2080s, maximum increases in dry and wet period flow were found for GISS-E2-H RCP 4.5 (moderate warming) and BCC-CSM1.1 RCP8.5 (wettest), respectively. Lowest dry and wet period flows were found for MRI-CGCM3 RCP6.0 (moderate wet) and GISS-E2-R RCP2.6 (coolest) scenarios, respectively.

Fischer et al. (2016) studied on reported peer-reviewed data relevant to sediment transport and perform a sensitivity analysis to identify sensitive and uncertain parameters, using the one-dimensional model HEC-RAS, considering both present and future climatic conditions. The results showed that there is considerable uncertainty in openly available estimates (260–720 Mt/year) of the annual sediment load for the Brahmaputra River at its downstream Bahadurabad gauging station (Bangladesh). This may aggravate scientific impact studies of planned power plant and reservoir construction in the region, as well as more general effects of ongoing land use change and climate change. They found that data scarcity on sediment grain size distribution, water discharge, and Manning's roughness coefficient had the strongest controls on the modelled sediment load. However, despite uncertainty in absolute loads, the study showed that predicted relative changes, including a future increase in sediment load by about 40 % at Bahadurabad by 2075–2100, were consistent across multiple model simulations.

Sediment transport dynamics strongly affect the region's ecology and agriculture. Suspended sediment is a natural part of river systems. It plays an important role in structuring the landscape, creating ecological habitats and transporting nutrients. Alterations to sediment quality and quantity negatively impact ecological communities, increase flood hazard and shorten the lifespan of infrastructure. The changes in global climate generates a lot of alterations in hydrological components like precipitation, evaporation, soil moisture, runoff etc. Anthropogenic and manmade activities can also consider in this type of assessment. The natural variability in hydrological conditions, as well as changes in land use, water use, and climate all affects the quantity and quality of sediments (e.g., Chalov et al. 2015).

Basin management problem usually occur due to unavailability of proper understanding about sediment load of a particular basin. The changes of sediment flows in future considering climatic variables alteration need to be assessed in order to proper control and management of sediment flows in large catchment, especially for that hydrological regions where people's livelihood depends on river systems and their natural processes. So, it is obvious to understand how a change in global climate could affect regional water supplies and amount of sediment load. The extensive literature review of present and past studies notes that climate change impact analysis for sediment load assessment generally done in four steps.

Step 1: Development of a calibrated and validated water level or runoff simulation model using historical data.

Step 2: Sediment load simulation under present climatic conditions for climate normal period (a 30-year period) using a hydrodynamic or a hydrologic model calibrated and validated with historical data.

Step 3: Generation of climate change scenarios for different future periods (usually three 30 years period of 21st century, namely, 2010-2039, 2040-2069, and 2070-2099).

Step 4: Sediment load simulation under changed climatic conditions for future periods based on the generated climate change scenarios.

2.5 Categorization of Mathematical Model

An event model simulates a single storm. The duration of the storm may range from a few hours to a few days. A continuous model simulates a longer period, predicting watershed response both during and between precipitation events.

A distributed model is one in which the spatial (geographic) variations of characteristics and processes are considered explicitly. In a lumped model, these spatial variations are averaged or ignored. HEC-HMS includes primarily lumped models. Lumped model is basically one dimensional and the equations are semi dimensional.

An empirical model is built upon observation of input and output, without seeking to represent explicitly the process of conversion. A conceptual model is built upon a base of

knowledge of the pertinent physical, chemical, and biological processes that act on the input to produce the output.

If all input, parameters, and processes in a model are considered free of random variation and known with certainty, then the model is a deterministic model. If instead the model describes the random variation and incorporates the description in the predictions of output, the model is a stochastic model.

A measured-parameter model is one in which model parameters can be determined from system properties, either by direct measurement or by indirect methods that are based upon the measurements. A fitted-parameter model, on the other hand, includes parameters that cannot be measured.

2.6 Constituents of a Model

All the models have the following common components:

State variable(s)

- Represent the state of the hydrologic system at a particular time and location.

Parameter(s) numerical

- Measure of the properties of the real-world system.
- They control the relationship of the system input to system output.

Boundary condition(s)

- The values of the system input—the forces that act on the hydrologic system and cause it to change.
- The most common boundary condition in HEC-HMS is precipitation.

Initial condition(s)

- The HEC-HMS models are unsteady-flow models.
- They describe changes in flow over time.
- They do so by solving, in some form, differential equations that describe a component of the hydrologic system.

2.7 Models of Watershed Hydrology and Sediment Yield

A model is a simplified representation of a complex process or phenomenon. Considering hydrologic cycle, mathematical model is the quantitative expression of observing,

analyzing or predicting a process by simulating it through the transformation of rainfall to runoff in catchments. The landscape gets affected in a numerous way when water flows over the land surface and through stream channels. Eroded surface soil and bed material due to shallow surface flow and steep headwater streams can be carried by the stream flow to lower reaches to the watershed. Therefore, erosion and sediment transport need to address as it leads to a number of problems. These problems can be best evaluated in conjunction with hydrologic simulation. Also, a good calibrated and validated model can be used for hydrologic prediction and future sediment load estimation. They are also providing valuable information for studying potential impacts of changes in land use and land cover or climate.

SWAT, HEC-HMS, VIC, HBV, MIKE-SHE, LISFLOOD are some widely used hydrological modeling tool for watershed analysis. SWAT, HEC-HMS and MIKE-SHE have surface erosion computing component which basically measures erosion due to rainfall or surface runoff by using USLE or MSULE equation. SWAT and HEC-HMS both have sediment routing component which basically represents sediment erosion and deposition processes within rivers. Though, HEC-HMS has Soil Moisture Accounting algorithm which theoretically more applicable for simulating continuous rainfall-runoff processes, it has been taken as a tool to develop a hydrological and surface erosion and sediment routing model of Brahmaputra River Basin.

2.8 Surface Runoff Model in HEC-HMS

2.8.1 Conceptual Basis

HEC HMS divides a watershed into subbasins. Each subbasin is connected through a junction in a channel. HEC-HMS omits any detailed accounting of movement of water within the soil. It includes models of infiltration from the land surface. But it does not model storage and movement of water vertically within the soil layer.

It implicitly combines the near surface flow and overland flow and models this as direct runoff. It does not include a detailed model of interflow or flow in the groundwater aquifer, instead representing only the combined outflow as baseflow. Most of the models included in HEC-HMS are event models but ModClark model is an exception. It includes both empirical and conceptual models. All models included in HEC-HMS are

deterministic. HEC-HMS uses a separate model to represent each component of the runoff process that is illustrated in Figure 2.4 including:

- Models that compute runoff volume
- Models of direct runoff (overland flow and interflow)
- Models of baseflow
- Models of channel flow

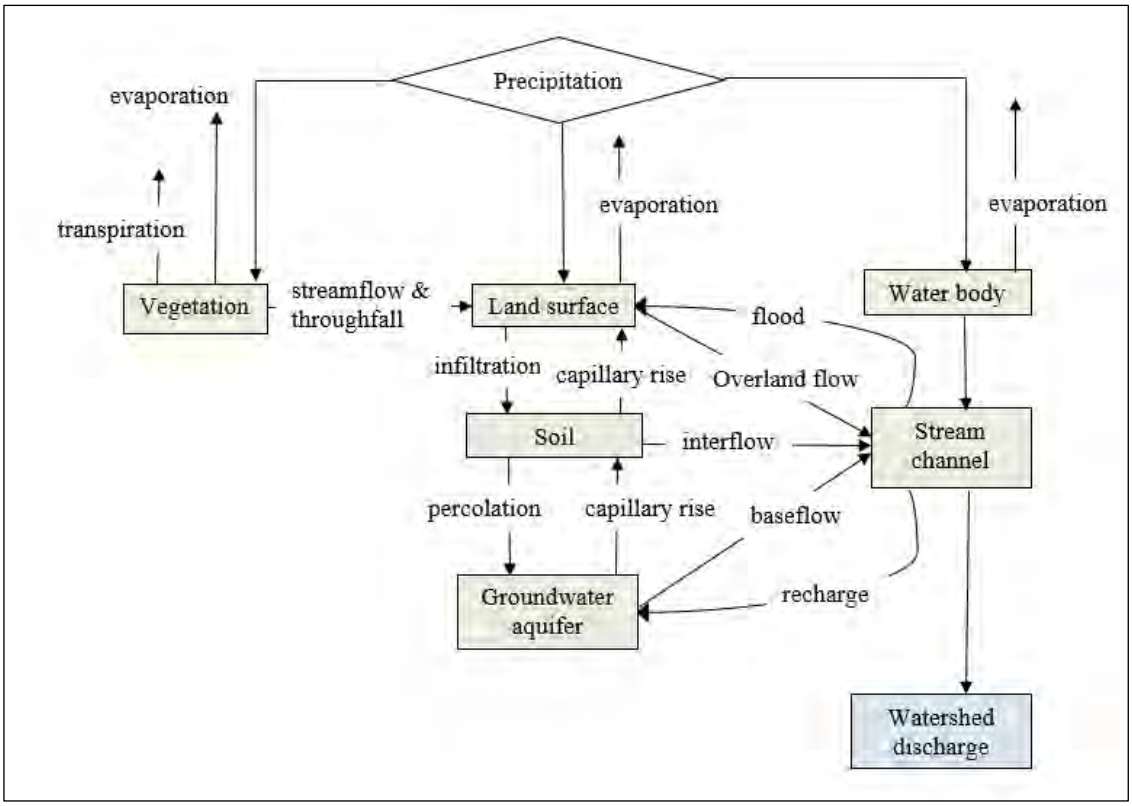

Figure 2.4: Typical HEC-HMS representation of watershed runoff (Scharffenberg, 2015)

2.8.2 Computing Runoff Volumes with HEC-HMS

HMS includes continuous model that simulates both wet and dry weather behaviour. The Soil Moisture Accounting model (SMA) shown in Figure 2.5 does this. The model simulates the movement of water through and storage of water on vegetation, on the soil surface, in the soil profile, and in groundwater layers. Given precipitation and potential evapotranspiration (ET), the model computes basin surface runoff, groundwater flow, losses due to ET, and deep percolation over the entire basin.

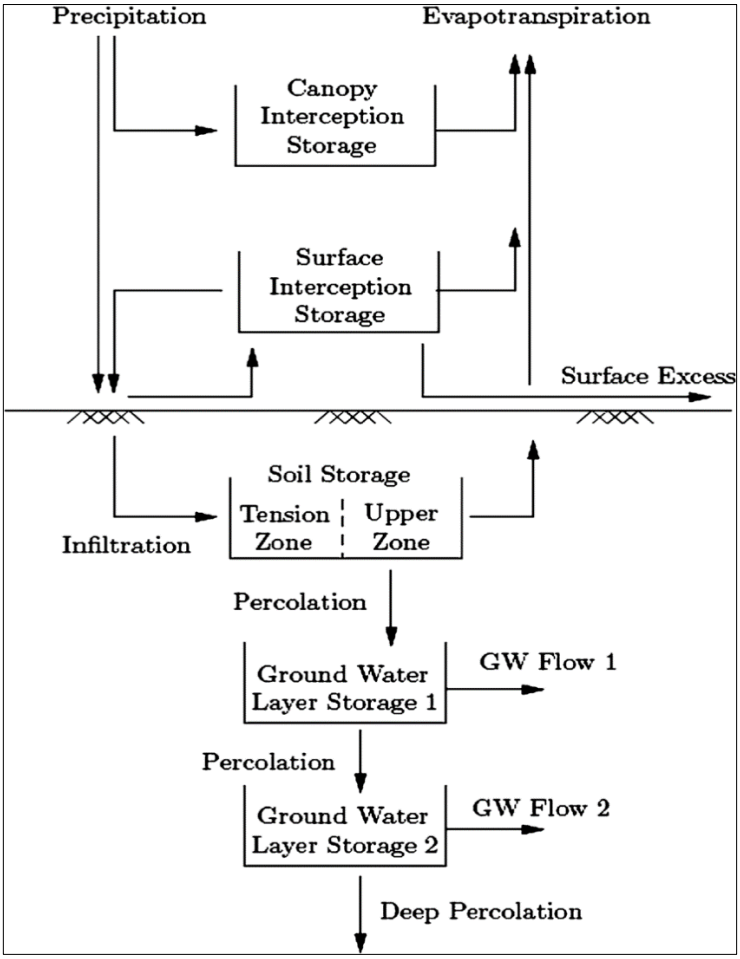

Figure 2.5: Soil Moisture Accounting losses module (Scharffenberg, 2015)

The SMA model computes flow into, out of, and between the storage volumes. This flow can take the form of:

Precipitation

Precipitation is an input to the system of storages. Precipitation first contributes to the canopy interception storage. If the canopy storage fills, the excess amount is then available for infiltration.

Infiltration

Infiltration is water that enters the soil profile from the ground surface. Water available for infiltration during a time step comes from precipitation that passes through canopy interception, plus water already in surface storage. The volume of infiltration during a time interval is a function of the volume of water available for infiltration, the state (fraction of

capacity) of the soil profile, and the maximum infiltration rate based om soil texture specified by the model user.

Percolation

Percolation is the movement of water downward from the soil profile, through the groundwater layers, and into a deep aquifer. In the SMA model, the rate of percolation between the soil-profile storage and a groundwater layer or between two groundwater layers depends on the volume in the source and receiving layers. The rate is greatest when the source layer is nearly full, and the receiving layer is nearly empty. Conversely, when the receiving layer is nearly full, and the source layer is nearly empty, the percolation rate is less.

Surface runoff and groundwater flow

Surface runoff is the water that exceeds the infiltration rate and overflows the surface storage. This volume of water is direct runoff. The resulting runoff hydrograph is computed with one of the models. Groundwater flow is the sum of the volumes of groundwater flow from each groundwater layer at the end of the time interval.

Evapotranspiration (ET)

ET is the loss of water from the canopy interception, surface depression, and soil profile storages. In the SMA model, potential ET demand currently is computed from monthly pan evaporation depths, multiplied by monthly-varying pan correction coefficients, and scaled to the time interval. The potential ET volume is satisfied first from canopy interception, then from surface interception, and finally from the soil profile. Within the soil profile, potential ET is first fulfilled from the upper zone, then the tension zone. If potential ET is not completely satisfied from one storage in a time interval, the unsatisfied potential ET volume is filled from the next available storage. When ET is from interception storage, surface storage, or the upper zone of the soil profile, actual ET is equivalent to potential ET. When potential ET is drawn from the tension zone, the actual ET is a percentage of the potential.

Flow into and out of storage layers is computed for each time step in the SMA model. Order of computations in each time step depends upon occurrence of precipitation or ET.

If precipitation occurs during the interval, ET is not modeled. Precipitation contributes first to canopy-interception storage. Precipitation in excess of canopy-interception storage, combined with water already in surface storage, is available for infiltration. If the volume available is greater than the available soil storage, or if the calculated potential infiltration rate is not sufficient to deplete this volume in the determined time step, the excess goes to surface-depression storage. When surface-depression storage is full, any excess is surface runoff.

Infiltrated water enters soil storage, with the tension zone filling first. Water in the soil profile, but not in the tension zone, percolates to the first groundwater layer. Groundwater flow is routed from the groundwater layer 1, and then any remaining water may percolate to the groundwater layer 2. Percolation from layer 2 is to a deep aquifer and is lost to the model.

If no precipitation occurs, ET is modeled. Potential ET is satisfied first from canopy storage, then from surface storage. Finally, if the potential ET is still not satisfied from surface sources, water is removed from the upper-soil profile storage. The model then continues as described above for the precipitation periods.

2.8.3 Modeling Direct Runoff with HEC-HMS

In HEC-HMS the following models are used to simulate the process of direct runoff of excess precipitation on a watershed as transformation of precipitation excess into point runoff.

- User-Specified Unit Hydrograph
- Clark's UH
- Snyder's UH
- SCS UH
- ModClark
- Kinematic Wave

In 1938, Snyder published a description of a parametric UH that he had developed for analysis of ungauged watersheds in the Appalachian Highlands in the US, and he provided relationships for estimating the UH parameters from watershed characteristics (Snyder, 1938). In this study, Snyder's Unit Hydrograph is used for direct runoff among all these

methods as Brahmaputra river basin is a data poor basin. Lag hour can be easily calculated from time of concentration and the range of peaking co-efficient is 0.4 to 0.8 (Bedient and Huber, 1992).

Snyder's Unit Hydrograph

HEC-HMS includes an implementation of Snyder's UH. For his work, Snyder selected the lag, peak flow, and total time base as the critical characteristics of a UH. He defined a Standard UH as one whose rainfall duration t_r, is related to the basin lag, t_p by

$$t_p = 5.5\ t_r \qquad \text{...2-1}$$

(Here lag is the difference in the time of the UH peak and the time associated with the centroid of the excess rainfall hyetograph, as illustrated in Figure 2.6) Thus, if the duration is specified, the lag (and hence the time of UH peak) of Snyder's standard UH can be found.

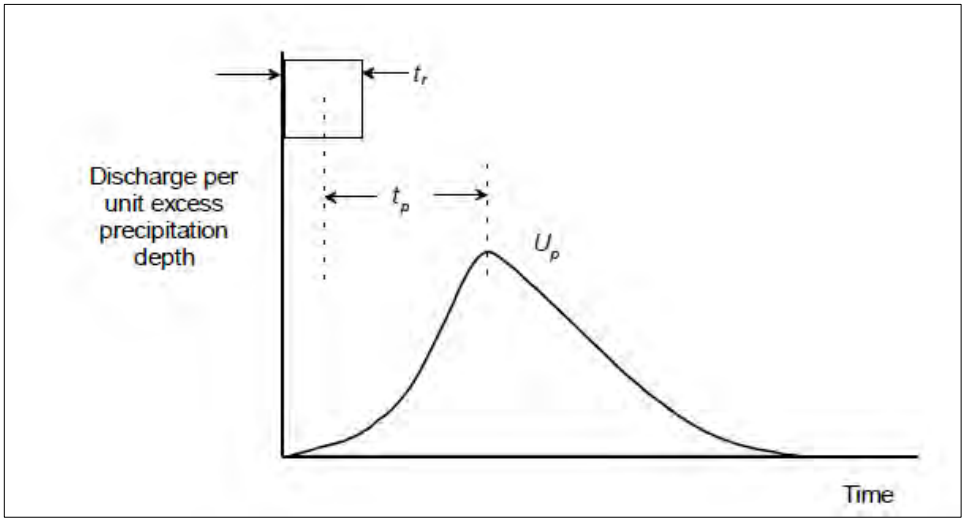

Figure 2.6: Discharge Vs time hydrograph (Feldman, 2000)

If the duration of the desired UH for the watershed of interest is significantly different from that specified by Equation 2-1, the following relationship can be used to define the relationship of UH peak time and UH duration

$$t_{pR} = t_p - \frac{t_r - t_R}{4} \qquad \text{...2-2}$$

in which t_R = duration of desired UH; and t_{pR} = lag of desired UH

For the standard case, Snyder discovered that UH lag and peak per unit of excess precipitation per unit area of the watershed were related by:

$$\frac{U_p}{A} = C\frac{C_p}{t_p} \quad \text{..... 2-3}$$

Where U_p = peak of standard UH (m^3/s)

A = watershed drainage area = km^2

C_p = UH peaking coefficient

and C = conversion constant = 2.75

For other durations, the UH peak, Q_{pR} is defined as

$$\frac{U_{pR}}{A} = C\frac{C_p}{t_{pR}} \quad \text{..... 2-4}$$

Snyder's UH model requires specifying the standard lag, t_p and the coefficient, C_p. HEC-HMS sets t_{pR} of Equation 2-2 equal the specified time interval and solves Equation 2-2 to find the lag of the required UH. Finally, HEC-HMS solves Equation 2-4 to find the UH peak. Snyder proposed a relationship with which the total time base of the UH may be defined. Instead of this relationship, HEC-HMS uses the computed UH peak and time of peak to find an equivalent UH with Clark's model (mentioned in the next section). From that, it determines the time base and all ordinates other than the UH peak.

Estimating Snyder's UH Parameters

Snyder collected rainfall and runoff data from gaged watersheds, derived the UH as described earlier, parameterized these UH, and related the parameters to measurable watershed characteristics. For the UH lag, he proposed:

$$t_p = CC_t (LL_c)^{0.3} \quad \text{.....2-5}$$

where C_t = basin coefficient; L= length of the main stream from the outlet to the divide (km); L_c = length along the main stream from the outlet to a point nearest the watershed centroid (km); and C = a conversion constant = 0.75.

C_t and C_p are best best found via calibration as they are not physically-based parameters. According to Bedient and Huber (1992) report, C_t typically ranges from 1.8 to 2.2 and C_p ranges from 0.4 to 0.8, where larger values of C_p are associated with smaller values of C_t.

Alternative forms of the parameter predictive equations have been proposed. According to Los Angeles District, USACE (1944),

$$t_p = CC_t (LL_c/\sqrt{S})^N \quad \text{..... 2-6}$$

Where, S = overall slope of longest watercourse from point of concentration to the boundary of drainage basin; and N = an exponent, commonly taken as 0.33.

Time of concentration is the time of flow from the most hydraulically remote point in the watershed to the watershed outlet and may be estimated with simple models of the hydraulic processes, as described here in the section on the SCS UH model. Various studies estimate t_p as 50-75% of t_c (Cudworth, 1989; USACE, 1987)

2.8.4 Modeling Baseflow with HEC-HMS

The following models are used to simulate the process of baseflow in HEC-HMS.

- Bounded Recession
- Constant Monthly
- Linear Reservoir
- Nonlinear Boussinesq
- Recession

In this study, the linear reservoir model is used with soil-moisture accounting model. It is best calibrated using procedures consistent with those used to calibrate that model (Feldman, 2000). This baseflow model simulates the storage and movement of subsurface flow as storage and movement of water through reservoirs. The reservoirs are linear: the outflow at each time step of the simulation is a linear function of the average storage during the time step. The outflow from groundwater layer 1 of the SMA is inflow to one linear reservoir, and the outflow from groundwater layer 2 of the SMA is inflow to another. The outflow from the two linear reservoirs is combined to compute the total baseflow for the watershed.

2.8.5 Modeling Channel Flow with HEC-HMS

It is a procedure to determine the flow hydrograph at a downstream point on a watershed from a known hydrograph at upstream. As the hydrograph travels, it

- attenuates
- gets delayed

Routing account for changes in flow hydrograph as a flood wave passes downstream. This helps in

- Accounting for storages
- Studying the attenuation of flood peaks

It is a method of channel routing. It uses a simple finite difference approximation of the continuity Equation 2-7.

$$\left(\frac{I_{t-1}+I_t}{2}\right)-\left(\frac{O_{t-1}+O_t}{2}\right)=\left(\frac{S_t-S_{t-1}}{\Delta t}\right) \quad \text{.....2-7}$$

Storage in the reach is modelled as the sum of prism storage and wedge storage. As shown in Figure 2.7, prism storage is the volume defined by a steady-flow water surface profile, while wedge storage is the additional volume under the profile of the flood wave. During rising stages of the flood, wedge storage is positive and is added to the prism storage. During the falling stages of a flood the wedge storage is negative and is subtracted from the prism storage.

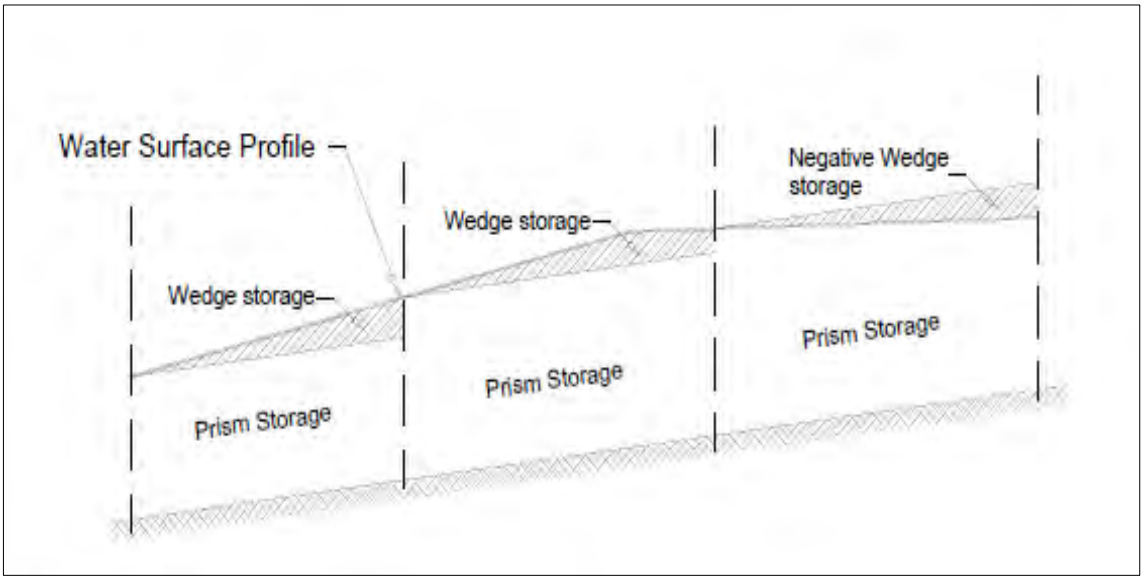

Figure 2.7: Wedge storage (Linsley,1982)

Muskingum model defines the storage as:

$$S_t = KO_t + KX(I_t - O_t) = K[XI_t + (1-X)O_t] \quad \text{.....2-8}$$

Where,

K = travel time of peak through the reach (hr)

X = weight on inflow versus outflow ($0 \leq X \leq 0.5$)

X = 0 for Reservoir, storage depends on outflow, no wedge

X = 0.0 - 0.3 for Natural stream

Equation 2-7 is substituted into Equation 2-8 and the result is rearranged to isolate the unknown values at time t, the result is in Equation 2-9.

$$O_t = \left(\frac{\Delta t - 2KX}{2K(1-X)+\Delta t}\right) I_t + \left(\frac{\Delta t + 2KX}{2K(1-X)+\Delta t}\right) I_{t-1} + \left(\frac{2K(1-X)-\Delta t}{2K(1-X)+\Delta t}\right) O_{t-1} \quad \text{.....2-9}$$

Muskingum Cunge model

Muskingum model is very easy and popular to use, but the parameters include in this model are not physically based and thus are difficult to estimate. Further, the model is based upon assumptions that often are violated in natural channels. An extension, the Muskingum-Cunge model, overcomes these limitations. For capturing the sediment load in a reach, it is very necessary to represent the river network like natural channels. In this regard, Muskingum-Cunge can surely give a better calibration of sediment load.

The model is based upon solution of the following form of the continuity Equation 2-10, (with lateral inflow, q_L, included):

$$\frac{\partial A}{\partial t} + \frac{\partial Q}{\partial x} = q_L \quad \text{.....2-10}$$

And the diffusion form of the momentum Equation 2-11:

$$S_f = S_o - \frac{\partial y}{\partial x} \quad \text{.....2-11}$$

Combining these and using a linear apptroximatiom yields the convective diffusion Equation 2-12 (Miller and Cunge, 1975):

$$\frac{\partial Q}{\partial t} + c\frac{\partial Q}{\partial x} = \mu\frac{\partial^2 Q}{\partial x^2} + cq_L \quad \text{.....2-12}$$

Where c = wave celerity and μ = hydraulic diffusivity. The wave celerity and the hydraulic diffusivity are expresses as Equation 2-13 and Equation 2-14:

$$c = \frac{dQ}{dA} \quad \text{……..2-13}$$

and

$$\mu = \frac{Q}{2BS_o} \quad \text{……..2-14}$$

Where B = top width of the surface. A finite difference approximation of the partial derivatives, combined with 2-9, yiels Equation 2-15:

$$O_t = C_1 I_{t-1} + C_2 I_t + C_3 O_{t-1} + C_4 (q_L \Delta x) \quad \text{……...2-15}$$

The coefficients are in Equation 2-16 to 2-19,

$$C_1 = \frac{\frac{\Delta t}{K} + 2X}{\frac{\Delta t}{K} + 2(1-X)} \quad \text{…….2-16}$$

$$C_2 = \frac{\frac{\Delta t}{K} - 2X}{\frac{\Delta t}{K} + 2(1-X)} \quad \text{……...2-17}$$

$$C_3 = \frac{2(1-X) - \frac{\Delta t}{K}}{\frac{\Delta t}{K} + 2(1-X)} \quad \text{……...2-18}$$

$$C_4 = \frac{2\left(\frac{\Delta t}{K}\right)}{\frac{\Delta t}{K} + 2(1-X)} \quad \text{……..2-19}$$

The parameters K and X are (Cunge, 1969; Ponce, 1978):

$$K = \frac{\Delta x}{c} \quad \text{……..2-20}$$

$$X = \frac{1}{2}\left(1 - \frac{Q}{BS_o c\Delta x}\right)$$ ……2-21

But c, Q and B change over time, so the coeffocients C_1, C_2, C_3 and C_4 must also change. The program recomputes C1, C2, C3 and C4 at each time step, Δt and Δx using the algorithm proposed by Ponce (1986).

$$\Delta x = c\Delta t$$ ……..2-22

$$\Delta x < \frac{1}{2}\left(c\Delta t + \frac{Q_o}{BS_o c}\right)$$ ……...2-23

Here, Q_0 = reference flow, computed from the inflow hydrograph as Equation 2-24.

$$Q_o = Q_B + \frac{1}{2}(Q_{peak} - Q_B)$$ ……2-24

where, Q_B = baseflow and Q_{peak} = inflow peak

2.9 Surface Erosion and Sediment Routing Model in HEC-HMS

2.9.1 Erosion Method

Erosion method computes the total sediment load transported out of the subbasin. The Modified USLE method (Williams, 1975) is adapted from the original Universal Soil Loss Equation. The original equation was based on precipitation intensity. With high infiltration, there is little surface runoff and little accompanying surface erosion and vice versa. The modifications to the original USLE equation changed the formulation to calculate erosion from surface runoff instead of precipitation shown in Equation 2-25 and Equation 2-26.

Sed = **95***(Q_{surf} *q_{peak})$^{0.56}$ × K × LS × C × P (fps unit)……2-25

Sed = **11.8** × (Q_{surf} *q_{peak})$^{0.56}$ × K × LS × C × P (metric unit)……..2-26

where,

Sed = sediment yield for a given event (tons)

Q_{surf} = surface runoff volume (ft^3 or m^3)

q_{peak} = peak runoff rate (ft^3/s or m^3/s)

K = Erodibility factor

C = Cover and management factor

LS = Topographic factor

P = Practice factor

Erodibility Factor (K):

- Describes the difficulty of eroding the soil
- A function of the soil texture, structure, organic matter content and permeability
- From 0.05 for unconsolidated loamy sand to 0.75 for silty and clayey loam soils

An algebraic approximation of the nomograph that includes five soil parameters (texture, organic matter, coarse fragments, structure, and permeability) is proposed by Wischmeier and Smith (1978) and Renard et al. (1995) in Equation 2-27.

$$K = [(2.1 \times 10^{-4} M^{1.14} (12 - OM) + 3.25 (s - 2) + 2.5 (p - 3)) / 100] * 0.1317 \text{.....} 2\text{-}27$$

Where:

M: the textural factor with M = (msilt + mvfs) * (100 - mc);

mc [%]: clay fraction content (<0.002 mm);

msilt [%]: silt fraction content (0.002 – 0.05 mm);

mvfs [%]: very fine sand fraction content (0.05 – 0.1 mm);

OM [%]: the organic matter content;

s: the soil structure class (s=1: very fine granular, s=2: fine granular, s=3, medium or coarse granular, s=4: blocky, platy or massive);

p: the permeability class (p=1: very rapid, …, p=6: very slow).

Topographic Factor (LS):

- Describes the susceptibility to erosion due to length and slope
- From 0.1 for short, flat slopes to 10 for long, steep slopes
- **Source: DEM data**
- Equation 2-28 is the topographic factor calculation equation and Table 2.2 represents coefficient NN values in this equation.

$$LS = [0.065 + 0.0456 (slope) + 0.006541 (slope)^2] (slope\ length \div constant)^{NN} \ldots\ldots 2\text{-}28$$

Where:

slope = slope steepness in %

slope length = length of slope in m

constant = 22.1 metric

Table 2.2: NN Values for Topographic Factor (Robert and Hilborn, 2015)

S	<1	1 ≤ Slope ≤ 3	3≤Slope ≤5	≥ 5
NN	0.2	0.3	0.4	0.5

Practice Factor (P):

- Describes the effect of specific soil conservation practices (BMPs)
- Difficult to establish range, may take 1 (Scharffenberg, 2015)

Cover & Management Factor (C):

- Describes the influence of plant canopy on surface erosion
- Bare ground: 1 (most susceptible to erosion)
- Fully mulched or covered soils: 0.1
- Forest soils with a well-developed soil) horizon (surface organic layer) under a dense tree canopy: 0.0001
- **Source: Land use data**

Threshold (CFS)

- Lower limit for runoff events that cause erosion
- Events with peak flow less than the threshold will have no erosion.

Exponent:

- Used to distribute the sediment load into a time series sedigraph
- Small value: flattens the sedigraph compared to the hydrograph
- Large Value: Heightens the sedigraph

Gradation Curve:

- Defines the distribution of the total sediment load into grain size classes and subclasses at each subbasin outlet
- Defined as a percentage function in the paired data manager
- **Source: Soil Data**

2.9.2 Sediment Transport Potential Method

- Transport capacity of the flow can be calculated from the flow parameters and sediment properties
- Sediment transport capacity> available sediment in stream flow = Erosion from stream bed
- Sediment transport capacity< available sediment in stream flow = Deposition to the reach bed

Table 2.3: Available methods for reach in HEC-HMS for transport potential function (Scharffenberg, 2015)

Transport potential functions for calculating the amount of sediment that can be carried by the stream flow. Type is non-cohesive (NC) or cohesive (CO). Method is excess shear (ES), stream power (SP), or regression (RE).

Method	Type	Method	Reference
Ackers-White	NC	SP	Ackers and White, 1973
Engelund-Hansen	NC	SP	Engelund and Hansen, 1967
Laursen-Copeland	NC	ES	Laursen, 1958; Copeland and Thomas, 1989
Meyer-Peter Muller	NC	ES	Meyer-Peter and Müller, 1948
Toffaleti	NC	RE	Toffaleti, 1968
Wilcock	NC	ES	Wilcock and Crowe, 2003
Yang	NC	SP	Yang, 1984
Krone Parthenaides	CO	–	Krone, 1962; Parthenaides, 1962

- Engelund Hansen from Table 2.3 will be applicable for all reaches as, in FAP 24, this equation has been found as prediction formulae having a high level of accuracy for Jamuna river. The generalized form of Engelund Hansen in Equation 2-29.

$$G = K((0.05WV^2h^{1.5}S^{1.5})/((s-1)^2*D*\sqrt{g})) \quad \text{2-29}$$

Where,

G = volumetric sediment transport rate (m^3/s)

K = calibration coefficient (=1 for standard equation)

W = width of flow (m)

V = water velocity (m/s)

h = flow depth (m)

S = water surface slope (m/m)

s = specific gravity of sediment (dimensionless)

D = sediment diameter (mm)

g = acceleration due to gravity (m/s^2)

- The detail of this equation can be found in Engelund and Hansen (1967).

2.9.3 Sediment Routing Method

The following methods are available in HEC-HMS for sediment method for reach:

- Fischer's Dispersion
- Linear Reservoir
- Uniform Equilibrium
- Volume Ratio
  - ✓ Links the transport of sediment to the transport of flow in the reach using a conceptual approach
  - ✓ For each time interval, sediment from upstream elements is added to the sediment already in the reach.
  - ✓ The deposition or erosion of sediment is calculated for each grain size to determine the available sediment for routing.
  - ✓ The proportion of available sediment that leaves the reach in each time interval is assumed equal to the proportion of stream flow that leaves the reach during that same interval.
  - ✓ All grain sizes are transported through the reach at the same rate, even though erosion and deposition are determined separately for each grain size.

Initial Bed Curve defines the distribution of the bed sediment by grain size at the beginning of the simulation. Erosion Limit or Deposition Limit is optional. Bed width which are used in computing the volume of the upper and lower layers of the bed model, should be typical of the reach. Field survey may provide more accuracy of the model. Bed depth should be typical of the total depth of the upper and lower layers of the bed. It represents the maximum depth of mixing over very long time periods. Active bed factor is used to calculate the depth of the upper layer of the bed model. At each time interval, upper layer depth is computed as the d90 of the upper layer, multiplied by the factor.

CHAPTER 3
METHODOLOGY

3.1 Introduction

A large number of pre-processing and post processing works are required to set up a hydrological model for a river basin. Researchers face numerous problems during these works. In the present work for BRB, initially several types of data such as, Digital Elevation Model (DEM), land use pattern, soil distribution, climate data, flow time series and available sediment load were collected to setup a hydrological model using HEC-HMS. Assessment of climate and land use change impact on the sediment load of any river basin using hydrological model involves several steps. Steps followed in the present research can be described as following:

Step 1-Data collection: This include DEM, land use pattern, soil distribution, climate data, flow time series and sediment load

Step 2- Bias correction: Correcting bias in the climate data (specifically precipitation)

Step 3- Surface runoff model setup: Surface runoff setup which includes watershed delineation, weather data file processing and selection of calculation methods

Step 4-Calibration and validation of surface runoff model: Calibration and validation of the model and evaluation of the performance

Step 5-Surface erosion and sediment routing model setup: It includes MUSLE factors estimation and selection of calculation methods

Step 6-Calibration and validation of surface erosion and sediment routing model: Calibration and validation of the model by comparing available sediment load with simulated sedigraph and estimating annual sediment load at Bahadurabad transit (SW 46.9L)

Step 7-RCM model Selection: Selection of Regional Climate Models of RCP 8.5 scenario for climate change impact assessment

Step 8- Climate and Land Use Change Impact Assessment: Run the model with RCM data and analyzed the impact of climate change on the flow and sediment load of Brahmaputra River Basin. Assessment on sediment load due to changing pattern of land use (urbanization) of BRB.

3.2 Data Collection

3.2.1 Digital Elevation Model, Land use and Soil Data

Digital Elevation Model (DEM) data of 90m resolution (Figure 3.1) for year 2003 has been collected from Shuttle Radar Topography Mission (SRTM) website (http://srtm.csi.cgiar.org). The SRTM DEM was found to contain more surface detail and roughness than the TOPO DEM. It has been produced using radar images gathered from NASA's shuttle.

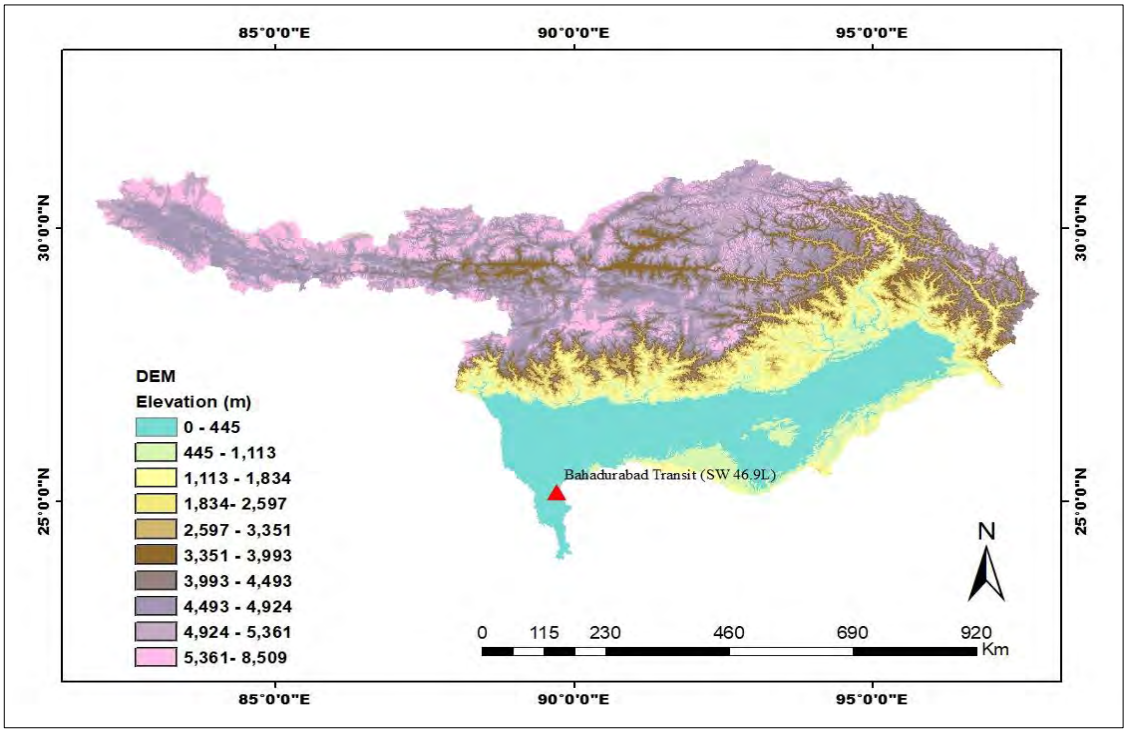

Figure 3.1: Digital Elevation Model (DEM) of Brahmaputra River Basin (BRB)

Land cover is one of the most important factors that affect surface erosion, runoff, and evapotranspiration in a watershed. Land cover map of 500 m resolution has been

collected from USGS (United State Geological Survey). It is a product of 0.5 km MODIS-based Global Land Cover analysis based on images of 2001-2010. 10 land cover classes have been found in the BRB basin which are shown in Figure 3.2.

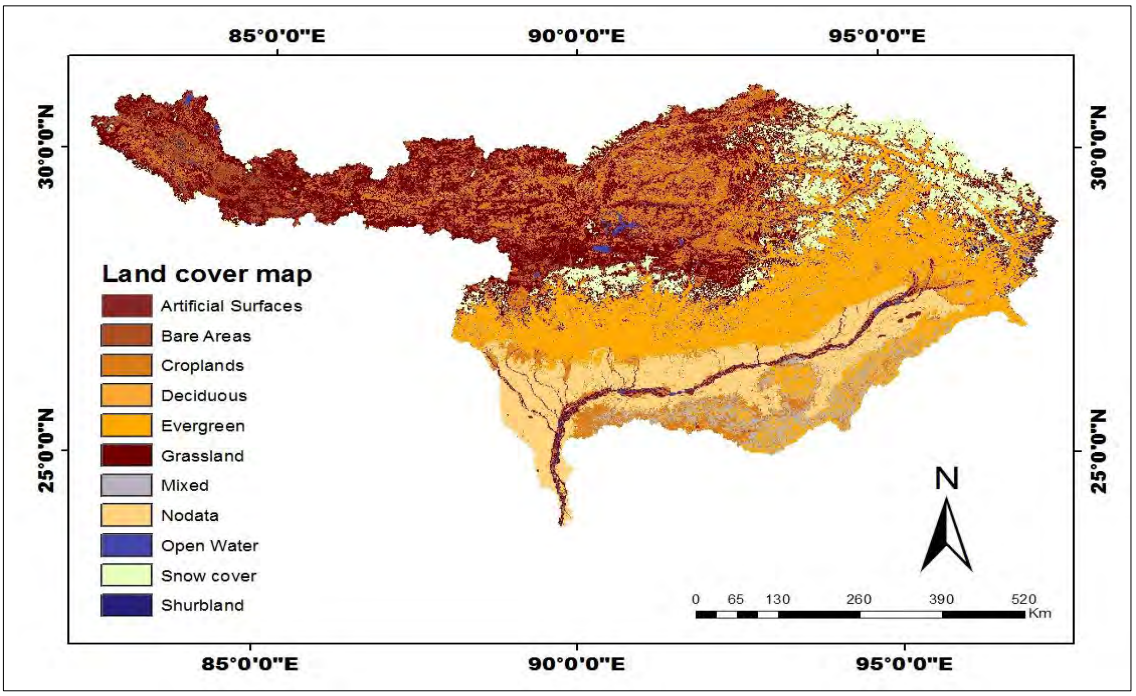

Figure 3.2: Land cover map of Brahmaputra River Basin (BRB)

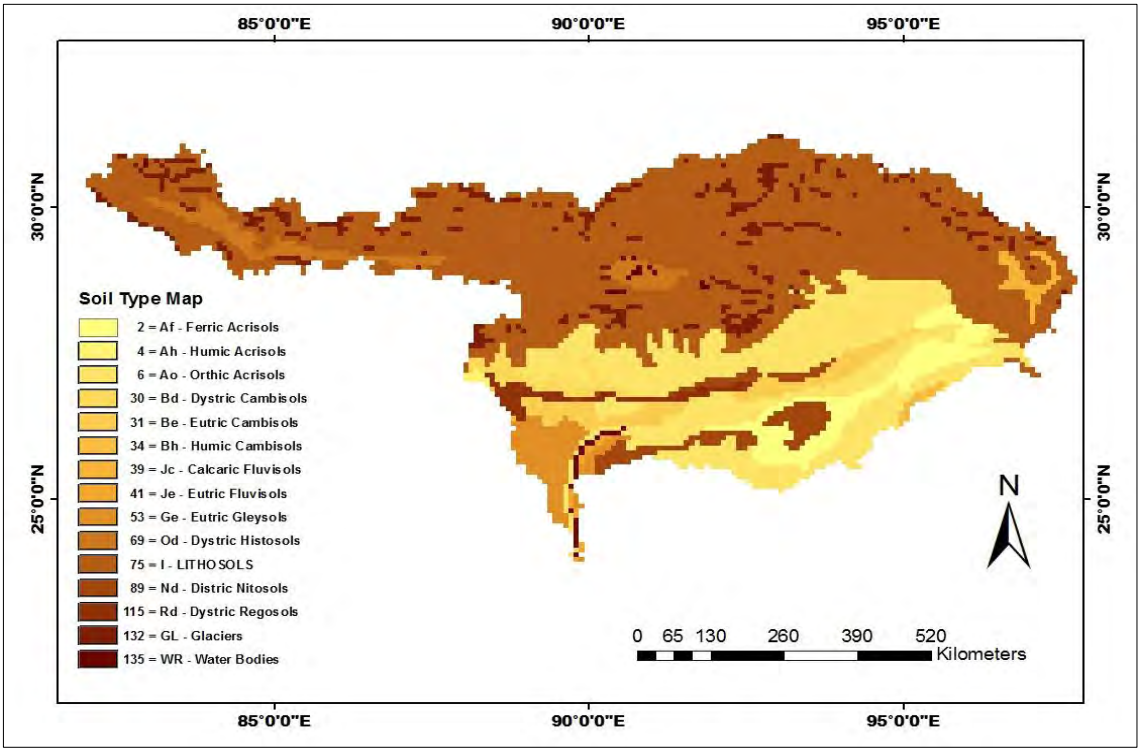

Figure 3.3: Soil use map of Brahmaputra River Basin (BRB)

Digital soil map (1:5,000,000) of year 2007 from FAO will be used. The FAO/UNESCO Legend for the Soil Map of the World 1974 is used as an international correlation system to indicate the dominant soil unit in each cell. It refers to the soil characteristics of the Digital Soil Map of the world but can be used as a reference for the dominant soil characteristics, as well. Dominant soil types for BRB are shown in Figure 3.3.

3.2.2 Weather, Discharge and Sediment Data

The HEC-HMS model requires daily values of precipitation, average temperature, solar radiation, relative humidity and wind speed. For this study, meteorological data for the BRB have been collected from the NASA-Prediction of Worldwide Energy Resource (link http://power.larc.nasa.gov) for the climate normal period (1983 to 2010).

Discharge and sediment load at Bahadurabad Transit (SW 46.9L) for the year of 1983-2010 have been collected from Bangladesh Water Development Board (BWDB). Future precipitation and temperature data considering RCP8.5 scenario have been collected from climate model run (CORDEX Database) for 1971-2099-time period from IWFM. Table 3.1 shows basic data used in this study including their source, resolution and time period.

Table 3.1: Basic input data used in this study

Data Type	Resolution/ Location	Source	Time period
Digital Elevation Model (DEM)	90m	Shuttle Radar Topography Mission (SRTM)	2003
Precipitation, temperature and other climatic variables	BRB	NASA-Prediction of Worldwide Energy Resource	1983-2012
Land cover map	500m	0.5 km MODIS-based Global Land Cover analysis	Based on images of 2001-2010
Digital soil map	1:5,000,000	FAO	2007
Discharge	Bahadurabad transit (SW46.9L)	BWDB	1983-2010
Sediment load	Bahadurabad transit (SW46.9L)	BWDB	1983-2010
Future precipitation and temperature data	RCP8.5	IWFM, BUET	1971-2099

3.3 Bias Correction of Rainfall Data

In hydrological modeling, precipitation is the most important variable. NASA POWER precipitation has showed a large difference with some observed rainfall data of Bangladesh Meteorological Department (BMD). To correct this mismatch, bias correction of NASA POWER precipitation data compared with some observed station of BMD has been done. Tangail, Bogra, Rangpur and Syedpur have been taken as observed station. The ratio of mean monthly observed precipitation and mean monthly precipitation from nearby NASA POWER grid has been determined for all four stations using the data of 1983-2012 period. These month ratios of four stations were averaged for each month separately. It has estimated the average monthly precipitation bias ratio for all the points on BRB. To remove bias, average monthly precipitation bias ratio has used to adjust all NASA POWER stations' precipitation.

3.4 Steps of Model Setup

The following steps have been taken to setup the surface runoff and sediment model for estimating present and future sediment load for BRB at Bahadurabad transit (SW 46.9L) station. Figure 3.4 represents the methodology of this study.

1. Delineation of watershed and stream network
2. Processing of necessary input data
3. Development of HEC-HMS surface runoff model using HEC-GeoHMS
4. Editing HEC-HMS surface runoff model inputs and simulation
5. Surface runoff model calibration and validation
6. Development and simulation of sediment model
7. Surface erosion and sediment routing model calibration and validation

3.5 Selection of RCM Models for RCP 8.5 Scenario

From Coordinated Regional Climate Downscaling Experiment (CORDEX) -South Asia domain database, an 11-member ensemble from three regional climate model (RCM) forced by eight general circulation model (GCM) is collected by IWFM, BUET. All the projections were made by forcing the corresponding GCM with Representative Concentration Pathway - RCP 8.5 (van Vuuren et al. 2011). For this study, precipitation obtained from different ensembles were average for three periods, viz. 2010-2039

(2020s), 2040-2069 (2050s) and 2070-2099 (2080s). For all the periods, changes of precipitations from the base period were analyzed separately. Finally, selection of RCM models was done based on the changes at the beginning, middle and end of 21st century which is represented by 2020s, 2050s and 2080s. The following steps are followed for selecting ensembles and scenarios.

Step 1: Annual average precipitation on BRB was determined for three-time periods, viz. 2020s (2010-2039), 2050s (2040-2069) and 2080s (2070-2099). Annual average precipitation was also calculated for base period (1981-2009).

Step 2: Percentage increase or decrease in precipitation for each model for these three different periods has been calculated.

Step 3: Model giving highest positive and negative change in precipitation were selected as the wettest the driest condition in future respectively. The model which gave nearest changes in precipitation to middle value was selected as moderate wet scenario.

3.6 Climate and Land Use Change Impact Assessment

Temperature and precipitation data of 3 RCM models selected from CORDEX database, viz. wettest, driest and moderate wet are used to estimate the range of potential impact of climate changes on sediment load as well as flow of Brahmaputra river basin (BRB). The changes in flow and sediment load at Bahadurabad transit (SW 46.9L) are analyzed for 2020s, 2050s and 2080s in monthly, seasonal and annual scale.

An additional increase in urbanization about 5% and 15% have been considered as land use changes to find out the impact on sediment load at Bahadurabad transit (SW 46.9L).

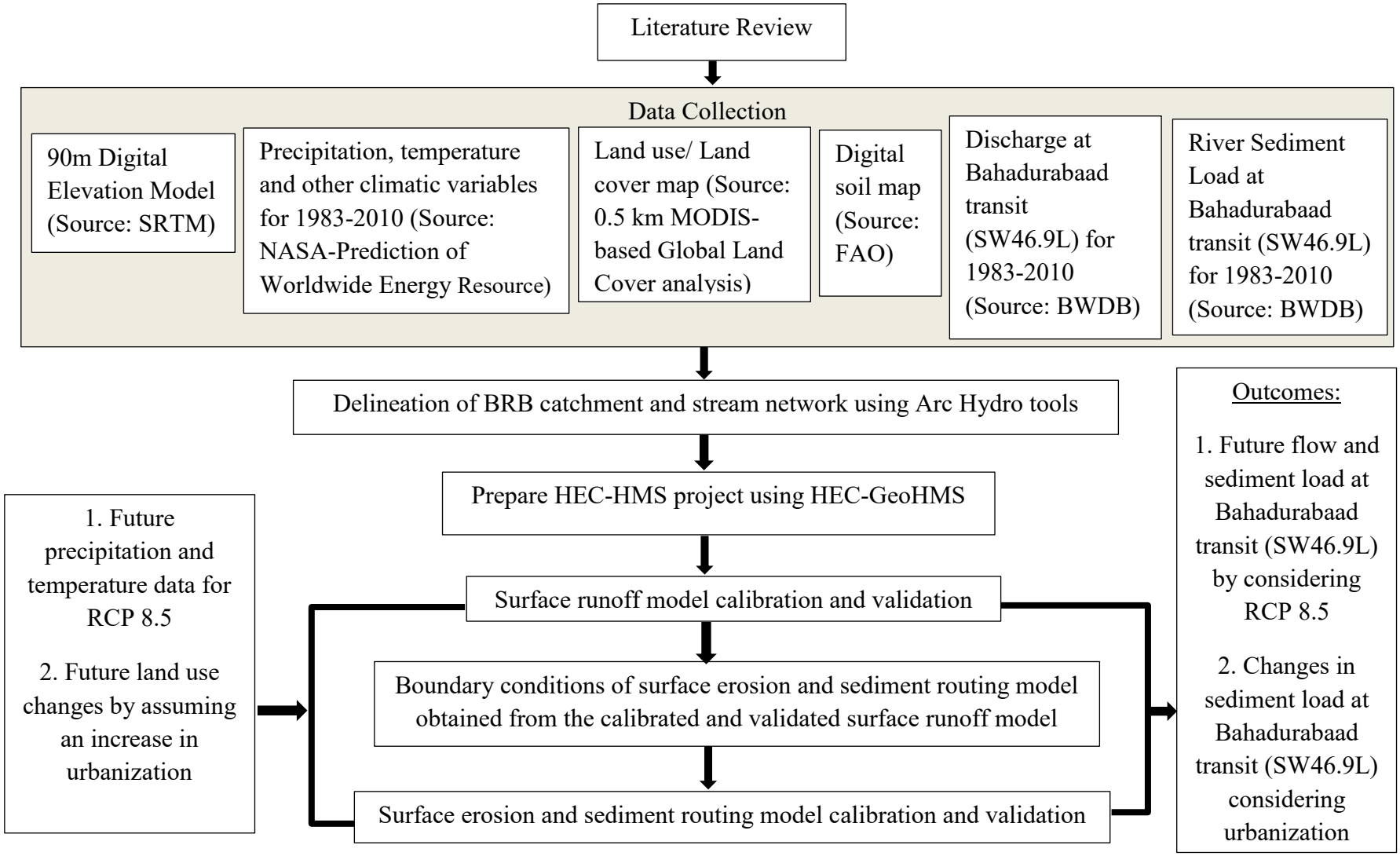

Figure 3.4: Methodology of the Study

CHAPTER 4
MODEL DEVELOPMENT

4.1 Bias Correction of NASA POWER Precipitation

In hydrological modeling, precipitation is an uncertain and the most variable (Islam and Gan, 2015). The difference between observed and NASA POWER precipitation may lead to greater uncertainty which may simulate less reliable outputs from the hydrologic assessment. It is possible the adjust some model parameters to reduce over-simulated and increase under-simulated runoff, whereas it is not possible to address the real problem like the uncertainty in precipitation. So, a question may arise about the validity of NASA POWER precipitation data. So, mean monthly precipitation of few observed stations and nearby NASA POWER stations have been compared to identify the extent of deviation. Four points have been selected within BRB based on the availability of data as shown in Figure 4.1. Tangail, Bogra, Rangpur and Syedpur have been taken as observed station. And the data has been collected from Bangladesh Meteorological station.

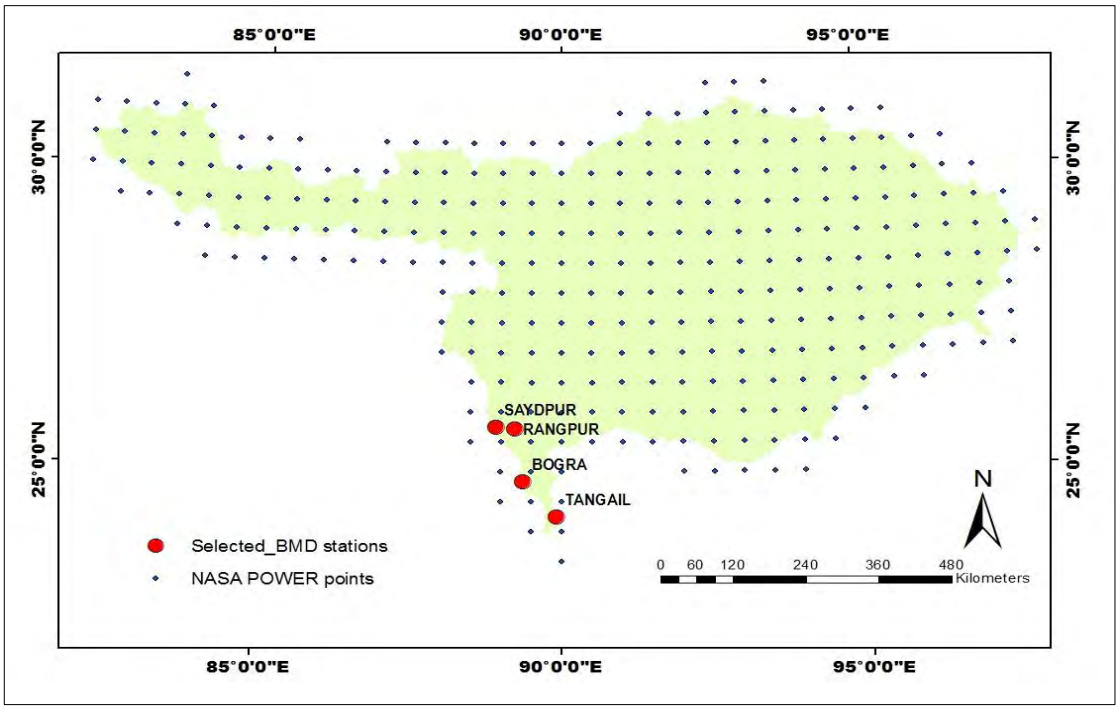

Figure 4.1: Selected four BMD stations with NASA POWER stations

To remove biases in NASA POWER data, a methodology applied in Islam and Gan (2015) has been adapted and will be discussed following:

Step 1: For all four stations, ratio of mean monthly observed precipitation and mean monthly precipitation from nearby NASA POWER grid has been determined.

Step2: Average monthly precipitation bias ratio for the BRB has been estimated by averaging month ratios of four stations for each month separately.

Step 3: NASA POWER precipitation data for all stations have been corrected by using the monthly ratio obtained from the previous step. This adjustment leads the bias corrected precipitation.

Table 4.1: Calculations to correct the bias in NASA POWER data

	Jan	Feb	Mar	Apr	May	Jun	Jul	Aug	Sep	Oct	Nov	Dec
NASA POWER (mm)	0.1837	0.2398	0.7897	2.0455	4.2147	9.589	11.4476	9.3996	8.6024	4.3055	0.4995	0.2412
Tangail (mm)	0.208	0.801	1.3103	3.6678	8.0456	10.8841	10.2247	8.5991	9.3131	5.0795	0.8595	0.3341
Tangail (mm)/NASA POWER (mm)	1.1323	3.3403	1.6592	1.7931	1.9089	1.1351	0.8932	0.9148	1.0826	1.1798	1.7207	1.3852
	Jan	**Feb**	**Mar**	**Apr**	**May**	**Jun**	**Jul**	**Aug**	**Sep**	**Oct**	**Nov**	**Dec**
NASA POWER (mm)	0.1925	0.2274	0.7399	1.7779	3.6201	8.9135	11.0657	8.9164	8.0304	3.8925	0.4078	0.2829
Bogra (mm)	0.2204	0.4227	0.6355	2.4744	6.7462	10.9765	11.7022	9.6527	10.0955	5.1957	0.3556	0.243
Bogra (mm)/NASA POWER (mm)	1.1449	1.8588	0.8589	1.3918	1.8635	1.2314	1.0575	1.0826	1.2572	1.3348	0.8720	0.8590
	Jan	**Feb**	**Mar**	**Apr**	**May**	**Jun**	**Jul**	**Aug**	**Sep**	**Oct**	**Nov**	**Dec**
NASA POWER (mm)	0.1569	0.1946	0.2881	0.665	1.3293	3.1018	4.688	4.8867	3.6556	0.8244	0.1715	0.0985
Rangpur (mm)	0.286	0.4298	0.8645	3.8251	8.7409	15.7422	15.7731	11.6925	12.9778	6.0247	0.2922	0.2183
Rangpur (mm)/NASA POWER (mm)	1.8228	2.2086	3.0007	5.7520	6.5756	5.0752	3.3646	2.3927	3.5501	7.3080	1.7038	2.2162
	Jan	**Feb**	**Mar**	**Apr**	**May**	**Jun**	**Jul**	**Aug**	**Sep**	**Oct**	**Nov**	**Dec**
NASA POWER (mm)	0.2106	0.2086	0.367	1.0487	2.7491	6.9251	9.0481	7.135	6.4647	2.4929	0.3112	0.1611
Syedpur (mm)	0.3045	0.272	0.7794	2.852	7.809	14.356	13.5363	10.9126	12.8417	5.3575	0.3042	0.1653
Syedpur (mm)/NASA POWER (mm)	1.4459	1.3039	2.1237	2.7196	2.8406	2.0730	1.4960	1.5294	1.9864	2.1491	0.9775	1.0261

Table 4.2: Monthly ratios obtained for bias correction

SL No	Jan	Feb	Mar	Apr	May	Jun	Jul	Aug	Sep	Oct	Nov	Dec
Tangail	1.1323	3.3403	1.6592	1.7931	1.9089	1.1351	0.8932	0.9148	1.0826	1.1798	1.7207	1.3852
Bogra	1.1449	1.8588	0.8589	1.3918	1.8635	1.2314	1.0575	1.0826	1.2572	1.3348	0.8720	0.8590
Rangpur	1.8228	2.2086	3.0007	5.7520	6.5756	5.0752	3.3646	2.3927	3.5501	7.3080	1.7038	2.2162
Syedpur	1.4459	1.3039	2.1237	2.7196	2.8406	2.0730	1.4960	1.5294	1.9864	2.1491	0.9775	1.0261
Average	1.3865	2.1779	1.9106	2.9141	3.2972	2.3787	1.7028	1.4799	1.9691	2.9929	1.3185	1.3716

Figure 4.2-4.5 show monthly comparison of average precipitation between NASA POWER and observed station.

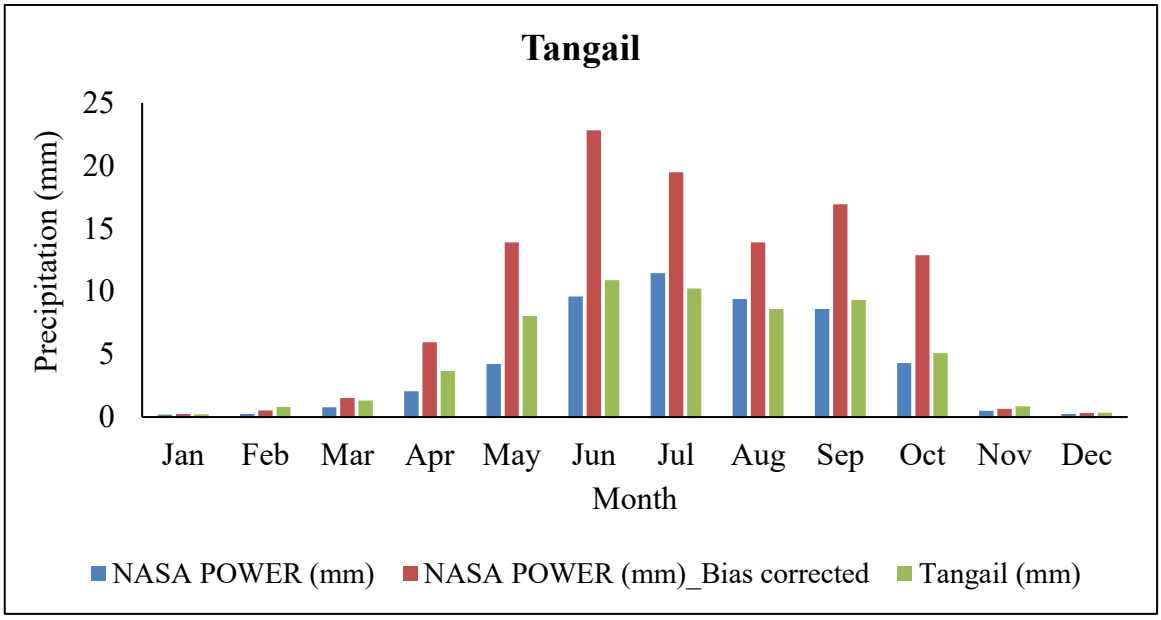

Figure 4.2: Bias correction at Tangail station

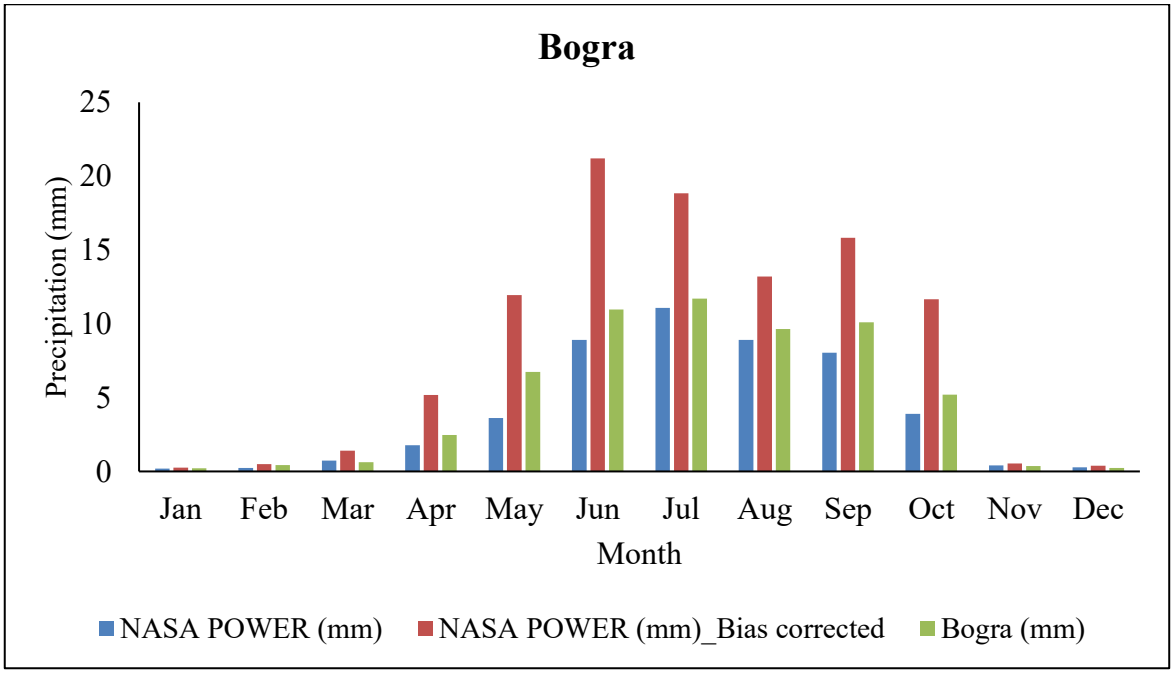

Figure 4.3: Bias correction at Bogra station

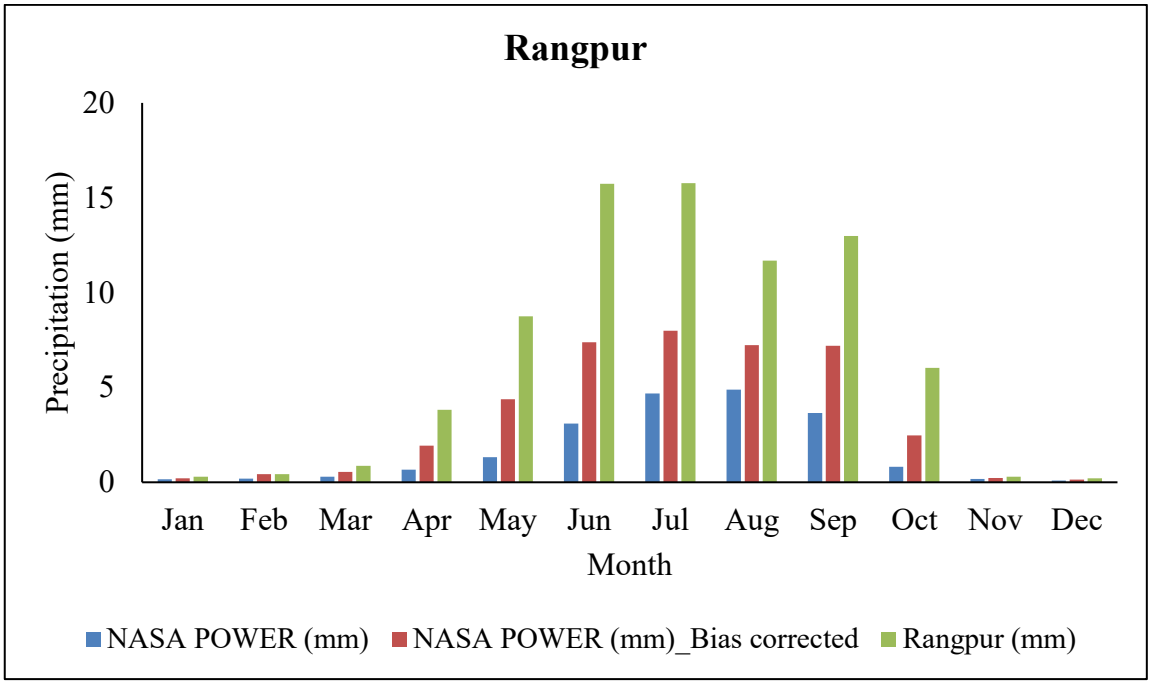

Figure 4.4: Bias correction at Rangpur station

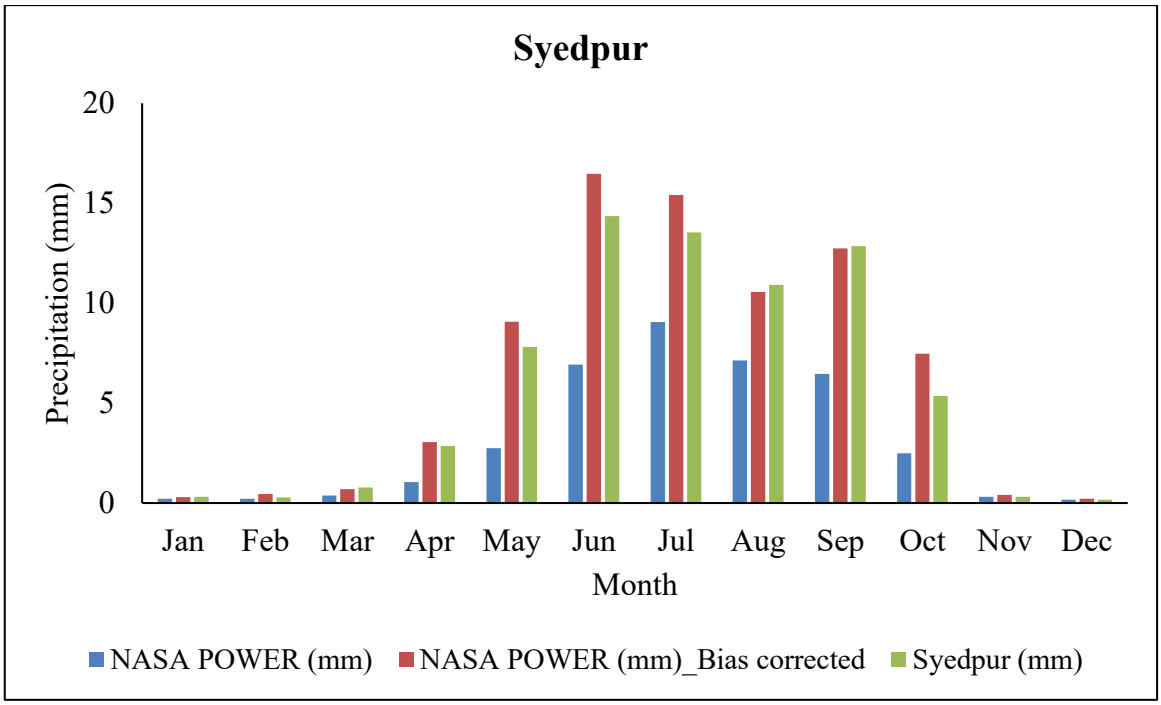

Figure 4.5: Bias correction at Syedpur station

4.2 Delineation of Watershed and Stream Network

Delineation of watershed boundary and streams is necessary prior to the management of study area as a watershed. It is the initial step of any hydrologic modeling to get some basic watershed properties area, slope, flow length, stream network density, etc. Figure 4.6 is the delineated watershed with stream network of the study area. To delineate the watershed, stream network and some watershed characteristics of the study area Arc Hydro tools (version that work with Arc GIS 10.1) is used. Output files from terrain pre-processing are used to create input files for HEC-HMS models using HEC-GeoHMS (Merwade, 2012).

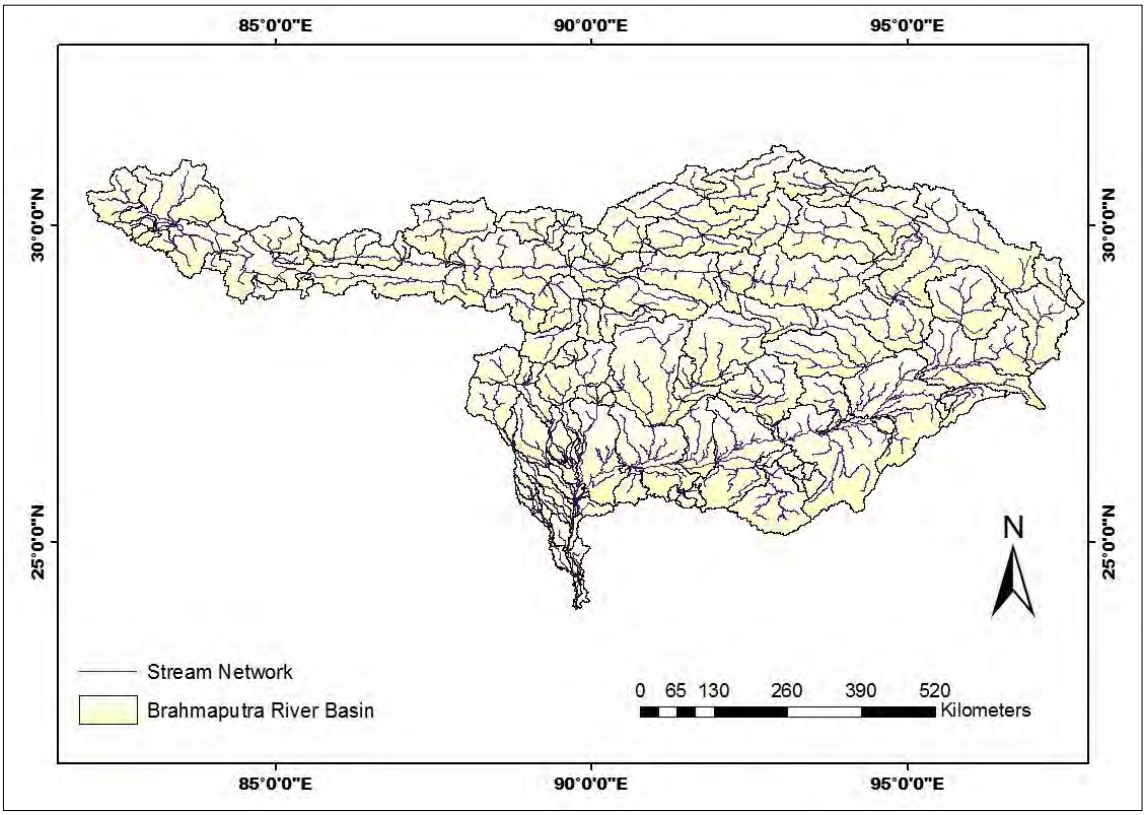

Figure 4.6: Brahmaputra River Basin (BRB) with stream network

4.3 Processing of Necessary Input Data

4.3.1 Determination of Gage Weight Factors

It is necessary to use interpolation methods to achieve accurate estimation of the spatial distribution of the rainfall. Thiessen polygons are an exact method of interpolation that

assumes that the values of unsampled locations are equal to the value of the nearest sampled point. To establish the area of influence of each precipitation gage method of Thiessen polygons are used. Thiessen polygons are created by subdividing lines joining nearest neighbour points, drawing perpendicular bisectors through these lines, and then using these bisectors to assemble polygon edges. If observed data points are irregularly spaced a surface of irregular polygons will be produced. Intersections of Thiessen polygons with the sub-basin polygons are shown in Figure 4.7. It introduces a new set of smaller polygons such that each Thiessen polygon is related to one Thiessen polygon and one sub-basin polygon. For calculating the average precipitation over an area in Thiessen polygon method weightage is given to the various stations on a rational basis.

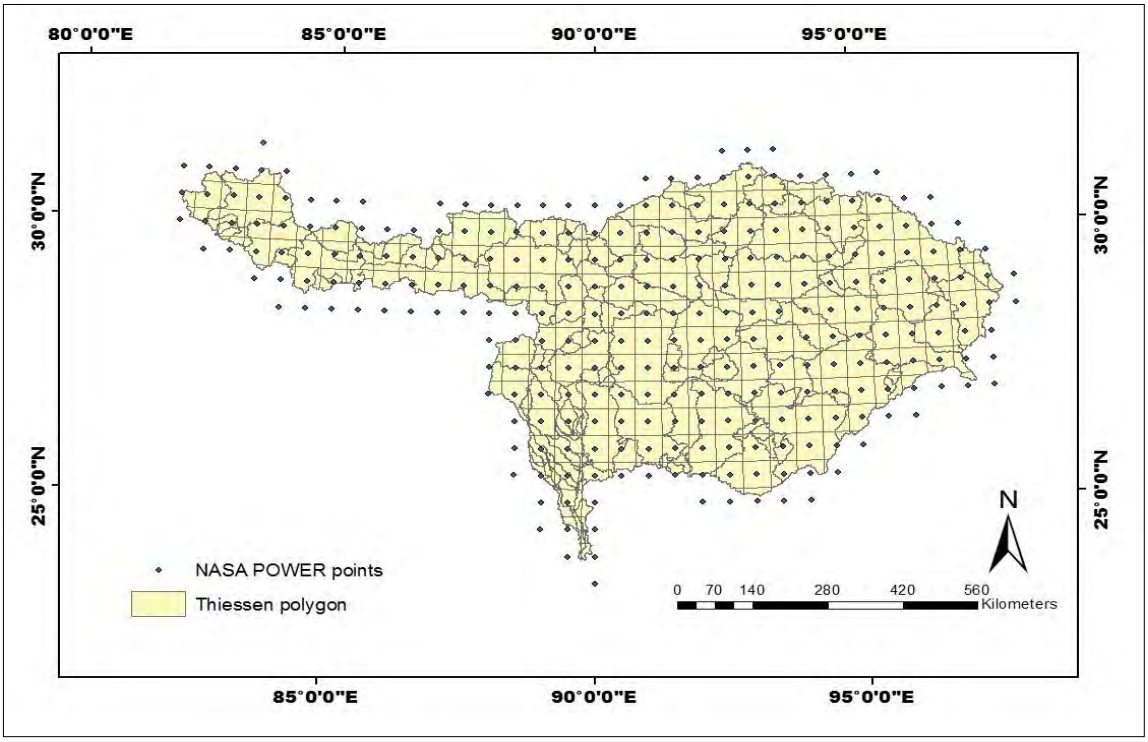

Figure 4.7: Intersections of Thiessen polygons with the subbasin polygons

The weightage factor is defined as the ratio of area of a Thiessen polygon to the area of its corresponding sub-basin polygon and can be expressed as-

$$W_{ij} = A_{ij}/S_j \quad \text{.....4-1}$$

Where,

A_{ij} = area of the polygon generated by the intersection of sub-basin j with Thiessen polygon of gage i.

S_j = area of sub-basin j.

W_{ij} = weightage factor of gage i for sub-basin j.

The sum of depth weights of a sub-basin should equal to unity. Table 4.3 represents intersected subbasin polygon with thiessen polygon for a selected area. Gage information including gage name, location, type and sub-basin information consisting name, identification code, name of each gage with corresponding weight is recorded after calculating the weightage based on subbasin and Thiessen polygon data sets.

Table 4.3: Estimated weightage factors for subbasins considering different NASA POWER stations

Subbasin Name	NASA POWER station ID	Subbasin Area_Sj	Polygon Area_Aij	Weightage factor of gage i for sub-basin j	
W10030	175	2704.281922	1105.142819	0.409	1
W10030	174	2704.281922	470.4136952	0.174	
W10030	207	2704.281922	403.3117821	0.149	
W10030	206	2704.281922	725.4055945	0.268	
W10110	136	15145.0853	91.34155053	0.006	1
W10110	169	15145.0853	357.9802344	0.024	
W10110	168	15145.0853	2282.503385	0.151	
W10110	138	15145.0853	27.37299694	0.002	
W10110	167	15145.0853	2700.199447	0.178	
W10110	166	15145.0853	2689.994424	0.178	
W10110	165	15145.0853	1219.655209	0.081	
W10110	137	15145.0853	282.8962152	0.019	
W10110	199	15145.0853	1348.188821	0.089	
W10110	198	15145.0853	1886.989331	0.125	
W10110	197	15145.0853	490.4285424	0.032	
W10110	201	15145.0853	526.183335	0.035	
W10110	200	15145.0853	1241.351798	0.082	
W10260	150	811.1250707	442.1162918	0.545	1
W10260	149	811.1250707	368.9447903	0.455	
W10270	151	718.2753523	715.416807	0.996	1
W10270	183	718.2753523	2.858543412	0.004	

4.3.2 Estimation of Impervious Area

Land cover map based on 0.5 km MODIS-based Global Land Cover analysis provides the information of different land cover types in BRB. HEC-HMS model needs the percentage of impervious area for each subbasin. Considering artificial surfaces area for each subbasin of BRB, percentage of impervious area for each subbasin has been estimated and the values are within 0 to 10% for each subbasin.

4.3.3 Estimation of Maximum Infiltration Rate

The saturation hydraulic conductivity is considered to be the maximum infiltration rate (mm/hr) and it is one of important inputs of SMA model in HEC-HMS. Digital soil map (1:5,000,000) of year 2007 from FAO provides the information of soil texture for BRB. The reference values considering soil texture are shown in the following Table 4.4. Using the sand, silt and clay percentage within each subbasin, saturated hydraulic conductivity (mm/hr) has been estimated using weighted average method and the values are within 12.57 to 156.64 mm/hr for each subbasin.

Table 4.4: Soil texture and properties (Rawls et al., 1982)

Soil Texture	Porosity, cm^3/ cm^3	Saturated hydraulic conductivity (cm/hr)
Sandy	0.437	21
Loamy sand	0.437	6.11
Sandy loam	0.453	2.59
Loam	0.463	1.32
Silt loam	0.501	0.68
Sandy clay loam	0.398	0.43
Clay loam	0.464	0.23
Silty clay loam	0.471	0.15
Sandy clay	0.43	0.12
Silty clay	0.479	0.09
Clay	0.475	0.06

4.3.4 Estimation of Erodibility Factor (K)

Erodibility factor describes the difficulty of eroding the soil. It is a function of the soil texture, structure, organic matter content and permeability ranges from 0.05 for unconsolidated loamy sand to 0.75 for silty and clayey loam soils. Soil use map is the

primary source to determine the erodibility factor for each subbasin showing in Figure 4.8.

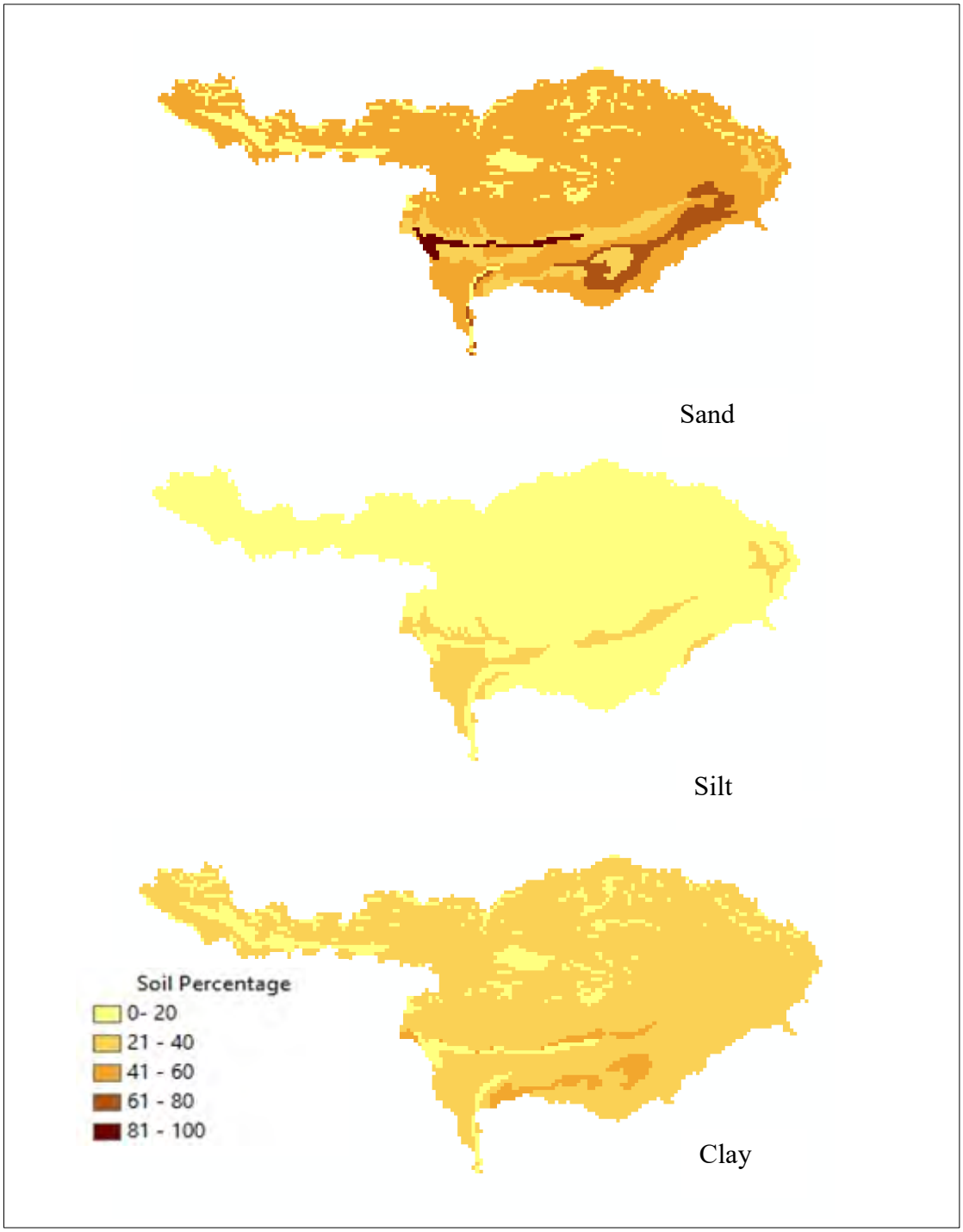

Figure 4.8: Percentages of sand, silt and clay in Brahmaputra River Basin

An algebraic approximation of the nomograph that includes five soil parameters (texture, organic matter, coarse fragments, structure, and permeability) is proposed by Wischmeier and Smith (1978) and Renard et al. (1995) in Equation 4-2.

$$K = [(2.1 \times 10^{-4} M^{1.14} (12 - OM) + 3.25 (s - 2) + 2.5 (p - 3)) / 100] * 0.1317 \ldots\ldots\ldots\ldots \quad 4\text{-}2$$

Where:

M: the textural factor with M = (msilt + mvfs) * (100 - mc);

mc [%]: clay fraction content (<0.002 mm);

msilt [%]: silt fraction content (0.002 – 0.05 mm);

mvfs [%]: very fine sand fraction content (0.05 – 0.1 mm);

OM [%]: the organic matter content;

s: the soil structure class (s=1: very fine granular, s=2: fine granular, s=3, medium or coarse granular, s=4: blocky, platy or massive);

p: the permeability class (p=1: very rapid, …, p=6: very slow).

Using the equation, erodibility factor for each subbasin has been calculated which is shown in Figure 4.9.

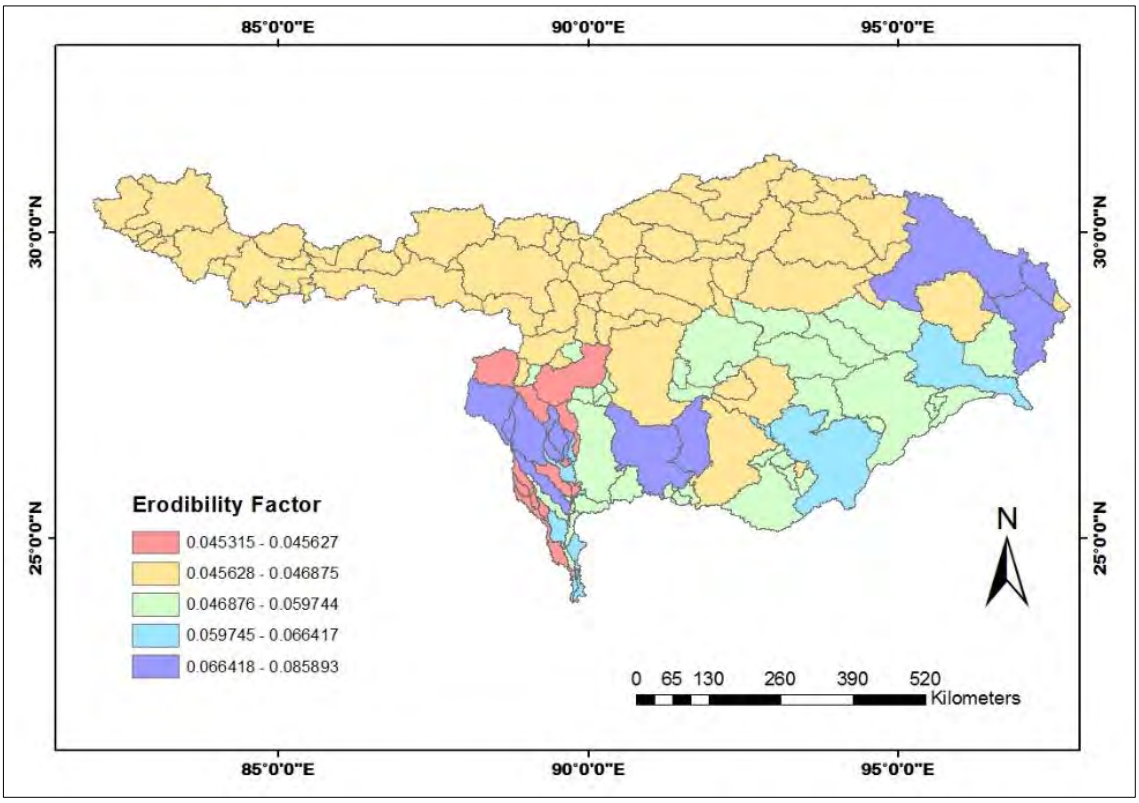

Figure 4.9: Erodibility factor in Brahmaputra River Basin

4.3.5 Estimation of Cover and Management Factor (C)

Cover and management factor describes the influence of plant canopy on surface erosion. For bare ground, value of CM factor is 1 which indicates the land is most susceptible to erosion. For fully mulched or covered soils, CM factor is 0.1. 0.0001 is considered for Forest soils with a well-developed soil horizon (surface organic layer) under a dense tree canopy. Using the land use map for BRB, CM factor for each subbasin is estimated by weighted average method which are shown in Figure 4.10.

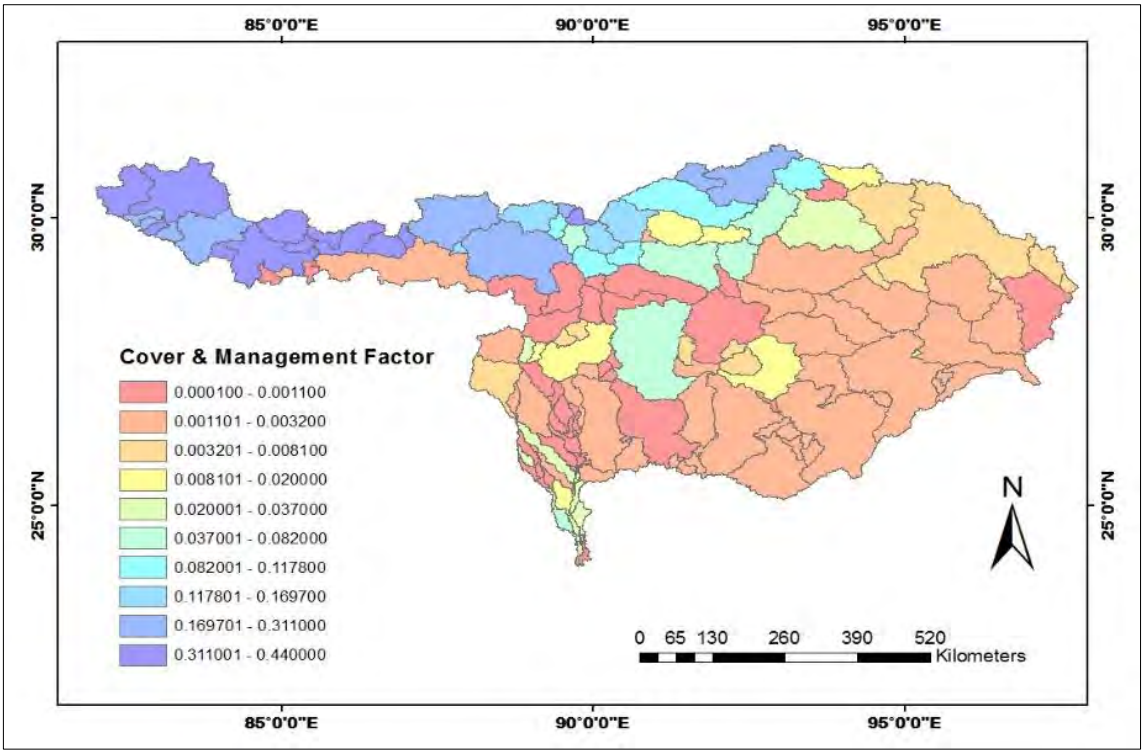

Figure 4.10: Cover and management factor in Brahmaputra River Basin

4.3.6 Estimation of Surface Storage

Surface storage represents the maximum amount of water that can pond on the soil surface before surface runoff begins. Surface runoff occurs when the storage is at full capacity and there is excess precipitation. With the help of soil map, this parameter for each subbasin was estimated by using Table 4.5.

Table 4.5: Standard depression storage from Bennett (1988)

Description	Slope, %	Surface Storage, mm
Paved impervious	NA	3.2 – 6.4
Steep	> 30	1
Moderate to gentle	5-30	12.7 – 6.4
Flat, furrow	0-5	50.8

4.4 Development of Surface Runoff Model using HEC-HMS

4.4.1 Initial Model Simulation

A basin input file is developed at the end of process in Hec-GeoHMS. Map is converted to HMS Units. HMS schematic tool creates a GIS representation of the hydrologic system using a schematic network with basin elements (nodes/links or junctions/edges) and their connectivity. Two shapefiles: one for river and one for sub-basin are created in the project folder. HMS legends and Coordinates are added. Coordinate tools add geographic coordinates to features in HMSLink and HMSNode feature classes. This is useful for exporting the schematic to other models or programs without losing the geospatial information. The project is created through Create HMS Project. This function copies all the project specific files that have created (.map and .met) to a specified directory and creates .hms file that will contain information on other files for input to HMS (Merwade, 2012).

In HEC-HMS window, the meteorological data set of weather stations have been generated using HEC-DSSVue. It is a data storage system where data for precipitation and temperature for present and future time line has been stored.

A base run with all necessary input data, hydrological models and meteorological model has been simulated to check the connections among the subbasins and junctions. Initially, Nash Sutcliffe Co-efficient for model run was 0.16 and it was in unsatisfactory stage. The rest of the parameters which were not estimated in this study using secondary data or literature are decided to be calibrated in that stage.

Table 4.6: Initial estimated values of parameters in HEC-HMS model

Parameter	Value	Source
Manning's roughness coefficient	0.018, 0.025, 0.035	Jung et al. (2010)
Effective river width	300 m -10000 m	Goswami (1985) and Coleman (1969), consistent with Datta and Singh 2004 and Mersel et al. (2013)
Length	184.7 m -200000 m	Estimated from GIS and Google Earth
Slope	0.000079 m/m - 0.0168 m/m	Mahanta et al. (2014)
Manning's n	0.025 – 0.04	Jung et al. (2010)
Surface storage	6.85 mm -50.8 mm	Bennett (1988)
Maximum infiltration rate	12.6 mm/hr – 137.1 mm/hr	Rawls et al. (1982)

4.4.2 Sensitivity Analysis of SMA Algorithm Parameters

HMS has the capabilities to process automated calibration in order to minimize a specific objective function, such as sum of the absolute error, sum of the squared error, percent error in peak, and peak-weighted root mean square error. However, in many cases, the resulted automated parameters are not reasonable and practical. In this study, manual calibrated method was adopted to determine a practical range of the parameter values preserving the hydrograph shape, minimum error in peak discharges and volumes. To identify the most sensitive parameter which is needed to calibrate first, a sensitivity analysis has been performed for 9 SMA algorithm parameters shown in Table 4.7.

Table 4.7: SMA algorithm parameters considered for sensitivity analysis

Parameter	Description	Unit
Soil storage	Max. amount of water that could held by the soil profile	mm
Soil percolation	Average rate of the percolation of water from soil into the GW1 layer	mm/hr
Tension storage	Portion of the soil storage from which water in this storage is lost through evapotranspiration only	mm
GW1 storage	Storage volume in GW1 layer	mm
GW1 Coefficient	GW1 delayed time	hr
GW1 Percolation	Percolation rate to GW2 layer	mm/hr
GW2 storage	Storage volume in GW2 layer	mm
GW2 Coefficient	GW2 delayed time	hr
GW2 Percolation	Deep percolation rate from GW2 layer	mm/hr

Initially, the model is run with the base data literature review and GIS analysis shown in Table 4.6. Thereafter, out of the 9 parameters, one parameter at a time was varied and analyzed from -40% to 40% with increments of 10%, keeping all other parameters constant. The model was used again, and the output runoff volume values were analyzed to determine variation with respect to the initial estimates of the parameters. Greater percentage change in the simulated volumes represents greater variable sensitivity. Five initial conditions for the five storage layers in the SMA model were not considered for sensitivity analysis. The percentage changes in simulated volume were then plotted against the percentage variation of each parameter shown in Figure. 4.11 and the sensitivity of each parameter was evaluated.

From the previous analysis shown in Figure 4.11, it has been found that soil percolation is the most sensitive parameter for simulated stream flow during the calibration period. GW2 storage and GW2 coefficient were the least sensitive parameters. Each parameter was ranked according to their sensitivity with respect to the change in simulated volume, as shown in Table 4.8.

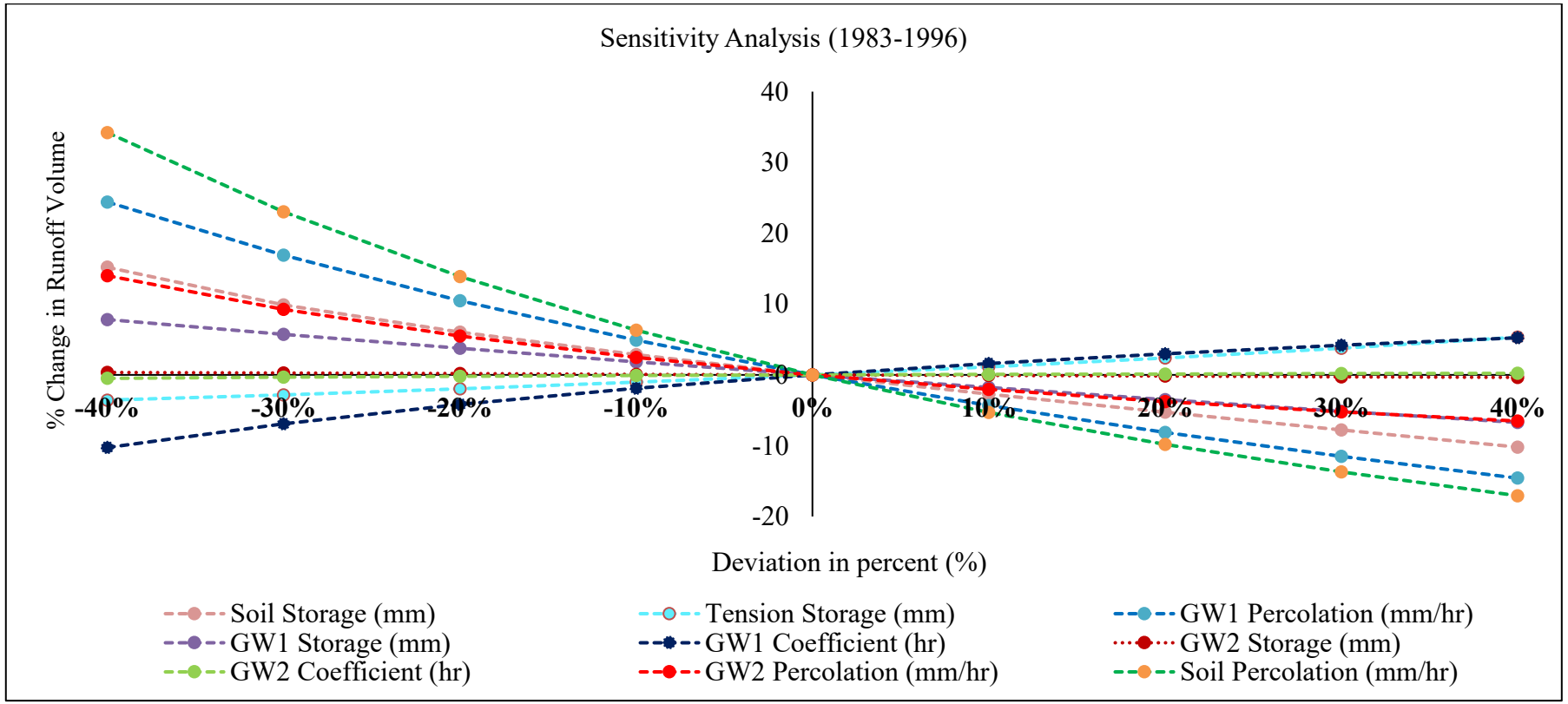

Figure 4.11: Sensitivity analysis of the HEC-HMS model for the calibration period

Table 4.8: Ranking of SMA Algorithm Parameters

Percent Changes in parameter	Soil Storage (mm)	Tension Storage (mm)	GW1 Percolation (mm/hr)	GW1 Storage (mm)	GW1 Coefficient (hr)	GW2 Storage (mm)	GW2 Coefficient (hr)	GW2 Percolation (mm/hr)	Soil Percolation (mm/hr)
-40%	15.20	-3.56	24.41	7.82	-10.26	0.35	-0.49	14.02	34.22
-30%	9.86	-2.82	16.90	5.74	-6.89	0.26	-0.33	9.24	23.01
-20%	6.04	-1.98	10.49	3.74	-4.15	0.18	-0.19	5.48	13.89
-10%	2.86	-1.04	4.88	1.85	-1.89	0.09	-0.08	2.46	6.32
0%	0.00	0.00	0.00	0.00	0.00	0.00	0.00	0.00	0.00
10%	-2.71	1.15	-4.31	-1.77	1.60	-0.09	0.07	-2.04	-5.29
20%	-5.27	2.40	-8.12	-3.49	2.99	-0.18	0.13	-3.79	-9.81
30%	-7.78	3.77	-11.51	-5.14	4.18	-0.26	0.17	-5.24	-13.68
40%	-10.19	5.33	-14.58	-6.72	5.24	-0.35	0.22	-6.52	-17.06
Ranking	**3**	**7**	**2**	**6**	**5**	**9**	**8**	**4**	**1**

4.4.3 Calibration and Validation of Surface Runoff Model

Calibration is the process whereby selected parameters and variables of the model are adjusted to make the model output match observations. Sorooshian and Gupta (1995) classified numerous parameters in hydrological models as physical parameters (i.e., parameters that can be physically measurable from the properties of watershed) and process parameters (i.e., parameters represent properties which are not directly measurable). So, the main purpose, is to obtain an economical and reproducible method of identifying a parameter set for a particular catchment under particular conditions, which gives the best possible fit between the simulated and observed discharge for a particular calibration i.e. the calibrated parameter set aims at minimizing the difference between simulated and observed discharge. This process is considered to be necessary because there may be uncertainties in the model input and because of that, models give only simplified representations of the catchment's physical processes. In calibration and validation stage, model performance is evaluated based on statistically and graphically.

Figure 4.12 shows the graphical representation of monthly observed and simulated flow for both calibration and validation period. It was found that the simulated flow is in great compliance with the observed discharge for both monsoon and dry season.

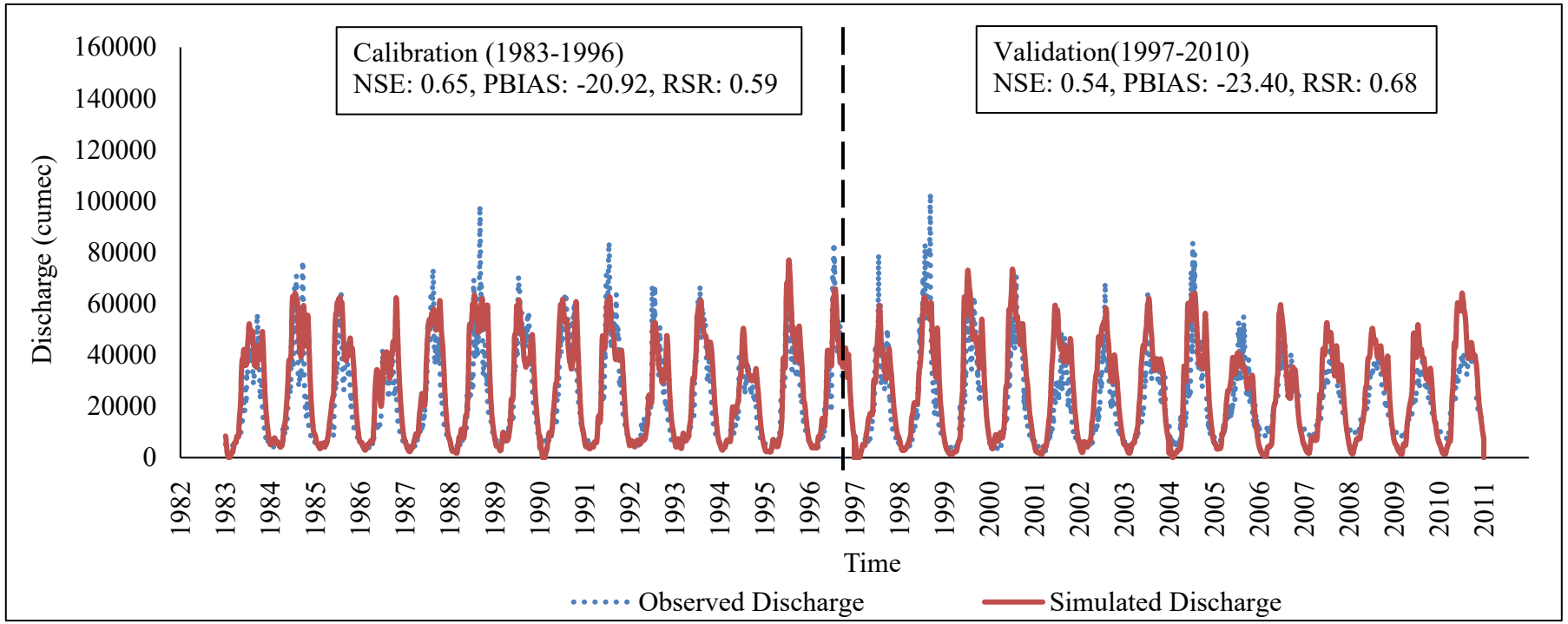

Figure 4.12: Observed and simulated flows for the calibration and validation period (1983-2010)

Table 4.9: Model performance statistics for calibration (1983-1996) and validation period (1997-2010) of the Brahmaputra river basin

Period	Observed Mean (m^3/s)	Simulated Mean (m^3/s)	Model Performance			
			NSE	R^2	PBIAS	RSR
Calibration	21971.05	26183.03	0.65	0.76	-20.92	0.59
Validation	21768.67	26864.04	0.54	0.71	-23.40	0.68

4.4.4 Surface Runoff Model Performance Evaluation

Some of model evaluation techniques (Error Index) are RMSE, MAE, MSE, NSE, RSR, PBIAS etc.

Nash-Sutcliffe efficiency (NSE)

The Nash-Sutcliffe efficiency (NSE) is a normalized statistic that determines the relative magnitude of the residual variance ("noise") compared to the measured data variance ("information") (Nash and Sutcliffe, 1970). NSE indicates how well the plot of observed versus simulated data fits the 1:1 line.

$$NSE = 1 - [\frac{\sum_{i=1}^{n}\left(Y_i^{obs} - Y_i^{sim}\right)^2}{\sum_{i=1}^{n}\left(Y_i^{obs} - Y_i^{mean}\right)^2}] \quad \text{.....4-3}$$

Where Yi^{obs} is the *i*th observation for the constituent being evaluated,

Yi^{sim} is the *i*th simulated value for the constituent being evaluated,

Y_i^{mean} is the mean of observed data for the constituent being evaluated

And *n* is the total number of observations.

Percent bias (PBIAS)

Percent bias (PBIAS) measures the average tendency of the simulated data to be larger or smaller than their observed counterparts. The optimal value of PBIAS is 0.0, with low-magnitude values indicating accurate model simulation. Positive values indicate model underestimation bias, and negative values indicate model overestimation bias (Gupta et al., 1999).

$$\text{PBIAS} = \left[\frac{\sum_{i=1}^{n}\left(Y_i^{obs} - Y_i^{sim}\right) * (100)}{\sum_{i=1}^{n}\left(Y_i^{obs}\right)}\right] \quad \text{.....4-4}$$

Where PBIAS is the deviation of data being evaluated, expressed as a percentage.

RMSE-observations standard deviation ratio (RSR)

RMSE is one of the commonly used error index statistics (Chu and Shirmohammadi, 2004). RSR standardizes RMSE using the observations standard deviation, and it combines both an error index and the additional information recommended by Legates and McCabe (1999). RSR is calculated as the ratio of the RMSE and standard deviation of measured data.

$$RSR = \frac{RMSE}{STDEV_{obs}} = \frac{\left[\sqrt{\sum_{i=1}^{n}\left(Y_i^{obs} - Y_i^{sim}\right)^2}\right]}{\left[\sqrt{\sum_{i=1}^{n}\left(Y_i^{obs} - Y^{mean}\right)^2}\right]} \quad \text{.....4-5}$$

Table 4.10: General Reported ratings for NSE, PBIAS and RSR for calibration and validation process (Moriasi et.al., 2007)

Performance Rating	NSE	RSR	PBIAS
Very good	$0.75 < NSE \leq 1.00$	$0.00 \leq RSR \leq 0.50$	$PBIAS < \pm 10$
Good	$0.65 < NSE \leq 0.75$	$0.50 < RSR \leq 0.60$	$\pm 10 \leq PBIAS < \pm 15$
Satisfactory	$0.50 < NSE \leq 0.65$	$0.60 < RSR \leq 0.70$	$\pm 15 \leq PBIAS < \pm 25$
Unsatisfactory	$NSE \leq 0.50$	$RSR > 0.70$	$PBIAS \geq \pm 25$

The statistical model performance is given in Table 4.9. General reported rating of NSE, R2, PBIAS and RSR are given in Table 4.10. The NSE values are 0.65 and 0.54 for calibration and validation period respectively. The PBIAS and RSR values are found to be -20.92 and 0.59 in calibration stage and -23.40 and 0.68 in validation stage, respectively. These statistics demonstrate HEC-HMS generally performed satisfactorily in both calibration and validation stages based on historical measured data for BRB (Moriasi et.al., 2007), which establishes the basis for developing sediment model and conducting climate and land use change impact on sediment load based on the simulations of HEC-HMS.

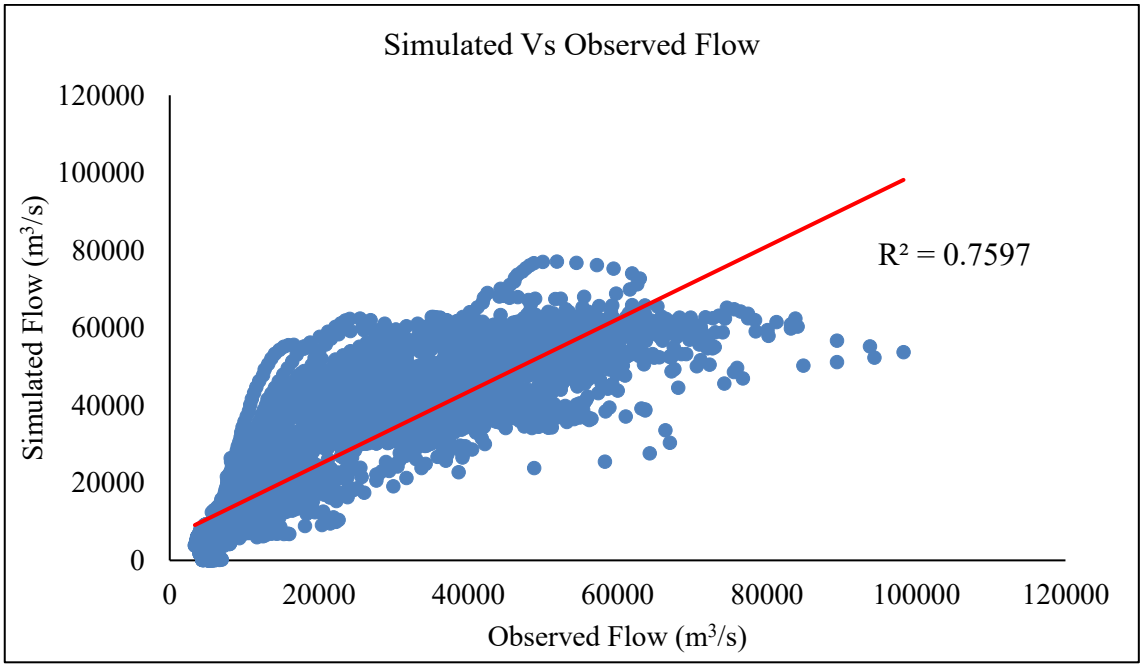

(a) Calibration Period (1983-1996)

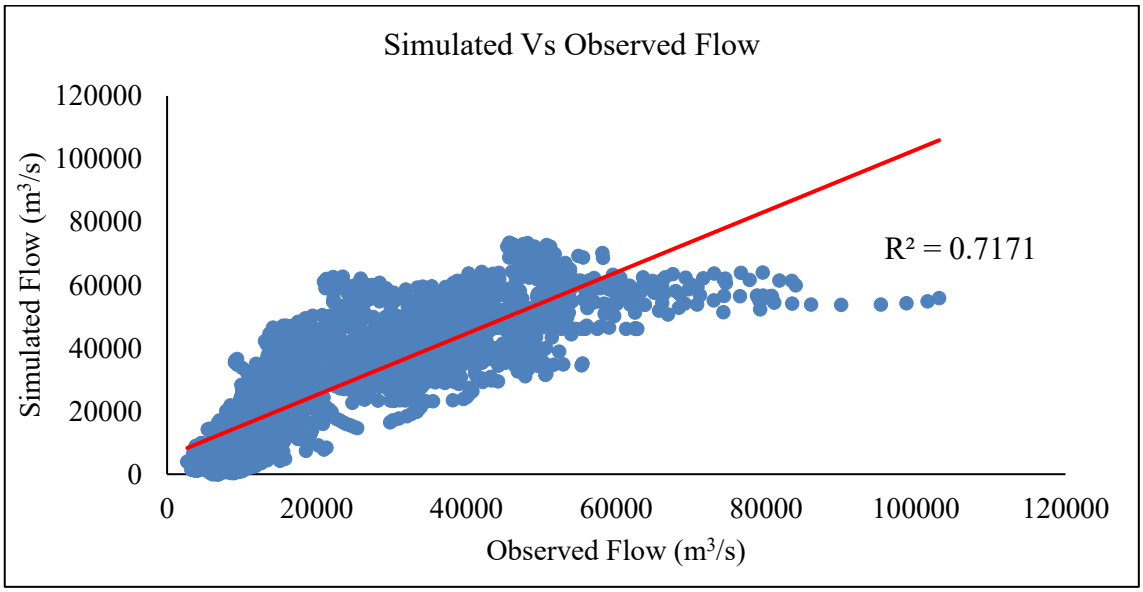

(b) Validation Period (1997-2010)

Figure 4.13: Scatter plot of simulated vs observed flow at Bahadurabad transit for (a) calibration period (1983-1996) and (b) validation period (1997-2010)

Scatter plot of simulated vs observed flow at Bahadurabad transit (SW 46.9L) for calibration and validation has been plotted in Figure 4.13. The co-efficient of determination (R^2) values are 0.76 for calibration and 0.71 for validation period.

4.5 Development of Surface Erosion and Sediment Routing model using HEC-HMS

Sediment routing studies in HEC-HMS requires a calibrated precipitation-runoff model, soil data, land use data, sediment grain size. This information is utilized in the development, calibration, and validation of surface erosion and sediment routing model which have been previously estimated. Soil gradation curve is obtained from literature review (Coleman, 1969) as field measurement for the BRB is not available.

Table 4.11: Initial values for developing surface erosion and sediment routing model

Parameter	Value	Source
Sediment grain size distribution	0.077-0.50 (d_{50} : 0.15)	Consistent with Coleman (1969)
Erodibility factor	0.05 – 0.086	Soil map
Practice factor	1	Scharffenberg (2015)
Topographic factor	0.3 – 1.9	Slope and length
Cover and management factor	0.0001 – 0.44	Land use map
Specific Gravity (Sediment grain)	2.65	Scharffenberg (2015)
Clay Density	480.55 kg/m^3	Scharffenberg (2015)
Silt Density	1041.2 kg/m^3	Scharffenberg (2015)
Sand and Gravel Density	1489.7 kg/m^3	Scharffenberg (2015)

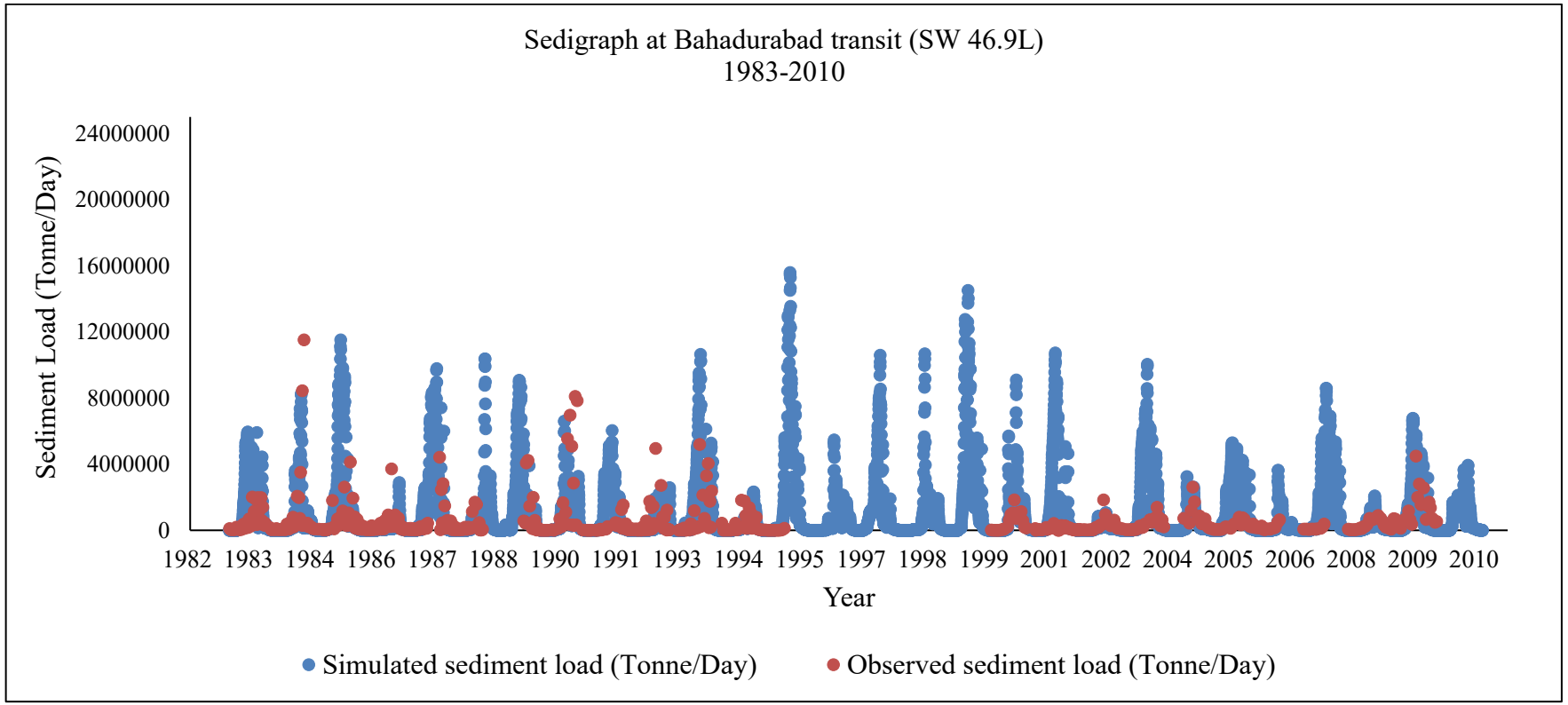

Figure 4.14: Calibration and validation of sediment model for 1983-2010

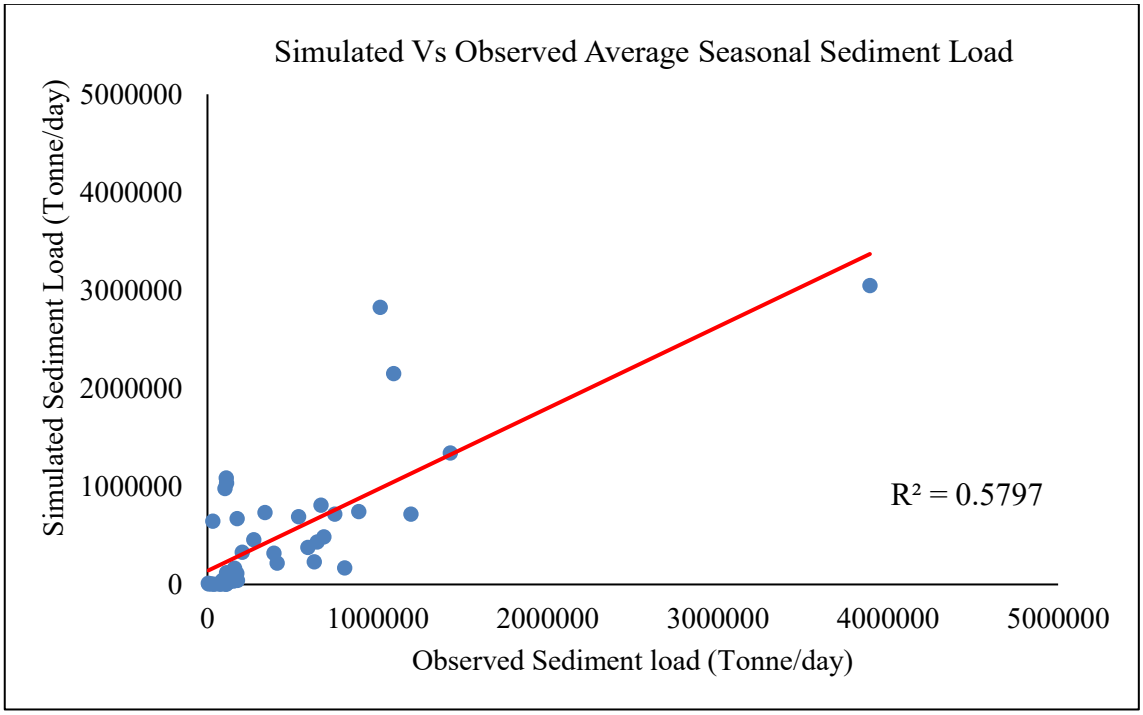

Figure 4.15: Scatter plot of simulated vs observed average seasonal sediment load at Bahadurabad transit for 1983-2010 period

Average seasonal sediment load at Bahdurabad Transit have been calculated by using the available data of 1983-2010 year collected from BWDB. Also, using the simulated sediment load for corresponding dates of observed sediment load at SW 46.9L, average seasonal sediment load of 1983-2010 year have been estimated. By plotting these results in Figure 4.15, the value of R^2 is about 0.6 which provides a satisfactory level of the surface erosion and sediment routing model.

4.6 Estimation of Annual Sediment Load at Bahadurabad Transit

From the calibrated and validated sediment model results at Bahadurabad transit (SW 46.9L), mean monthly sediment load has been estimated in Mt/month which is shown in Table 4.12. It has been found that annual average sediment load at Bahadurabad transit (SW 46.9L) for Brahmaputra river basin is about 370.20 Mt/year for 1983-2010 shown in Table 4.12. Particularly, for year 1993-1996, it has been found about 379.08 Mt/year shown in Table 4.13 which is close to the analysis done by Delft Hydraulics.

Table 4.12: Average annual sediment load at Bahadurabad transit (SW 46.9L) from calibrated model

Month	Calibration/Validation Period (Mt/month)
Jan	0.037
Feb	0.063
Mar	1.771
Apr	6.966
May	41.510
Jun	92.664
Jul	109.319
Aug	56.092
Sep	37.326
Oct	20.118
Nov	3.941
Dec	0.393
Total average annual sediment load (Mt/year)	**370.20**

Table 4.13: Average annual sediment load at Bahadurabad transit (SW 46.9L) for 1993-1996

Year	Simulated Sediment Load (Mt/year)	Sediment Load from Previous Literature/ Analysis (Mt/year)	Source
1993-1996	379.08	402	Delft Hydraulics/DHI (1996c)

CHAPTER 5
RESULTS AND DISCUSSIONS

5.1 Sensitivity Analysis

The changes in streamflow under the impact of climate change was investigated by using several hypothetical scenarios (synthetic approach) applied to the climate normal (1983–2010) meteorological data. Incremental climate change scenarios were applied with a hypothetical temperature increase (+2 °C and +6 °C) and a change in precipitation (-25%, +10%, +25%, +40%) to examine the change of the HEC-HMS simulated streamflow and sediment load at Bahadurabad transit (SW 46.9L).

5.1.1 Sensitivity to Precipitation Change

For the BRB changes in mean monthly discharge and mean monthly sediment load at Bahadurabad transit due to the changes in precipitation, while keeping the temperature unchanged are shown in Figure 5.1 and Figure 5.2. Various precipitation scenarios are analyzed which include -25%, 0%, 10%, 20%, 30% and 40% changes with respect to the base period of 1983-2010.

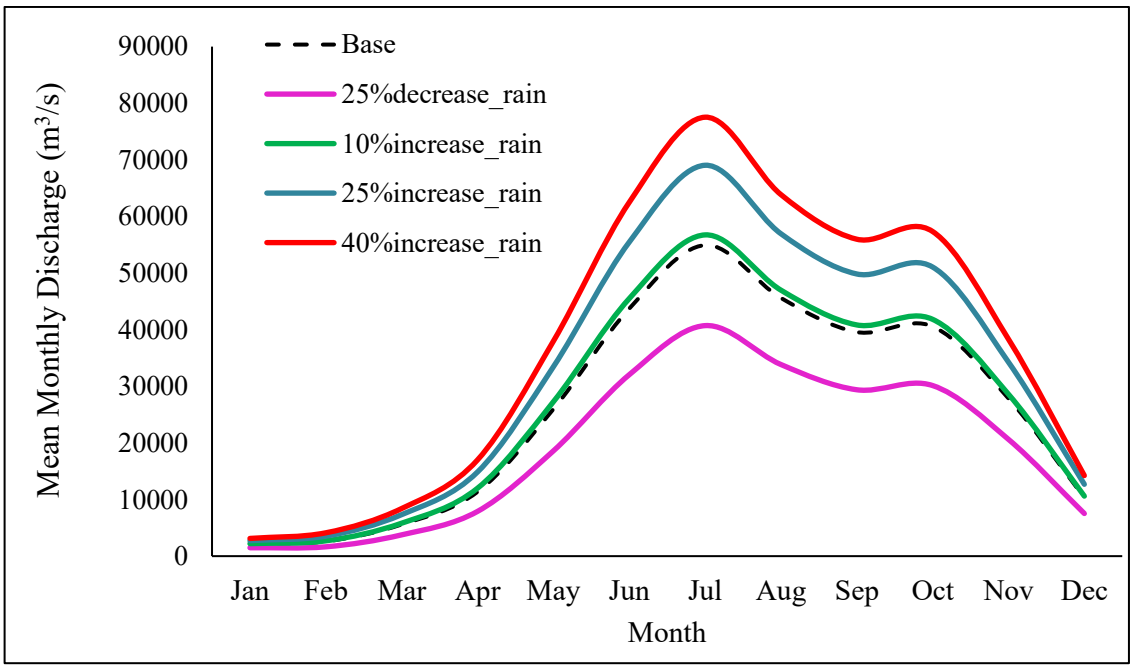

Figure 5.1: Mean monthly discharge at Bahadurabad transit due to precipitation change from -25% to +40%

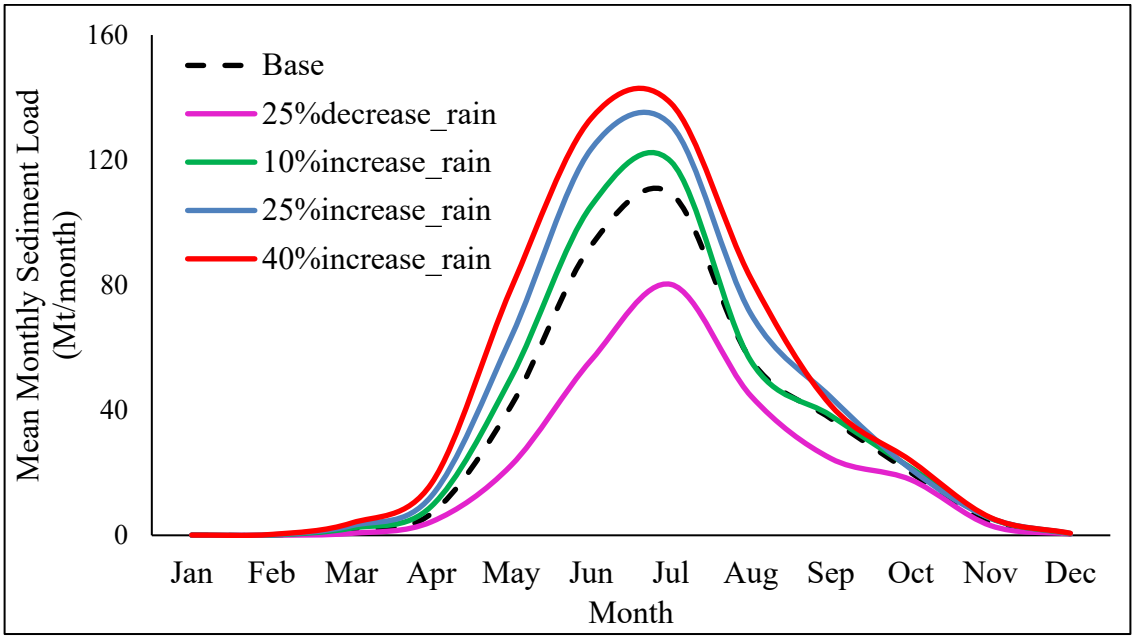

Figure 5.2: Mean monthly sediment load at Bahadurabad transit due to precipitation change from -25% to +40%

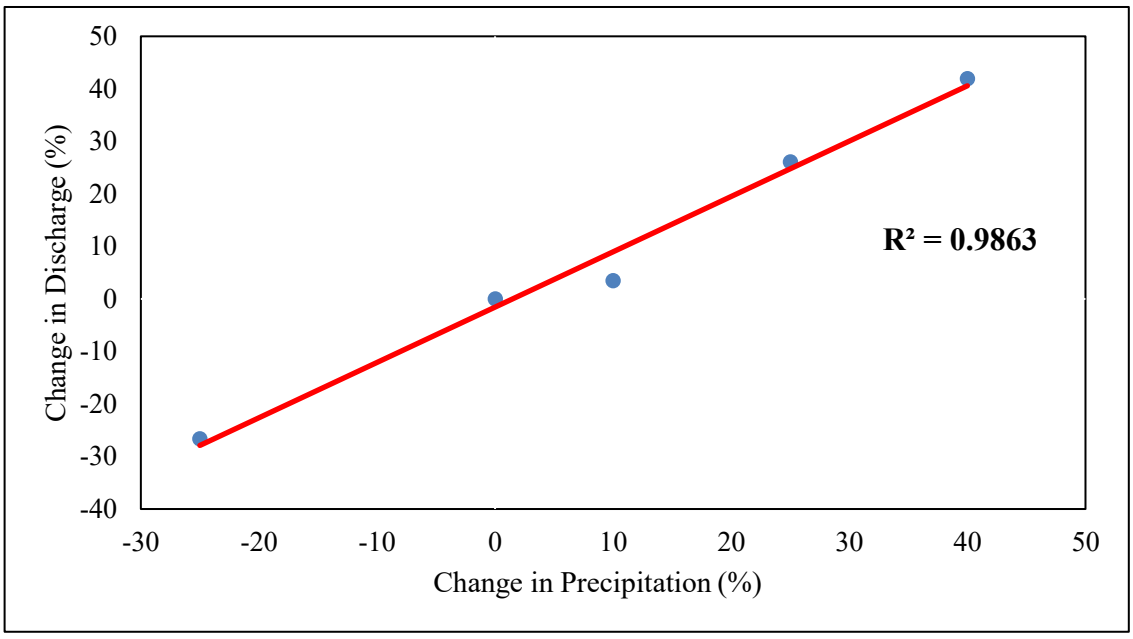

Figure 5.3: Changes in annual average discharge (%) at Bahadurabad transit due to changing precipitation

As a first approximation, a linear regression analysis of the streamflow and sediment load responses for the various scenarios indicated that a 25 % change in precipitation would produce a 26.1 % change in streamflow and 28.7% change in sediment load for Brahmaputra river basin. Table 5.1, Table 5.2, Figure 5.3 and Figure 5.4 shows that the

BRB is almost equally sensitive to a reduction and increase in precipitation for discharge and sediment load.

Table 5.1: Average annual discharge (m^3/s) due to the changes in precipitation

Change in Precipitation (%)	Average Annual Discharge (m^3/s)
-25	18972.92
0	25855.77
10	26757.58
25	32601.89
40	36698.01

Table 5.2: Average annual sediment load (Mt/year) due to the changes in precipitation

Change in Precipitation (%)	Base	-25%	+10%	+25%	+40%
Average Annual Sediment Load (Mt/year)	370.20	254.19	408.75	476.41	525.38
% Increase in Sediment Load		-31.34	10.41	28.69	41.92

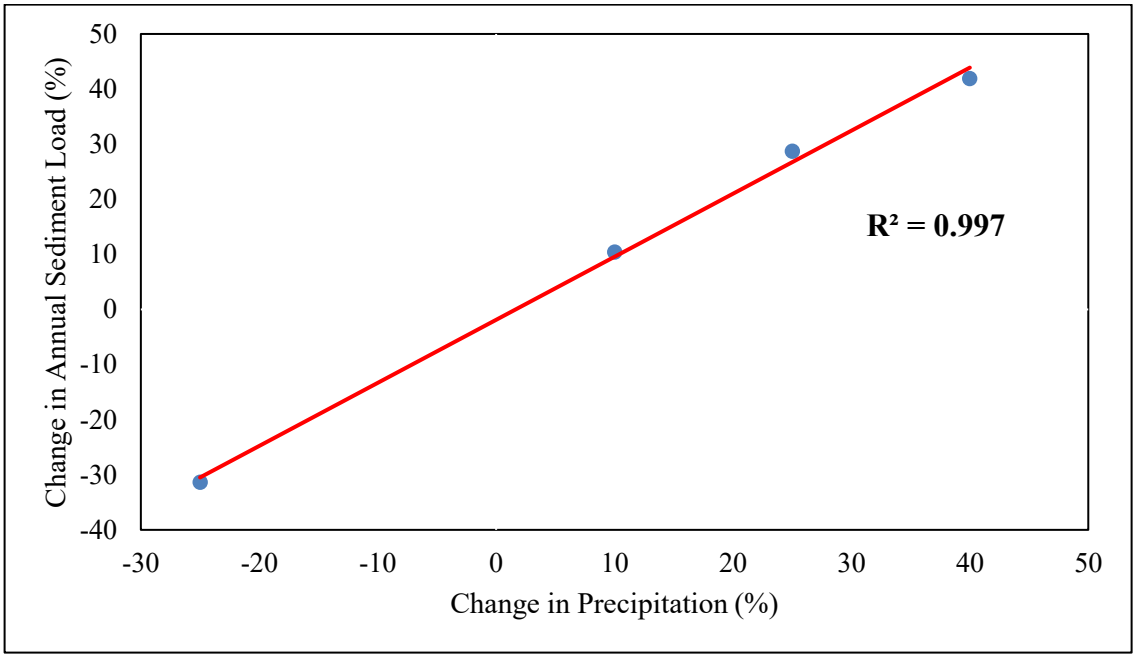

Figure 5.4: Changes in average annual sediment load (%) at Bahadurabad transit due to changing precipitation

5.1.2 Sensitivity to Temperature Change

For the BRB changes in mean monthly discharge and mean monthly sediment load at Bahadurabad transit (SW 46.9L) due to the changes in temperature, while keeping the precipitation unchanged are shown in Figure 5.5 and Figure 5.6. Table 5.3 shows percentage change in mean annual sediment load due to temperature change.

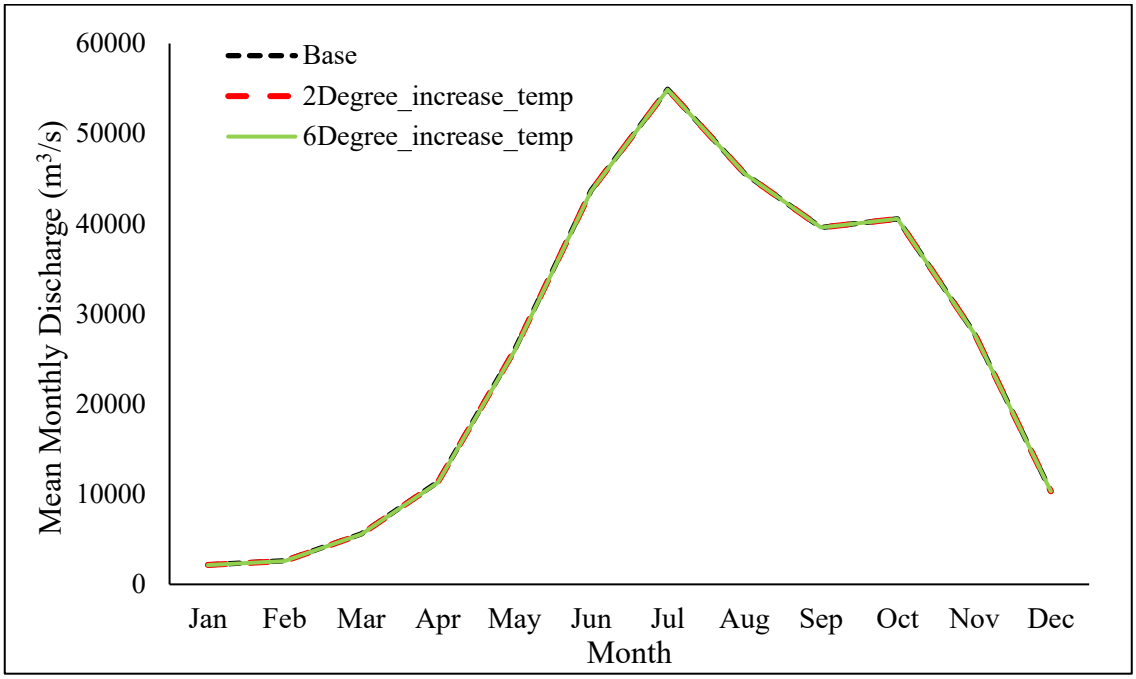

Figure 5.5: Mean monthly discharge (m^3/s) at Bahadurabad transit due to temperature increase

From the values it can be concluded that this model is not sensitive to temperature change. It may occur as snow melt option is not considered during the model setup due to lack of computational capacity of HEC-HMS. In future, the enhanced precipitation will cause an increase in discharge while the enhanced temperature will cause decrease in discharge by increasing evaporative losses. From previous studies, it was revealed that for BRB increased discharge due to enhanced precipitation offset the decreased discharge due to enhanced evaporation (Alam, 2015) So, lacking in sensitiveness of the model due to temperature produce very negligible error in dry season flow and sediment load estimation.

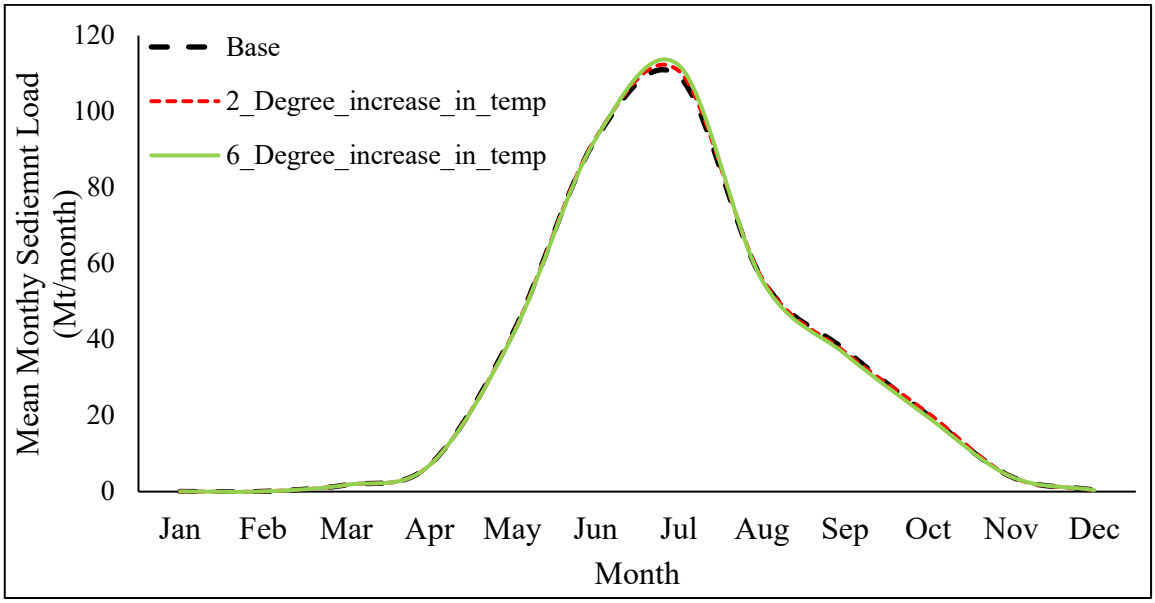

Figure 5.6: Mean monthly sediment load at Bahadurabad transit due to temperature increase

Table 5.3: Percentage change in mean annual sediment load due to temperature change

	Base	2 Degree Temperature Increase	4 Degree Temperature Increase
Mean Annual Sediment Load (Mt/year)	370.20	371.704	370.685
% increase in Sediment Load		0.41	0.13

5.2 Selection of RCM Models for RCP 8.5 Scenario

An 11-member ensemble from three regional climate model (RCM) forced by eight general circulation model (GCM) was selected from Coordinated Regional Climate Downscaling Experiment (CORDEX) -South Asia domain database. The selection of the ensemble member is based on the availability in the database at the time of the study. All the projections were made by forcing the corresponding GCM with Representative Concentration Pathway - RCP 8.5 (van Vuuren et al., 2011). This scenario represents no change in current trend of greenhouse gas emission, i.e. business as usual. So far, the actual trend in emission is found to follow this pathway (Piontek et al., 2013; Friedlingstein et al., 2014).

Table 5.4: Selection of RCM for climate impact analysis on discharge and sediment load

	2020s	2050s	2080s	
MPI-M-MPI-ESM-LR_MPI-CSC-REMO2009	**-0.74**	**-0.93**	**-8.93**	**Driest**
ACCESS1-0_CSIRO_CCAM_1391M	0.92	0.45	-2.40	
CNRM-CM5_CSIRO-CCAM-1391M	0.78	-2.58	-2.22	
MPI-ESM-LR_CSIRO-CCAM-1391M	-0.86	-0.15	-1.43	
CCSM4_CSIRO-CCAM-1391M	-1.26	-1.63	-0.33	
MPI-M-MPI-ESM-LR_SMHI-RCA4	**0.39**	**6.97**	**12.13**	**Moderate Wet**
NOAA-GFDL-GFDL-ESM2M_SMHI-RCA4	1.29	7.56	15.24	
CNRM-CERFACS-CNRM-CM5_SMHI-RCA4	3.47	10.19	18.90	
ICHEC-EC-EARTH_SMHI-RCA4	8.53	15.23	23.09	
MIROC-MIROC5_SMHI-RCA4	8.94	18.12	27.06	
IPSL-CM5A-MR_SMHI-RCA4	11.81	15.4	**33.53**	**Wettest**

The changes in annual average precipitation for 2010-2039, 2040-2069 and 2070-2099 from the climatic base period (1980-2009) for all three RCMs forced by eight GCMs have been analyzed which are shown in Table 5.4. The work has been done to select specific models for doing impact analysis on sediment load considering driest, moderate and wettest condition. For RCM SMHI-RCA4 forced by GCM IPSL-CM5A-MR, the percentage increase in precipitation are 11.81, 15.4 and 33.53 for 2020s, 2050s and 2080s respectively. For 2020s and 2080s, the values are the highest among all the results. So, RCM SMHI-RCA4 forced by GCM IPSL-CM5A-MR has been considered as wettest condition in which highest precipitation will occur in future. Analysis on precipitation from RCM CSC-REMO2009 forced by GCM MPI-M-MPI-ESM-LR_MPI output have percentage decrease in precipitation which are 0.74, 0.93 and 8.93 for 2020s, 2050s and 2080s respectively and this has been considered as driest condition. RCM SMHI-RCA4 forced by GCMMPI-M-MPI-ESM-LR has considered as the moderate condition of precipitation in future. Only changes in precipitation has been considered for further

climate change impact assessment as the model is found as highly sensitive for precipitation in the previous section.

5.3 Climate Change Impact Analysis on Flow of BRB

After selection of the models, HEC-HMS sediment model has been simulated for future RCP 8.5 scenario. To capture range of uncertainty in flow for RCP 8.5, HEC-HMS model has been simulated in the periods of 2020s, 2050s, and 2080s projections.

5.3.1 Change of Monthly Flow at Bahadurabad Transit for 2020s Projections

In the Figure 5.7 shows the volume of monthly flow for 2020s projections and Figure 5.8 shows the box plot about future change of flow from baseline at Bahadurabad transit (SW 46.9L) which is outlet of Brahmaputra basin. The maximum change of monthly flow for March, April and May might increase 350%, 125% and 75% respectively. The range of uncertainty of change monthly flow for March, April has been found greater than February, May and June. The difference of maximum and minimum range for November and December are greater than August, September and October, so there might be uncertainty in the change of monthly flow for November and December.

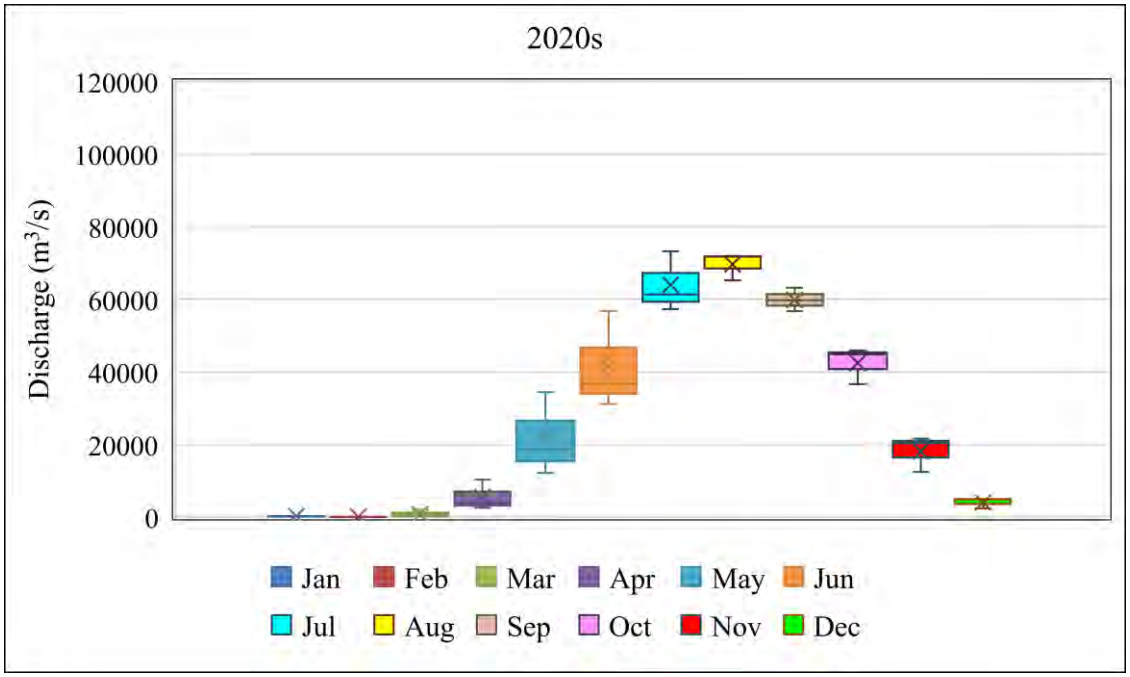

Figure 5.7: Future monthly flow for 2020s

The Highest discharge values may occur in the month of July and it is within 57000 m^3/s to 73000 m^3/s. The difference of maximum and minimum range October, November and December has been found as 5%, 23% and 30% respectively.

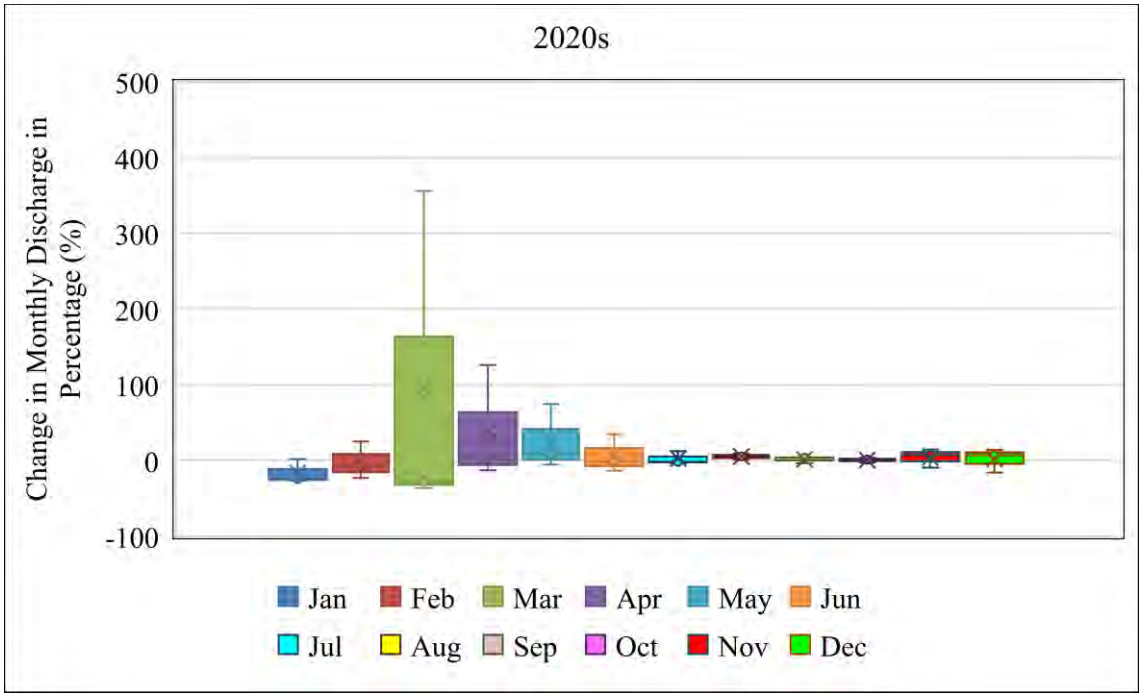

Figure 5.8: Change of future monthly flow from baseline for 2020s

5.3.2 Change of Monthly Flow at Bahadurabad Transit for 2050s Projections

Figure 5.9 shows the volume of monthly flow for 2050s projections and Figure 5.10 shows the box plot about future change of flow from baseline at Bahadurabad transit (SW 46.9L) which is outlet of Brahmaputra River Basin. The Highest discharge values may occur in the month of July and it is within 60000 m^3/s to 85000 m^3/s. The difference of maximum and minimum range October, November and December has been found as 30%, 45% and 75% respectively.

The maximum change of monthly flow for March, April and May might increase 385%, 220% and 125% respectively. The range of uncertainty of change monthly flow for March, April has been found greater than February, May and June. It has been found that the change of monthly flow for August, September might increase 10% for 2050s projections. There is minor difference between maximum and minimum range for August

and September. The difference of maximum and minimum range for November and December are greater than August, September and October, so there might uncertainty in the change of monthly flow for November and December.

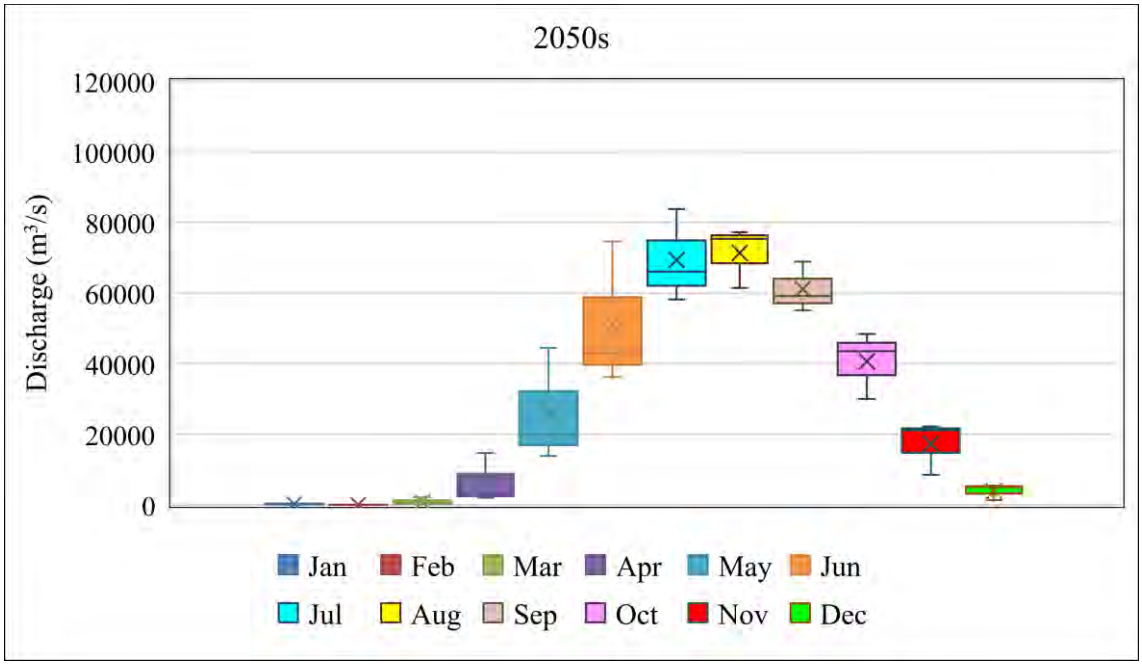

Figure 5.9: Future monthly flow for 2050s

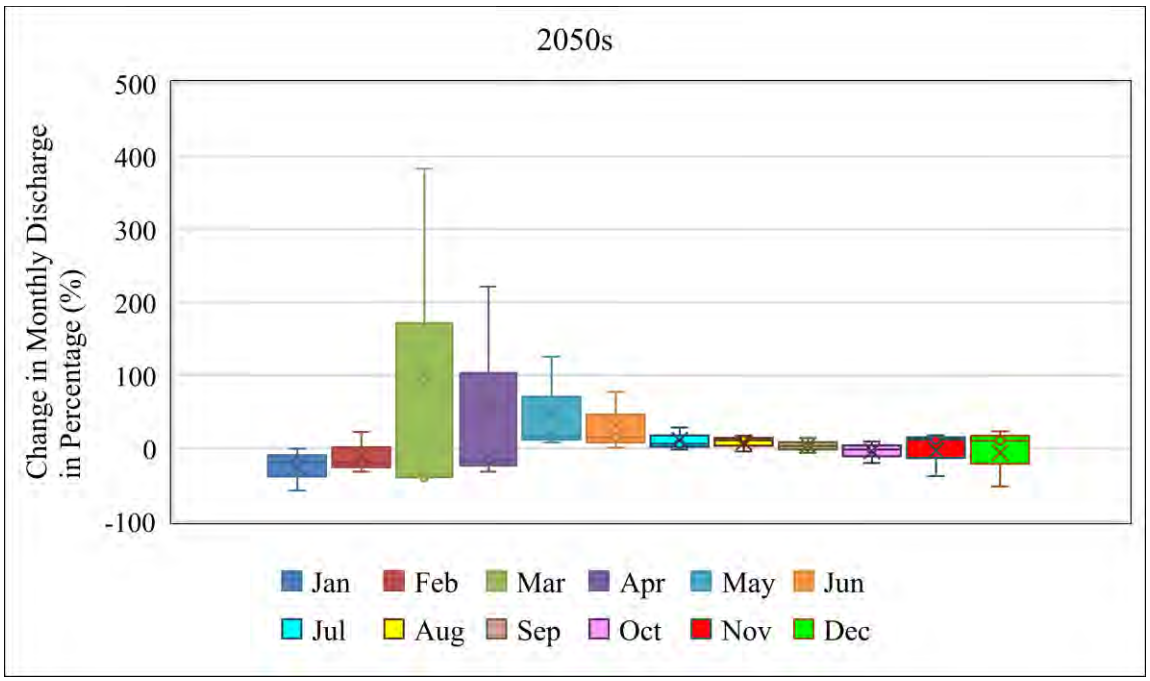

Figure 5.10: Change of future monthly flow from baseline for 2050s

5.3.3 Change of Monthly Flow at Bahadurabad Transit for 2080s Projections

For Bahadurabad transit (SW 46.9L), Figure 5.11 and Figure 5.12 show the volume of monthly flow for 2080s projection and box plot about future change of flow from baseline respectively.

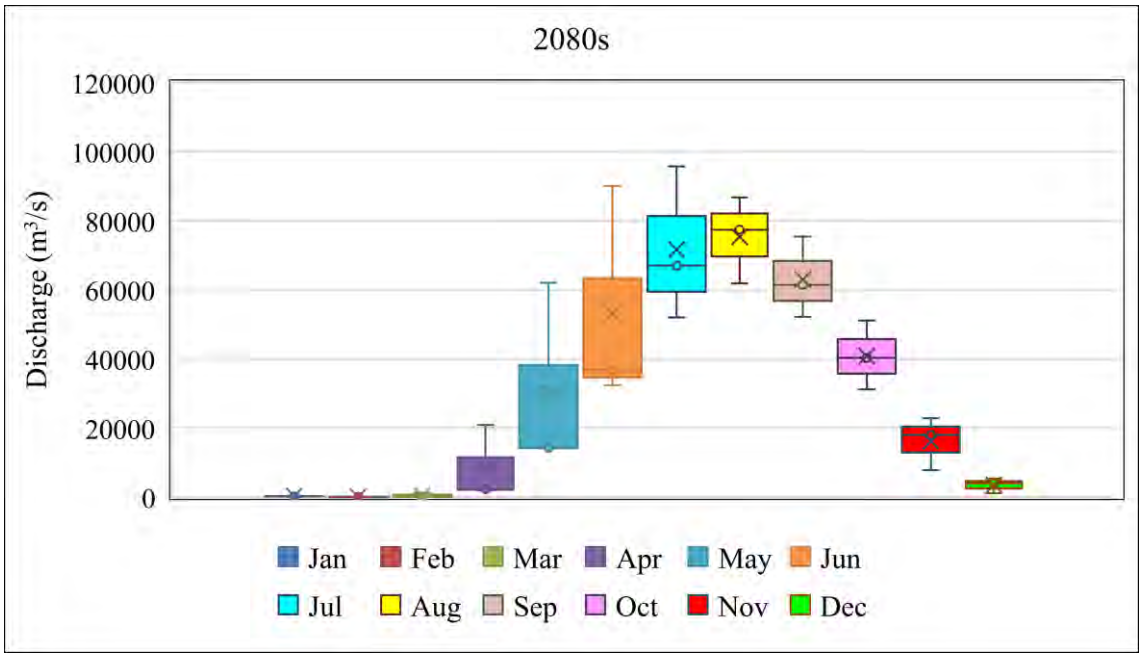

Figure 5.11: Future monthly flow for 2080s

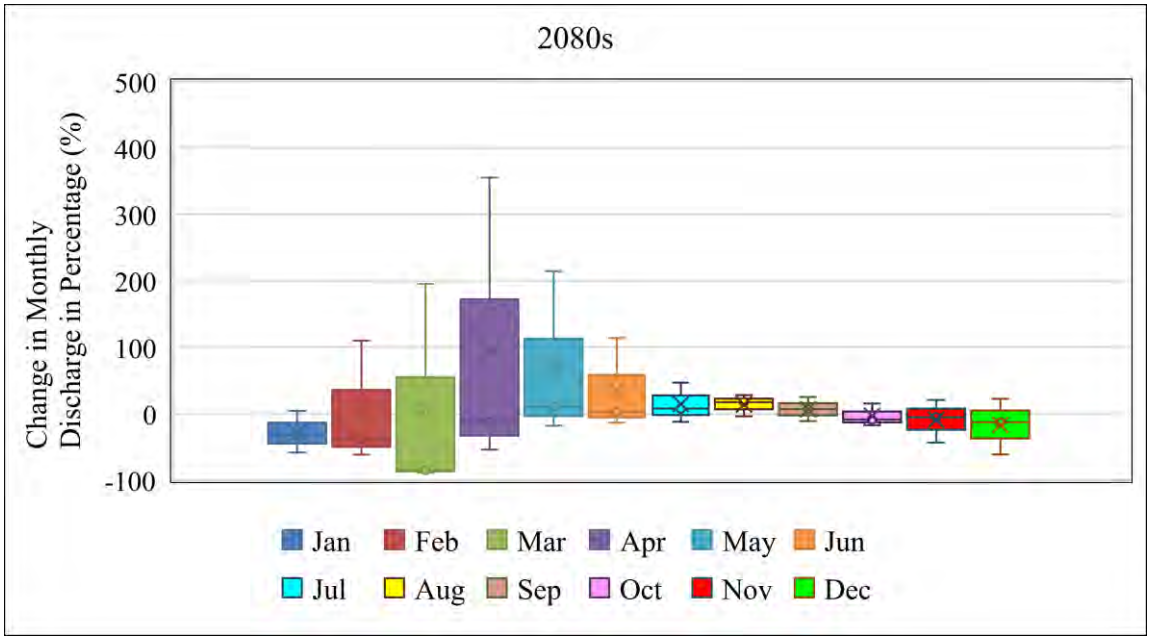

Figure 5.12: Change of future monthly flow from baseline for 2080s

The highest discharge values may occur in the month of July and it is within 52000 m^3/s to 96000 m^3/s. The difference of maximum and minimum range October, November and December has been found as 32%, 63% and 83% respectively.

The maximum change of monthly flow for March, April and May might increase 200%, 350% and 210% respectively. The range of uncertainty of change monthly flow for April is the highest one. Also, the range of uncertainty of change monthly flow for February, March, May and June is higher than the remaining months. The difference of maximum and minimum range for July, November and December are greater than August, September and October, so there might uncertainty in the change of monthly flow for July, November and December.

5.3.4 Change of Seasonal flow at Bahadurabad Transit

The Figure 5.13 shows the volume of seasonal flow for 2020s, 2050s and 2080s projections. Figure 5.14 describes change of seasonal flow from baseline at Bahadurabad transit of Brahmaputra Basin. It also analyzed the comparison of future seasonal change of flow among the three future projections. The change in the quartiles of the pre-monsoonal (MAM) seasonal discharges has been found to be increasing from 2020s towards the 2050s and 2080s projections that the change of seasonal flow of 2020, 2050s and 2080s has been found as 94%, 150% and 245% respectively.

The change in the quartiles of the monsoonal (JJAS) seasonal discharges has been found to be increasing from 2020s towards the 2050s and 2080s projections that the change of seasonal flow of 2020, 2050s and 2080s has been found as 14%, 35% and 57% respectively. The changes in flow for pre-monsoon is found higher than monsoon period.

For post-monsoon (ON) and Dry (DJF) season, the change in the quartiles seasonal discharges has been found to be decreasing from 2020s towards the 2050s and 2080s projections. For post monsoon, the change of seasonal flow of 2020, 2050s and 2080s are 11%, 37% and 40% respectively and for dry season, these values are 23%, 71% and 75%.

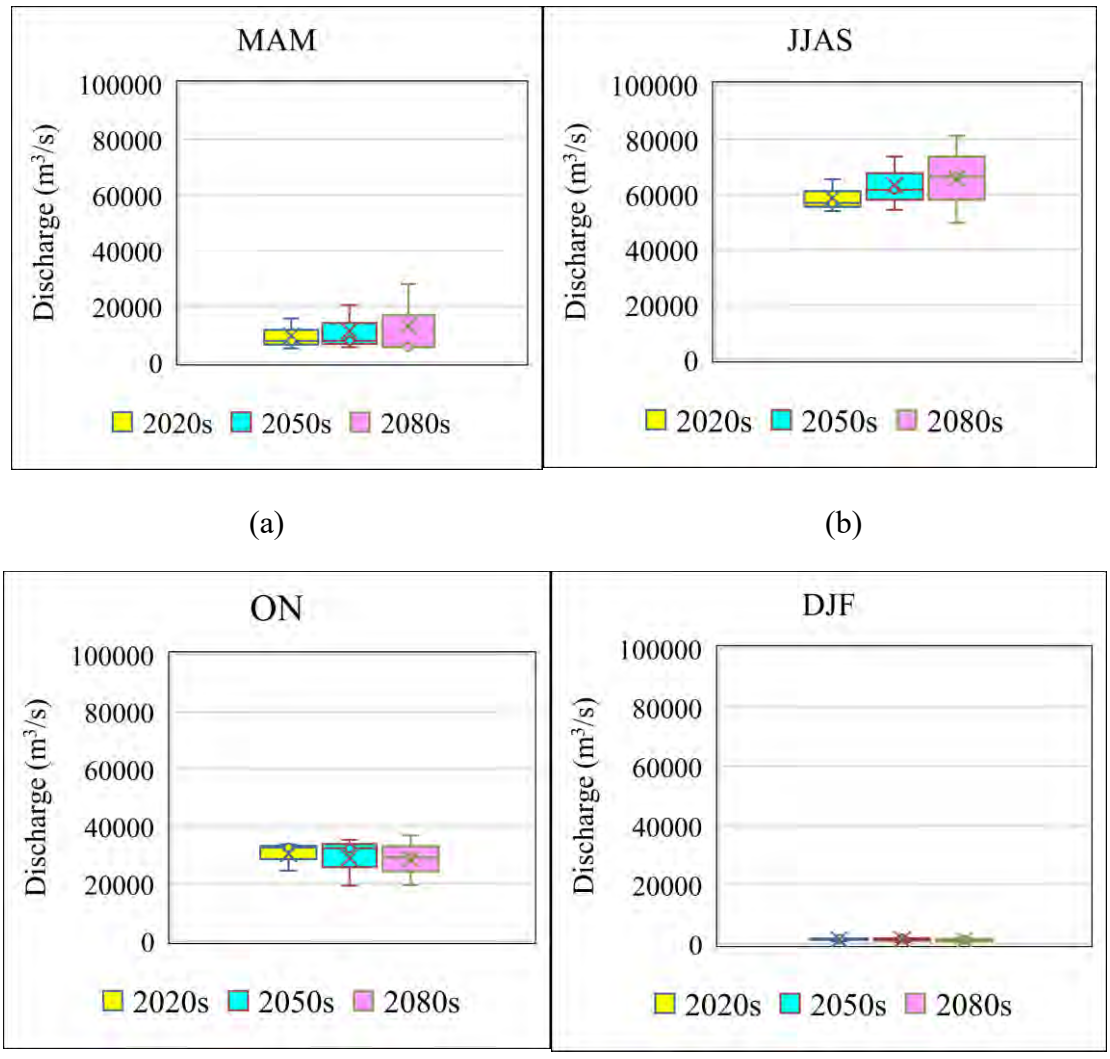

Figure 5.13: Future seasonal monthly flow for (a) MAM (b) JJAS (c) ON and (d) DJF

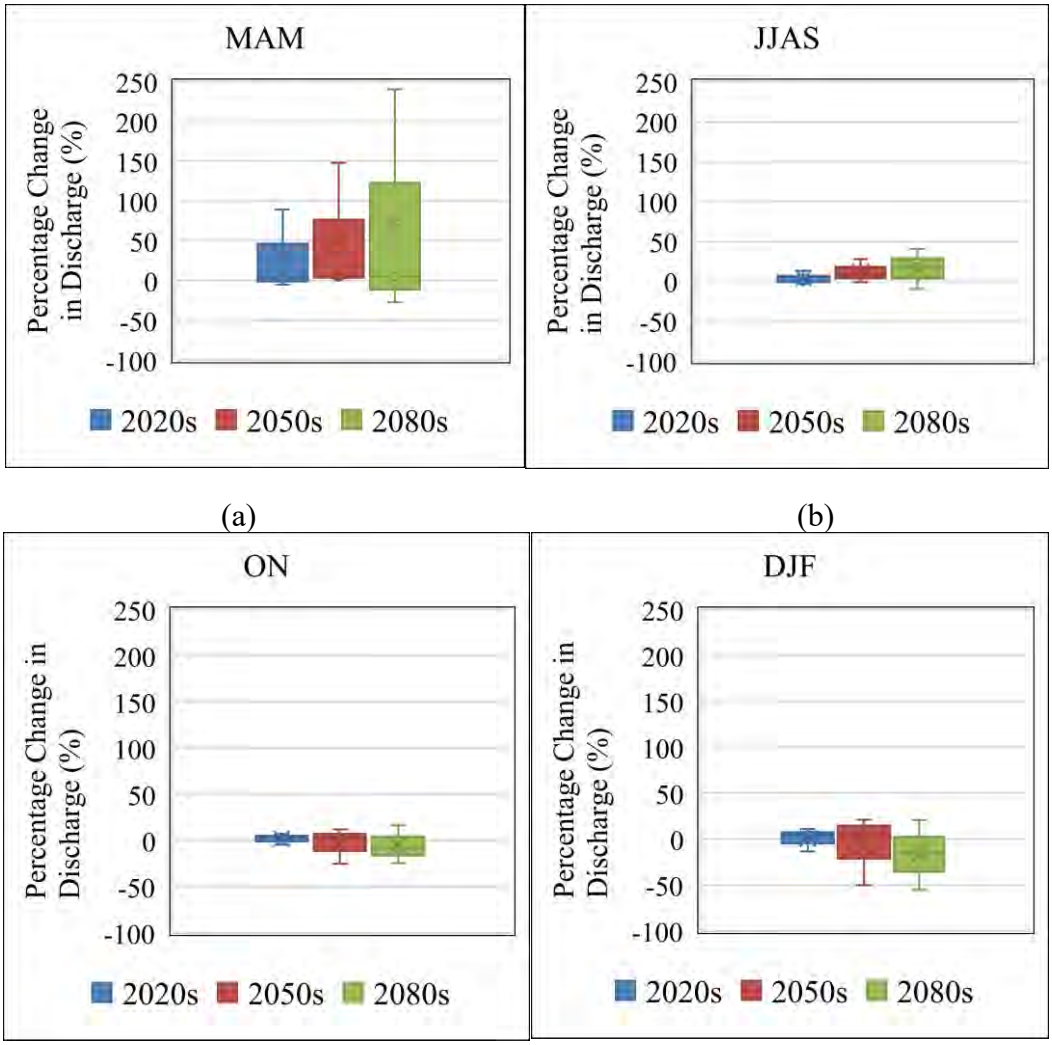

Figure 5.14: Change of future seasonal flow from baseline for (a) MAM (b) JJAS (c) ON and (d) DJF

5.3.5 Change of Mean Annual Flow at Bahadurabad Transit

Figure 5.15 shows boxplots of differences in the mean annual average streamflow simulated by the selected RCM models with respect to the climate normal period. The percentage changes of model simulated mean annual streamflow from the climate base period with respect to climate change scenario RCP 8.5 has been plotted in Figure 5.16. The percentage changes in average annual flow from baseline period for 2020s, 2050s and 2080s are 18%, 27% and 61% respectively. A gradual increase in annual average flow is found from 2020s to 2080s. The range of 75th and 25th percentile grows from 2020s to 2080s which indicates that uncertainty associated with the projected streamflow of BRB increases as we go distant future.

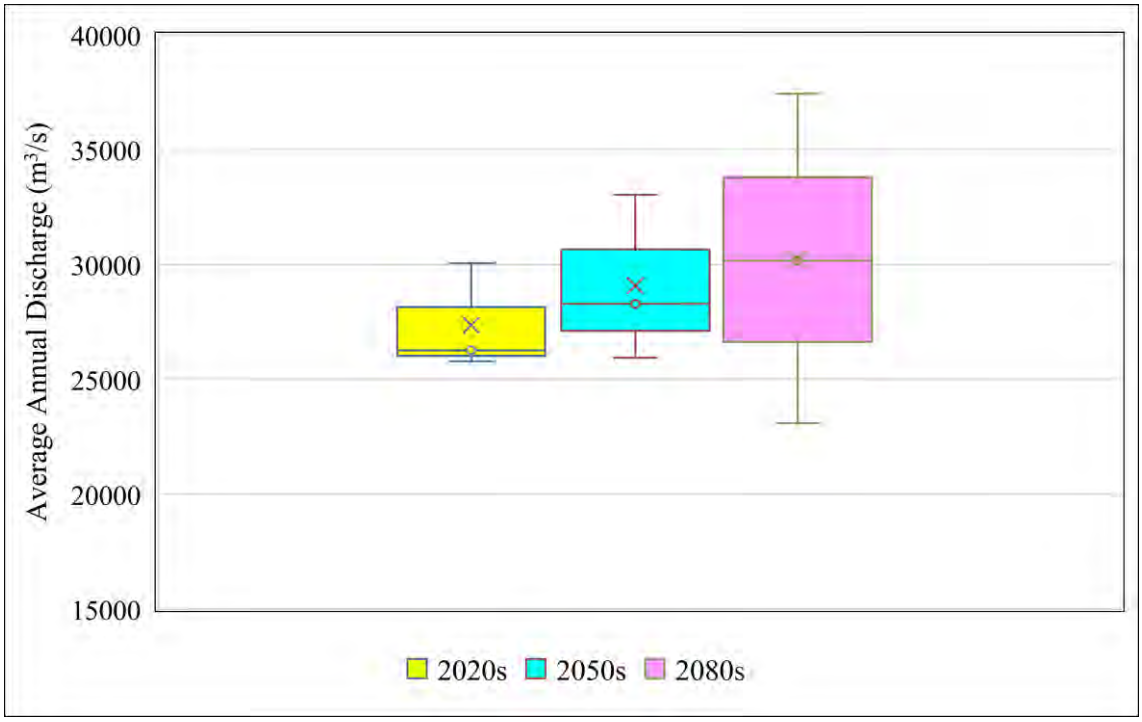

Figure 5.15: Average annual discharge (m^3/s) of RCP 8.5 for 2020s, 2050s and 2080s

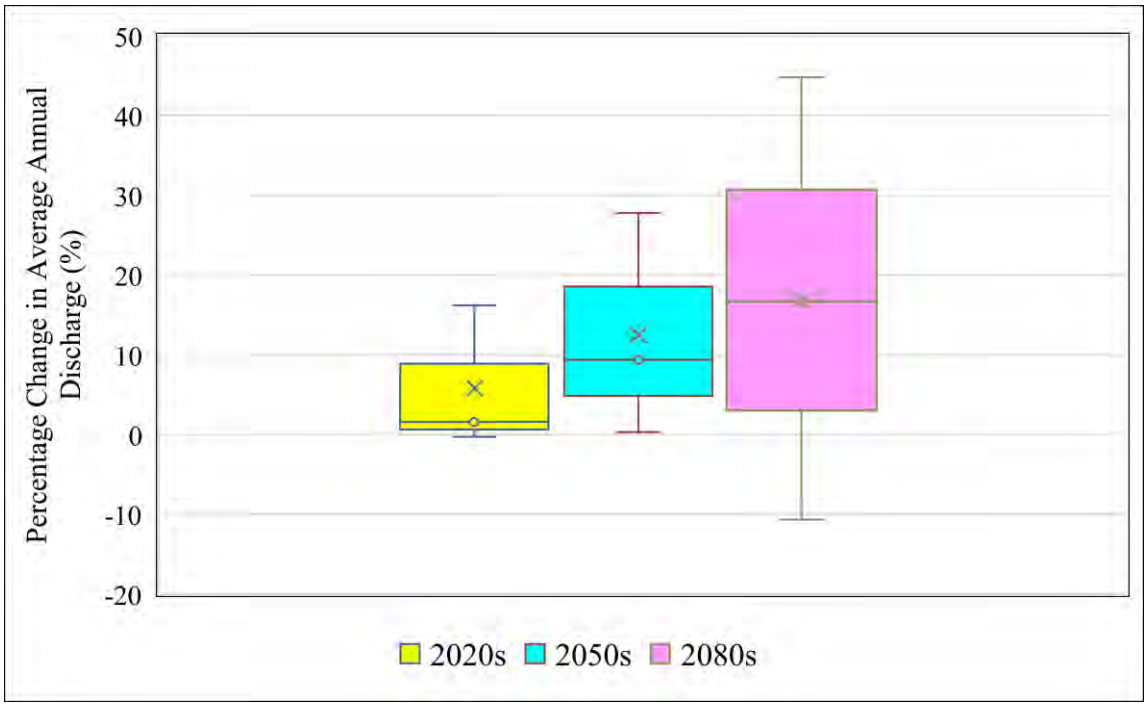

Figure 5.16: Change of future average annual flow from baseline

5.4 Climate Change Impact Analysis on Sediment Load of BRB

After analysing the uncertainty in flow for RCP 8.5 scenario, HEC-HMS model has also been simulated in the periods of 2020s, 2050s, and 2080s projections for capturing the uncertainty in sediment load at Bahadurabad transit (SW46.9L) of BRB.

5.4.1 Change of Monthly Sediment Load at Bahadurabad Transit for 2020s Projections

Figure 5.17 shows the volume of monthly sediment load in Mt/month for 2020s projections. The difference of maximum and minimum range for June and July is comparatively higher than May, August, September and October. So, there might be a high uncertainty in the change of monthly sediment load for particularly these two months. The highest sediment load (Mt/month) values may occur in the month of August and it is within 118 Mt/month to 147 Mt/month.

On the other hand, the difference of maximum and minimum range for November is highest among the remaining months (January, February, March, April, November and December) and the value is within 1.5 Mt/month to 6 Mt/month.

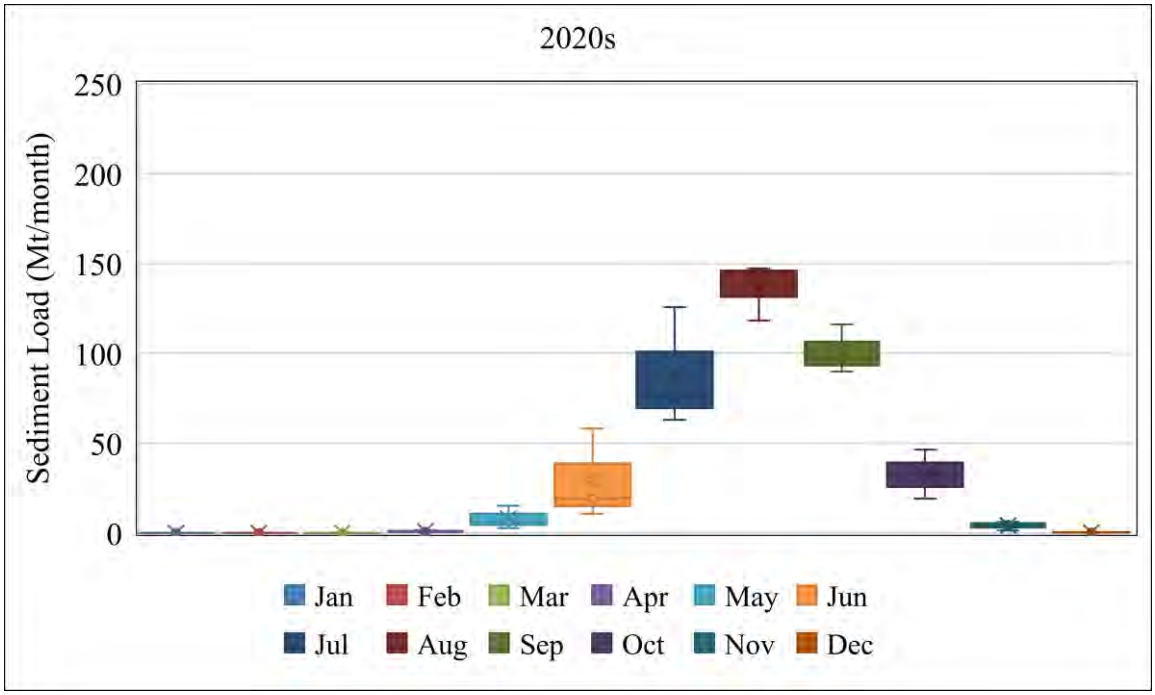

Figure 5.17: Future monthly sediment load(Mt/month) for 2020s

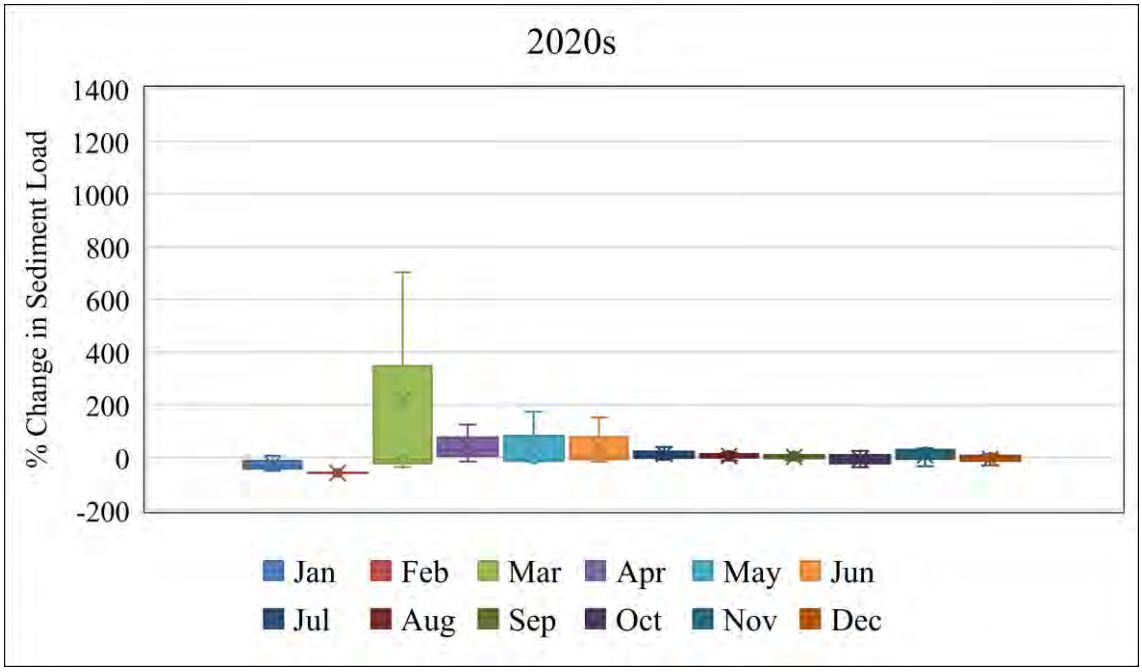

Figure 5.18: Change of future monthly sediment load from baseline for 2020s

In Figure 5.18, it has been found that, the maximum change of monthly sediment load occurs in March. The range of uncertainty of change monthly sediment load for April, May and June has also been found greater than the remaining months. Though, high level uncertainty has been found for March, the amount of sediment load is very minor in this month and that is why it has a very low impact on total sediment load than the other months.

5.4.2 Change of Monthly Sediment Load at Bahadurabad Transit for 2050s Projections

Figure 5.19 shows the volume of monthly sediment load in million tonnes per month for 2050s projections. The difference of maximum and minimum range for June and July is comparatively higher than May, August, September and October. So, there might be a high uncertainty in the change of monthly sediment load for particularly these two months. The highest sediment load (Mt/month) values may occur in the month of July and it is within 92 Mt/month to 182 Mt/month.

On the other hand, the difference of maximum and minimum range for April and November is comparatively higher than the remaining months (January, February, March and December). The sediment load value of the month April is within 0.3 Mt/month to 4

Mt/month. The sediment load value of the month November is within 1 Mt/month to 5 Mt/month.

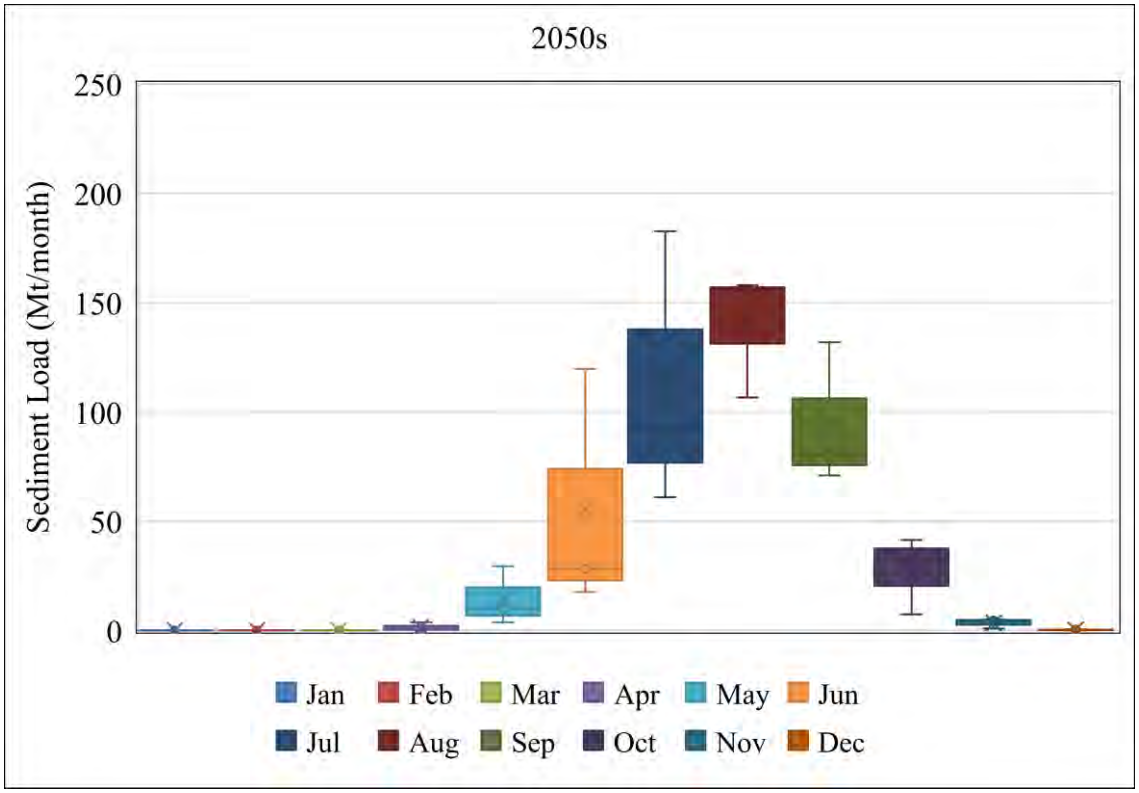

Figure 5.19: Future monthly sediment load(Mt/month) for 2050s

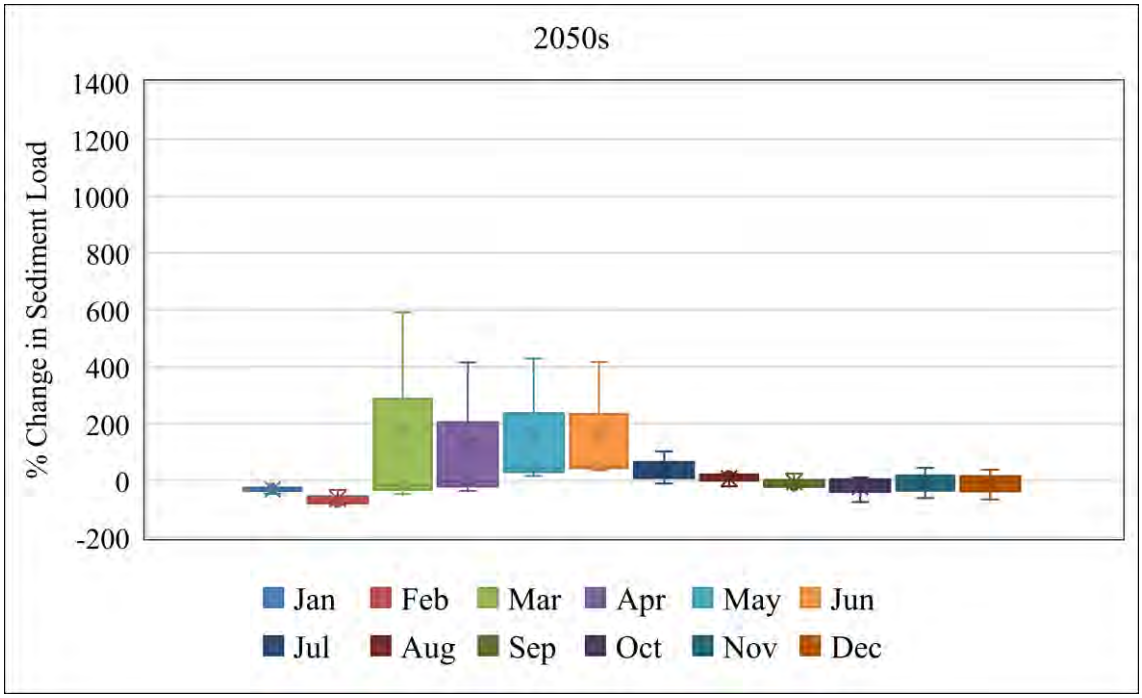

Figure 5.20: Change of future monthly sediment load from baseline for 2050s

Figure 5.20 shows the percentage change in monthly sediment load for Bahadurabad transit on 2050s. The maximum change of monthly sediment load occurs in March. The range of uncertainty of change monthly sediment load for April, May and June has also been found greater than the remaining months. Though, high level uncertainty has been found for March, the amount of sediment load is very minor in this month and that is why it has a very low impact on total sediment load than the other months.

5.4.3 Change of Monthly Sediment Load at Bahadurabad Transit for 2080s Projections

Figure 5.21 and Figure 5.22 show the volume of monthly sediment load in Mt/month and percentage change in monthly sediment load from climatic base for 2080s projections. The difference of maximum and minimum range for June and July is comparatively higher than May, August, September and October. So, there might be a high uncertainty in the change of monthly sediment load for particularly these two months. The highest sediment load value may occur in the month of July and it is within 98 Mt/month to 223 Mt/month.

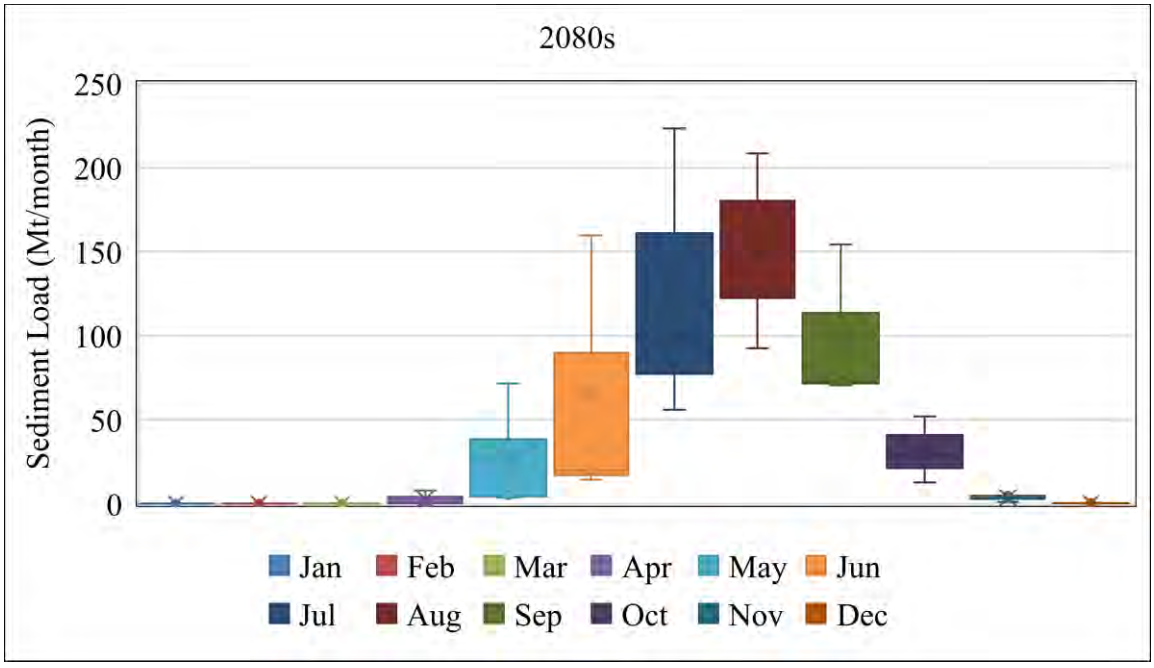

Figure 5.21: Future monthly sediment load(Mt/month) for 2080s

On the other hand, the difference of maximum and minimum range for April is highest among the remaining months (January, February, March, April, November and

December). The sediment load value of the month April is within 0.2 Mt/month to 8 Mt/month. The highest uncertainty in percent change in monthly sediment load occurs for May in 2080s. The range of uncertainty is also high for March and April month.

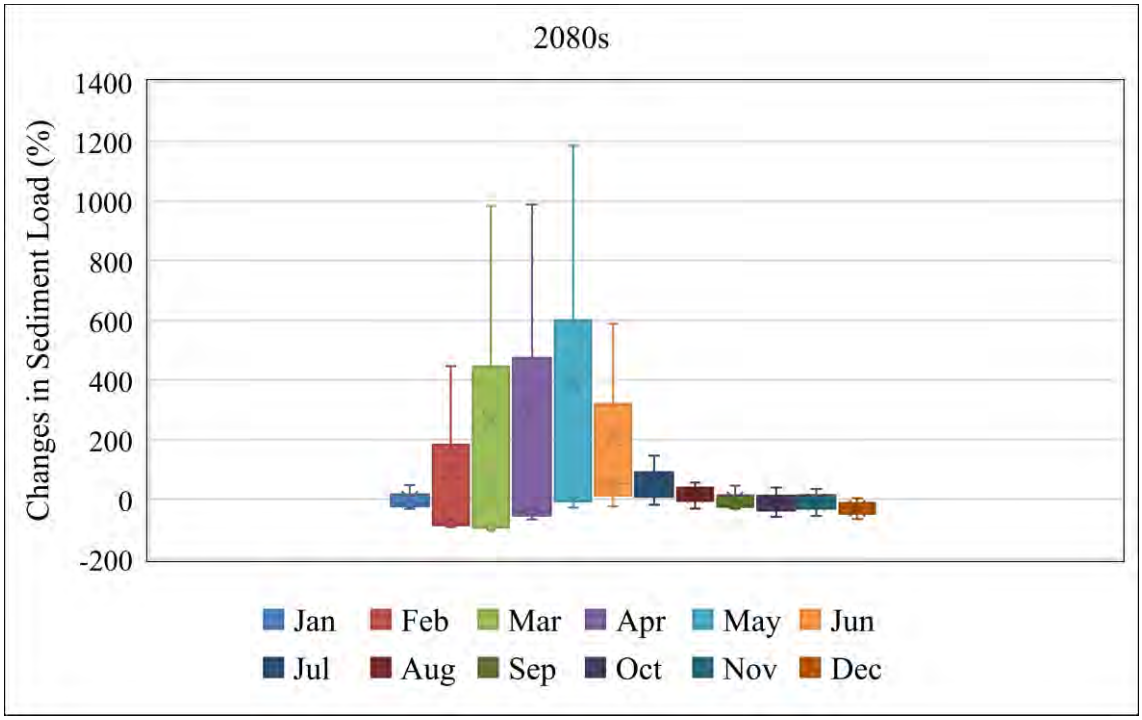

Figure 5.22: Change of future monthly sediment load from baseline for 2080s

5.4.4 Change of Seasonal Sediment Load at Bahadurabad Transit

Pre-monsoon (MAM), monsoon (JJAS), post-monsoon (ON) and dry (DJF) season have been considered for analysing changes in sediment load at Bahadurabad transit of BRB. Figure 5.23 shows the volume of seasonal sediment load for 2020s, 2050s and 2080s projections. Figure 5.24 describes change of seasonal sediment load from baseline for all three projections at Bahadurabad transit of Brahmaputra River Basin.

The change in the quartiles of the pre-monsoonal (MAM) seasonal sediment load has been found to be increasing from 2020s towards the 2050s and 2080s projections that the change of seasonal sediment load of 2020, 2050s and 2080s has been found as 182%, 441% and 1170% respectively. The change in the quartiles of the monsoonal (JJAS) seasonal sediment load has been found to be increasing from 2020s towards the 2050s and 2080s projections that the change of seasonal sediment load of 2020, 2050s and 2080s has been found as 40%, 74% and 111% respectively. The changes in sediment load for

pre-monsoon is found higher than monsoon period. For post-monsoon (ON) and Dry (DJF) season, the change in the quartiles seasonal sediment load has been found to be decreasing from 2020s towards the 2050s and 2080s projections. For post monsoon, the change of seasonal sediment load of 2020, 2050s and 2080s are 61%, 83% and 92% respectively and for dry season, these values are 36%, 98% and 107%.

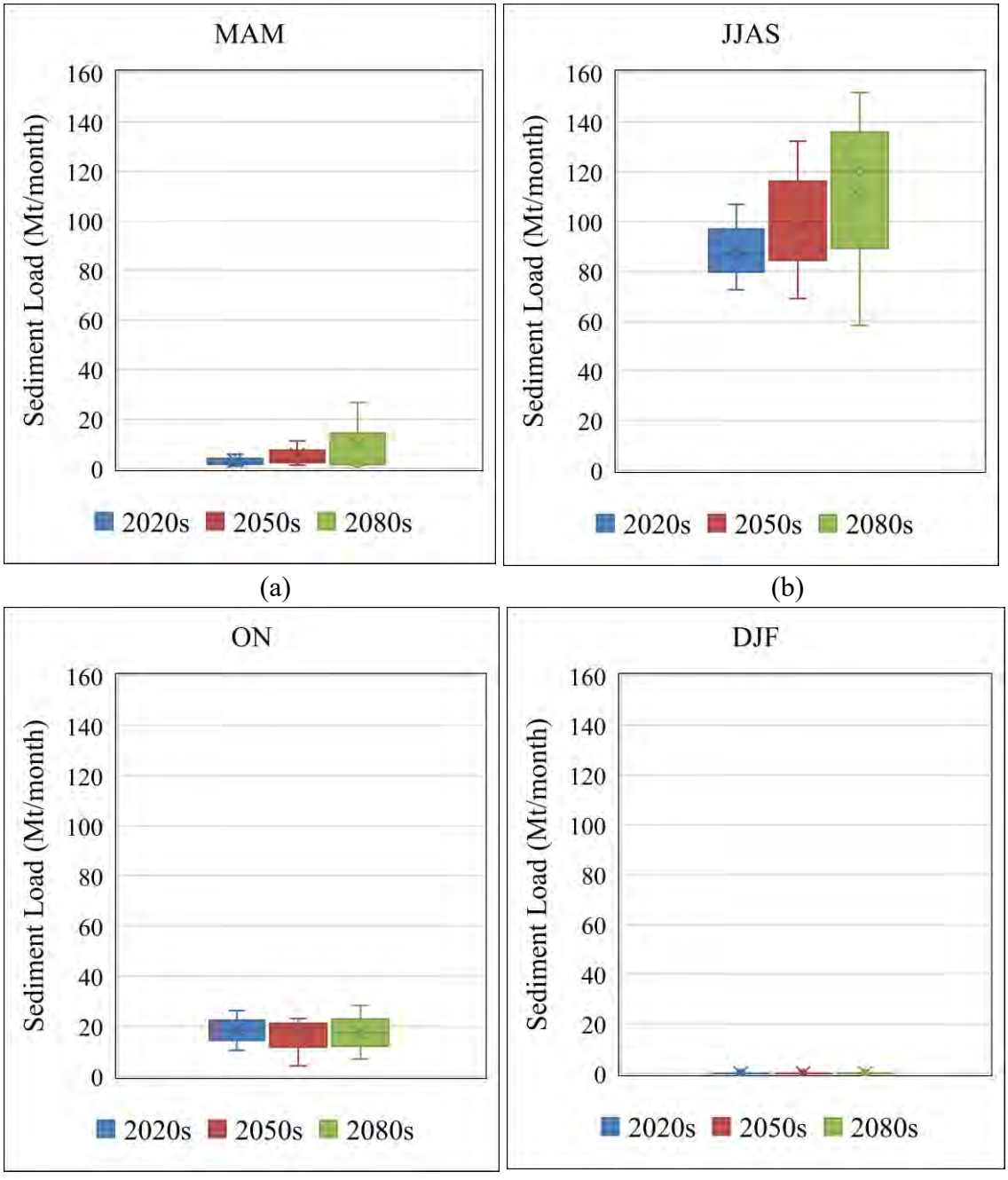

Figure 5.23: Seasonal sediment load for (a) MAM, (b) JJAS (c) ON and (d) DJF

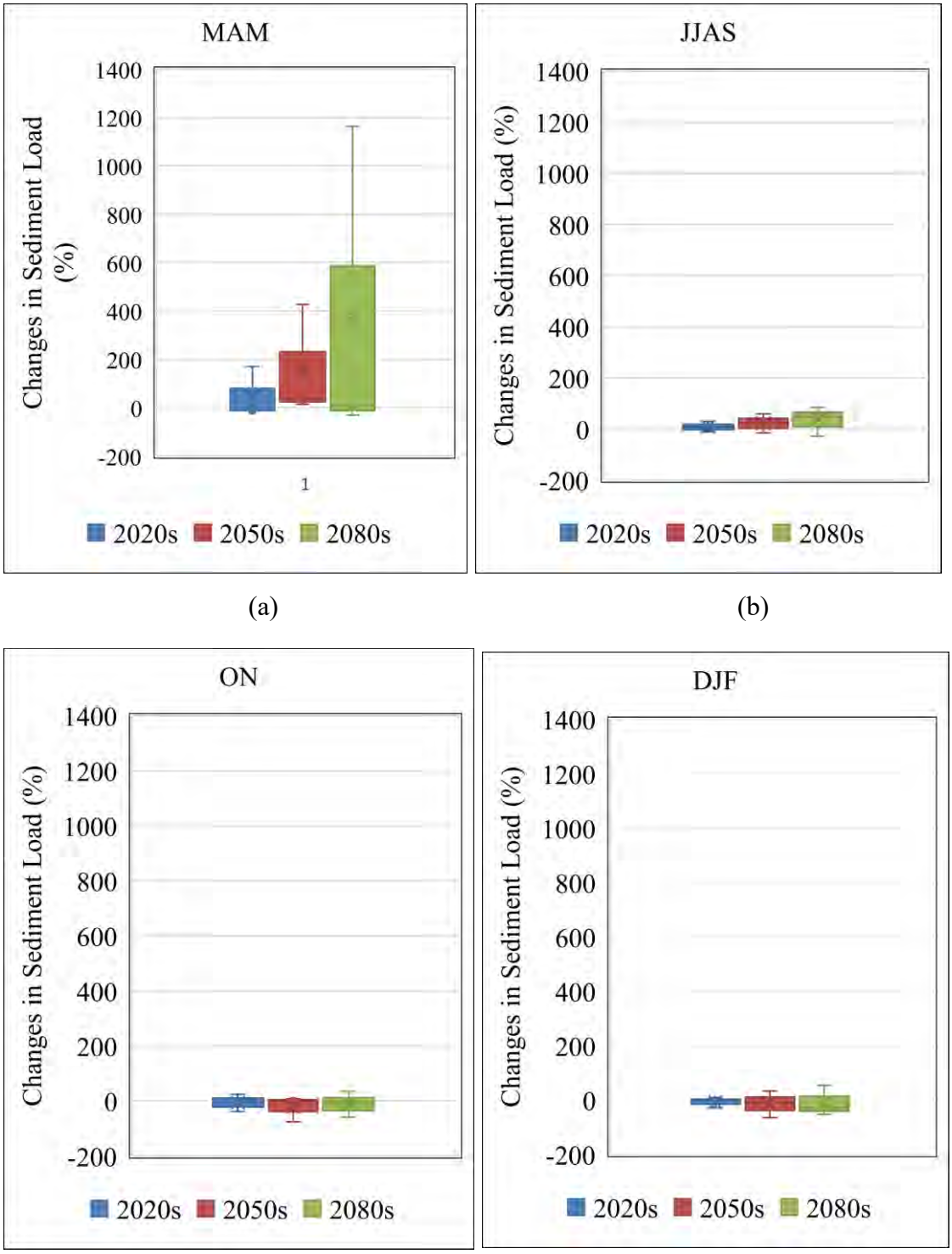

Figure 5.24: Percentage change in sediment load for (a) MAM, (b) JJAS (c) ON and (d) DJF

It reveals that though the uncertainty in percentage change in seasonal sediment load of pre-monsoon is higher than the monsoon season, the contribution of sediment load of pre-

monsoon is very much lower than the monsoon season. So, increase in sediment load for monsoon season will have much effect on changes in total sediment load at Bahadurabad transit of BRB.

5.4.5 Change of Mean Annual Sediment Load at Bahadurabad Transit

The model simulated percentage changes in the mean annual sediment load from the climate base period with respect to climate change scenario RCP 8.5 has been plotted in Figure 5.25. Figure 5.26 shows boxplots of differences in the annual average sediment load simulated by the selected RCM models with respect to the climate normal period. The percentage changes in average annual sediment load from baseline period for 2020s, 2050s and 2080s are 34%, 67% and 115% respectively. A gradual increase in average annual sediment load is found from 2020s to 2080s. The range of 75th and 25th percentile grows from 2020s to 2080s which indicates that uncertainty associated with the projected sediment load of BRB increases as we go distant future.

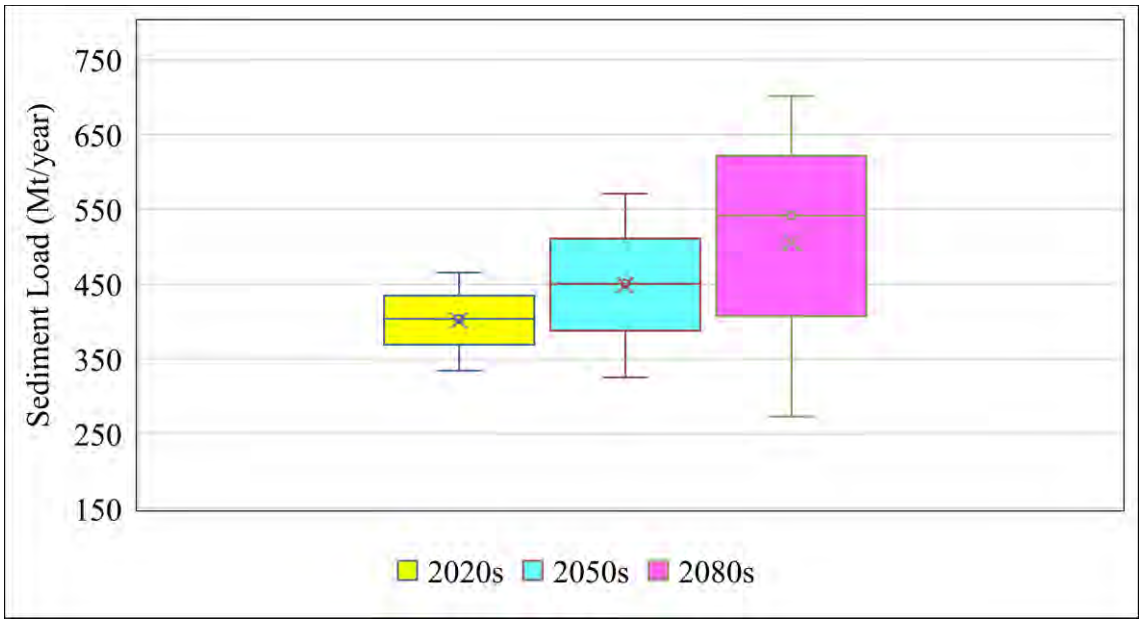

Figure 5.25: Future average annual sediment load for 2020s, 2050s and 2080s

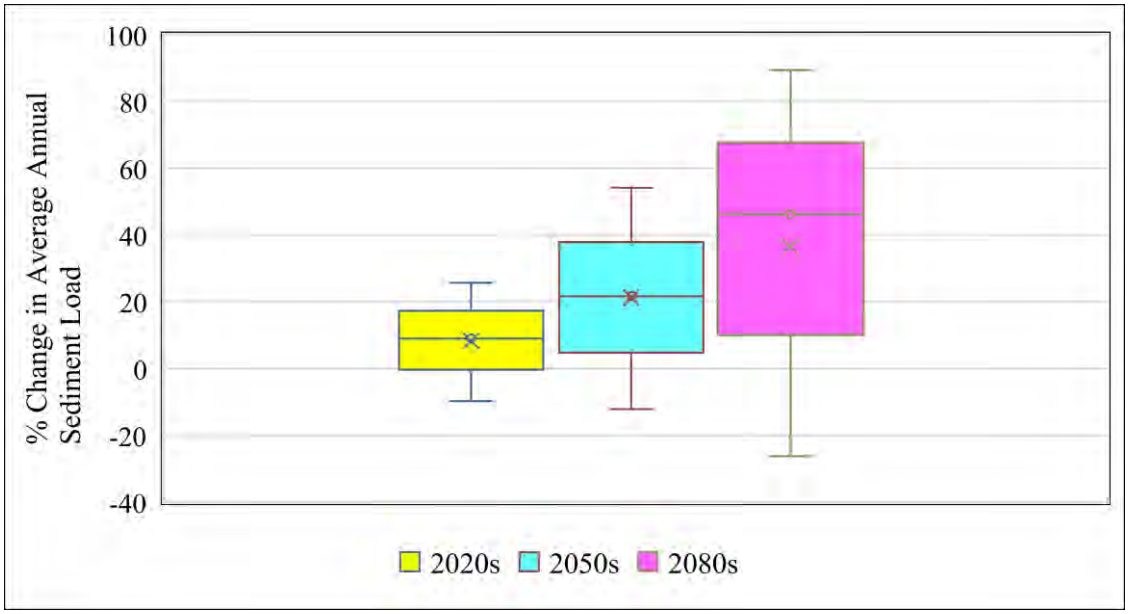

Figure 5.26: Change of future average annual sediment load from baseline

5.5 Impact of Land Use Changes on Sediment Load

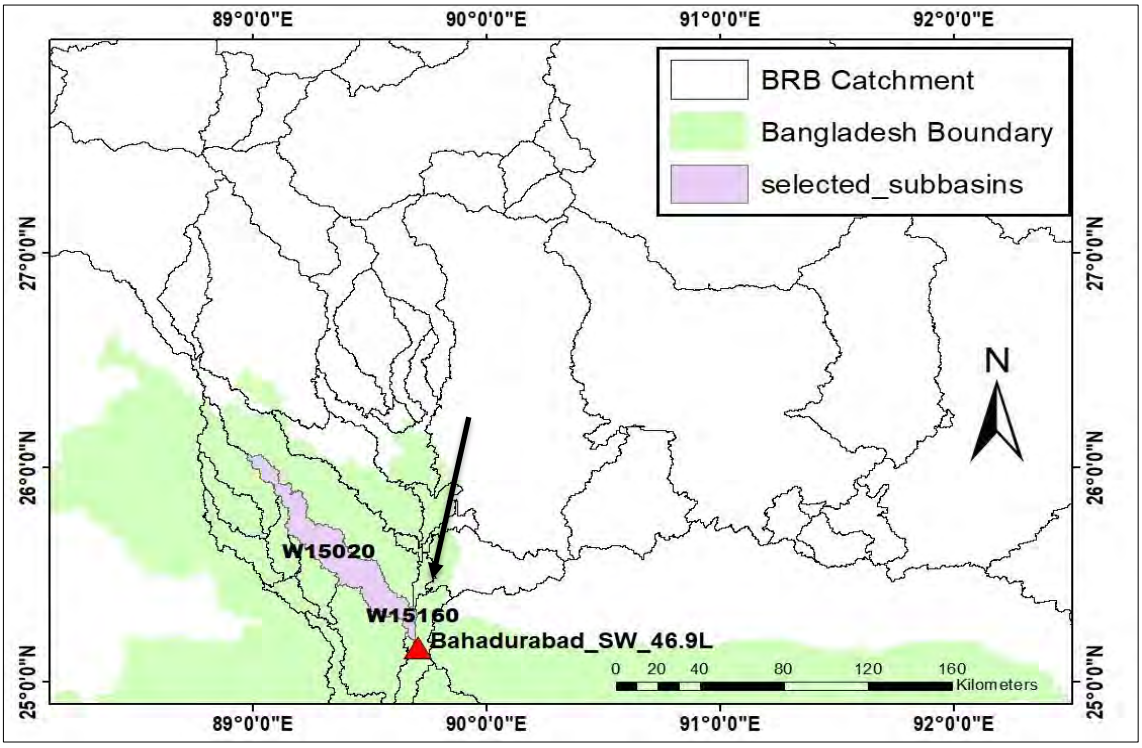

Figure 5.27: Selected subbasins for analysing urbanization effect on sediment load

At Bahadurabad Transit, total sediment load is coming through a reach and two lateral subbasins shown in Figure 5.27. The reach basically carries sediment load from the all subbasins located at upstream of that point. To analyse the impact on land use changes

on sediment load coming from basin area, additional 5% and 15% area of BRB has been considered as urbanized. Two lateral subbasins (W15020 and W15160) have been taken as example for showing the further analysis at Bahadurabad transit (SW 46.9L). The cover and management factor of these particular two subbasins are given in Table 5.5.

Table 5.5: Cover and management factor for urbanization of selected subbasins

	W15020	**W15160**
Present	0.0032	0.0670
Additional 5% urbanization	0.0030	0.0637
Additional 15% urbanization	0.0027	0.0569

Figure 5.28 and Figure 5.29 represent the monthly mean sediment load coming from these two subbasins to Bahadurabad transit (SW 46.9L). For increasing in urbanization, sediment load for two subbasins have decreasing trend.

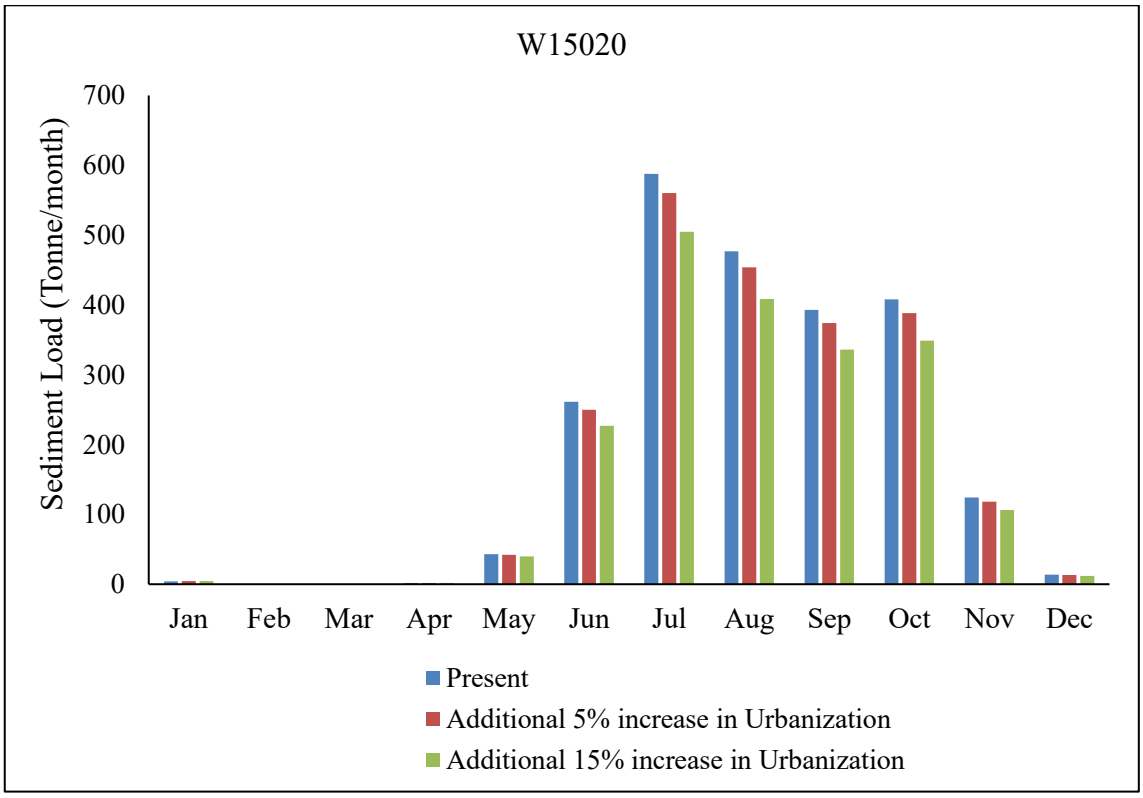

Figure 5.28: Mean monthly sediment load for subbasin W15020

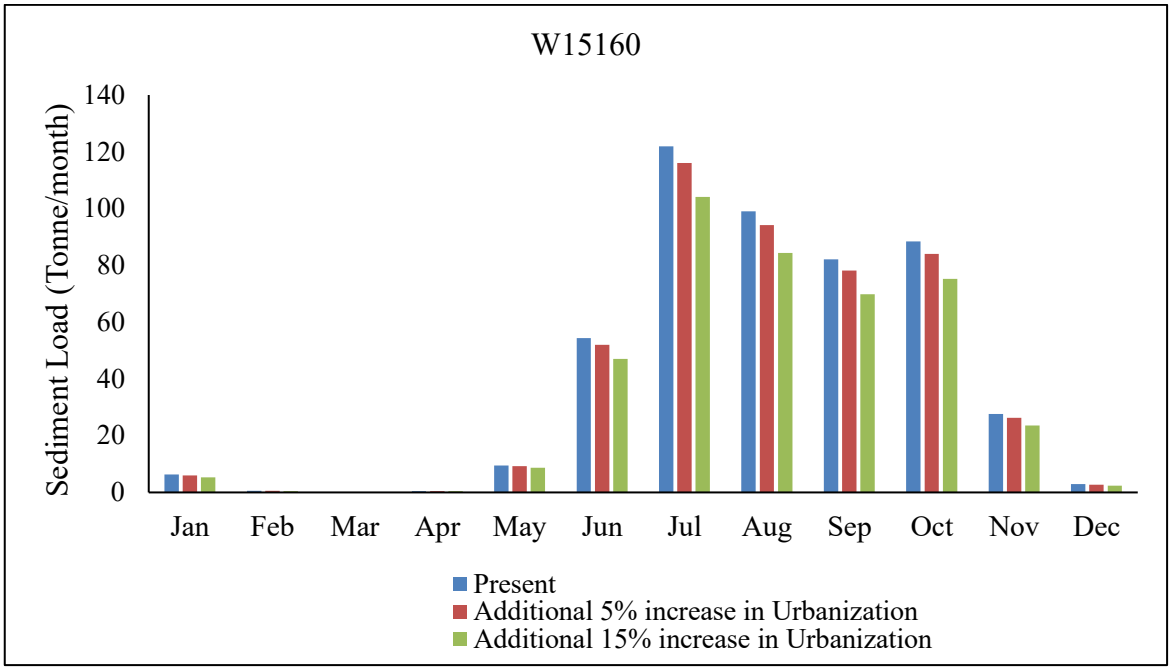

Figure 5.29: Mean monthly sediment load for subbasin W15160

Figure 5.30 and Figure 5.31 represent the mean seasonal sediment load coming from these two subbasins to Bahadurabad transit (SW 46.9L). Figure 5.32 indicates percentage change in seasonal sediment load for two representative subbasins of BRB. For increasing in urbanization, sediment load for two subbasins for all four seasons have decreasing trend.

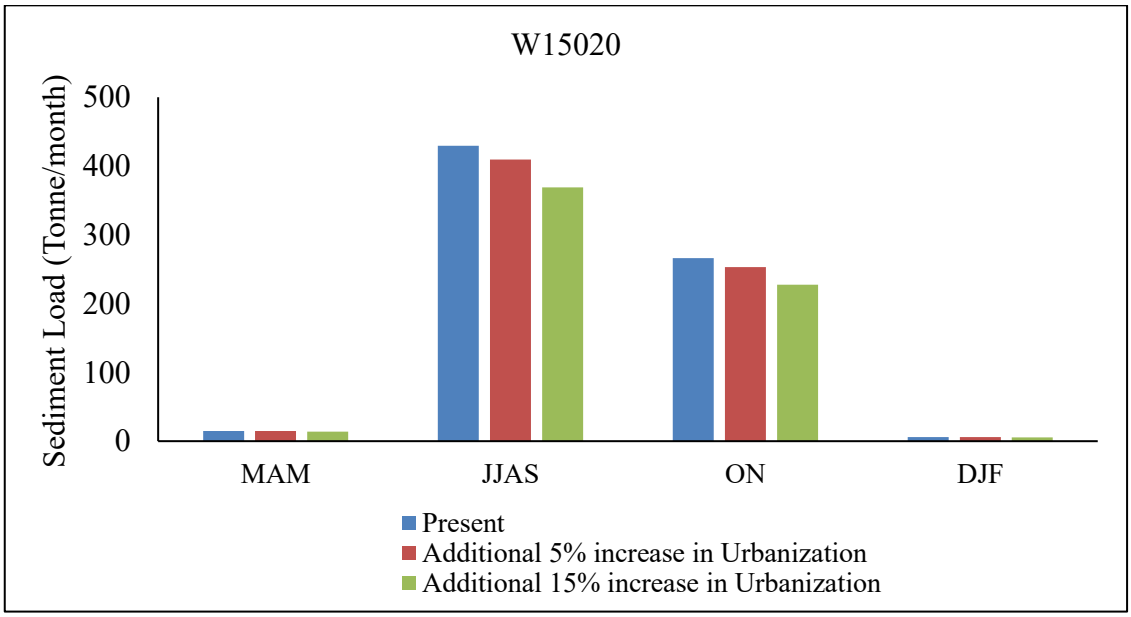

Figure 5.30: Mean seasonal sediment load for subbasin W15020

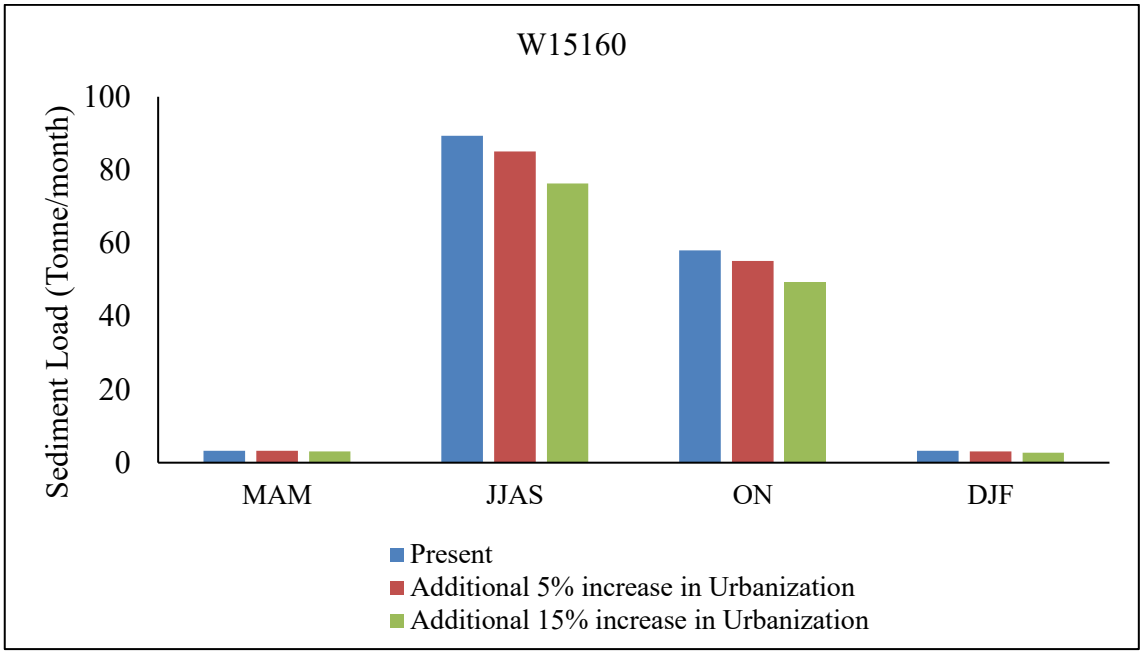

Figure 5.31: Mean seasonal sediment load for subbasin W15160

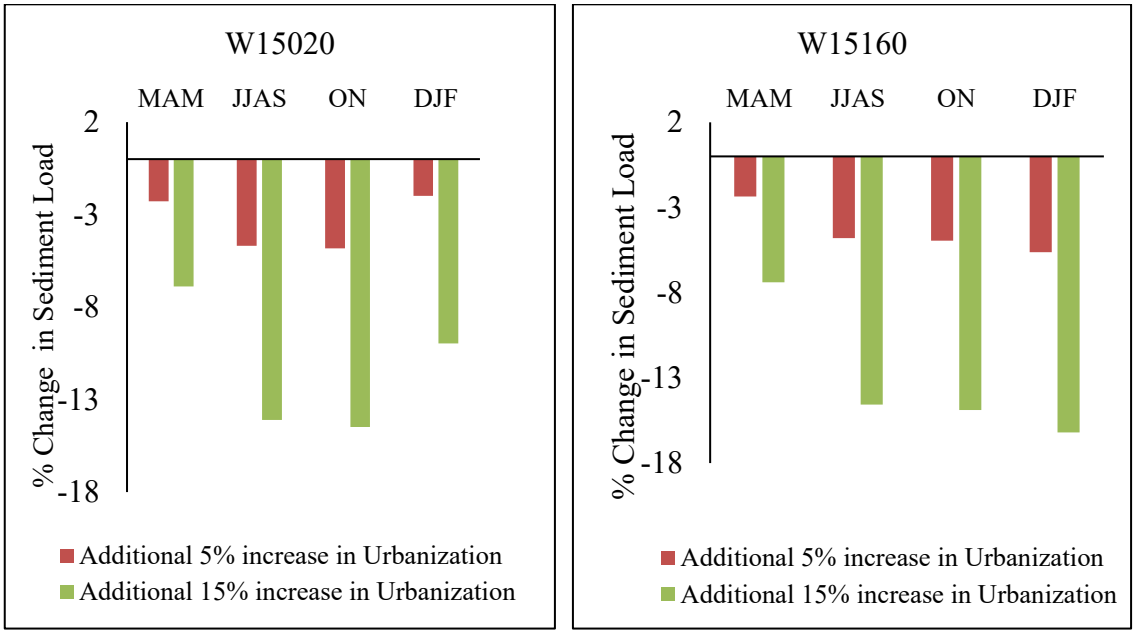

Figure 5.32: Change of seasonal sediment load for subbasin W15020 and W15160

Table 5.6: Percentage change in average annual sediment load for urbanization

Subbasin name	Additional 5% urbanization	Additional 15% urbanization
W15020	-4.64	-14.02
W15160	-4.80	-14.54

The percentage changes in average annual sediment load for both subbasins are shown in Table 5.6. It has been found that for increase in urbanization, average annual sediment load for both subbasins decrease linearly. For assuming 5 and 15% additional increase in urbanization in BRB, sediment load coming from basin area at Bahadurabad transit decreases about 4.7% to 14.3%.

From Table 5.7, it has been found that, for additional increase in urbanization about 5% and 15% in BRB, the changes in annual average sediment load are about -0.54% and 0.26%. It reveals that for a hypothetical addition about 5% and 15% urbanization throughout the basin will not make any representative change in average annual sediment load at Bahadurabad transit (SW 46.9L).

Table 5.7: Average annual sediment load at Bahadurabad Transit considering urbanization in BRB

	Calibrated/validated Model	Additional 5% urbanization	Additional 15% urbanization
Jan	0.04	0.04	0.04
Feb	0.06	0.07	0.07
Mar	1.77	1.81	1.87
Apr	6.97	7.07	7.42
May	41.51	41.54	41.96
Jun	92.66	93.19	93.17
Jul	109.32	108.77	107.67
Aug	56.09	53.83	56.41
Sep	37.33	36.83	38.07
Oct	20.12	20.71	20.11
Nov	3.94	3.98	3.98
Dec	0.39	0.39	0.39
Total sediment load (Mt/year)	370.20	368.22	371.17
% change		-0.54	0.26

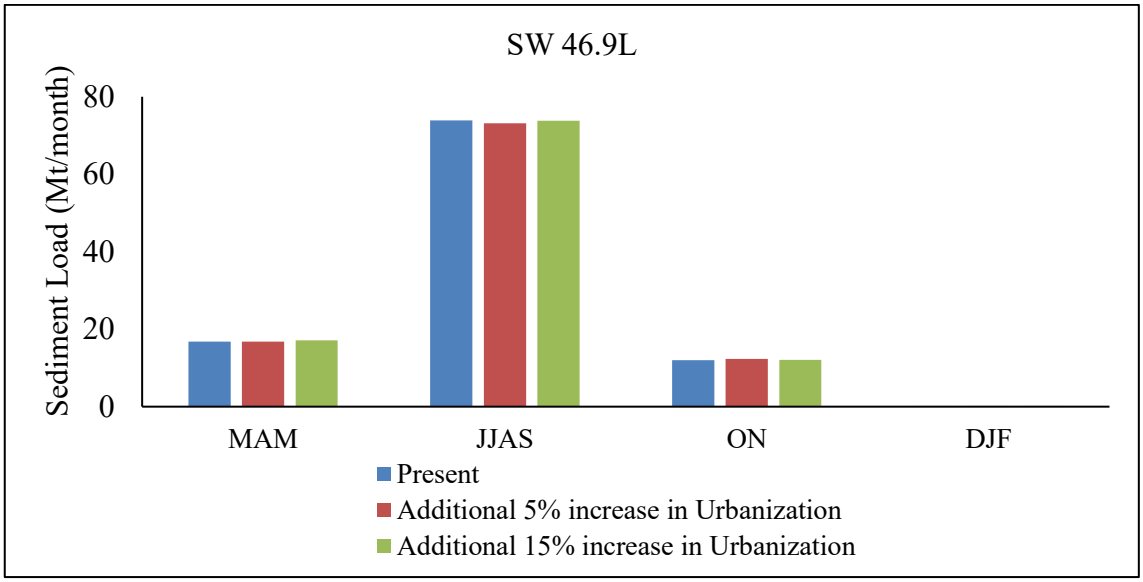

Figure 5.33: Mean seasonal sediment load at Bahadurabad transit (SW46.9L)

Figure 5.33 represents variation of average seasonal sediment load at Bahadurabad transit for present condition together with 5% and 15% additional increase in urbanization by changing impervious area and cover and management factor of BRB. The seasonal estimation of sediment load for BRB also do not show any representative change for additional 5% and 15% urbanization from the present condition.

5.6 Discussions

In 1960s sediment load for BRB was about 555 Mt/year measured by BWDB (Coleman, 1969). The measurements of FAP 24 in the early 1990s shows that suspended bed material load was about 402 Mt/year in this river which is much less than in the 1960s. Fischer et al. (2016) estimated annual sediment load using HEC-RAS which was about 368 Mt/year sediment load at Bahadurabad Transit of the Brahmaputra river. In this study, average annual sediment load at Bahadutrabad Transit was 370.20 Mt/year for the calibration/validation period.

The change in discharge considering an increase and decrease in precipitation was found almost linearly shown in Figure 5.3 similar like previous study (Alam et al., 2016). For sediment load at Bahadurabad Transit, model has been found linearly sensitive for increase/decrease in rainfall (Figure 5.4). But for temperature change from 2 to 6 Degree C, simulated discharge and sediment load are not found sensitive (Figure 5.5 and Figure 5.6) as snow melting process for around 5% area of BRB is not considered in this study.

For impact analysis of climate, Fischer et al. (2016) increased about 26% in flow in HEC-RAS model and for this, sediment load was increased about 49% at Bahadurabad Transit. In this study, the percentage changes in average annual flow and average annual sediment load at Bahadurabad transit (SW 46.9L) from baseline period for 2020s, 2050s and 2080s are 18%, 27%, 61% (Figure 5.16) and are 34%, 67%, 115% (Figure 5.26) respectively.

Due to a hypothetical addition in urbanization area about 5% and 15% for BRB, the sediment load coming from basin area decreases almost linearly with respective increase in urbanization. But, at Bahadurabad transit (SW 46.9L), the average annual and seasonal sediment load remains almost same as the present condition. It reveals that the decrease amount of sediment load coming from the basin area has been adjusted with the volume of sediment load carried by the increased amount of overland flow due to urbanization.

CHAPTER 6
CONCLUSIONS AND RECOMMENDATIONS

6.1 Conclusions

Brahmaputra River Basin (BRB), like other watersheds in many parts of the world, is poorly gauged or not gauged. Streamflow and sediment data are not available. In this study, grid-based rainfall data products from NASA POWER have been considered as precipitation source. Soil Moisture Accounting model (SMA) has been used instead of SCS curve number model to simulate continuous runoff at Bahadurabad transit (SW 46.9L) of BRB. Sensitivity analysis of SMA algorithm parameters has been done to provide a ranking of these parameters which provide a good assistance during calibration process. Soil percolation (mm/hr) and GW2 storage (mm) are the most and least sensitive parameter have been found for BRB.

The NSE, PBIAS and RSR values are 0.65, -20.92, 0.59 and 0.54, -23.40, 0.68 for calibration and validation period of hydrological model respectively. These statistics establishes the basis for developing sediment model and conducting climate change impact on sediment load based on the simulations of HEC-HMS. The co-efficient of determination (R^2) values are 0.76 for calibration and 0.71 for validation period respectively has shown a satisfactory correlation between simulated and observed discharge at Bahadurabad transit of BRB.

Surface erosion and sediment model has been calibrated from 1983-1996 and validated for 1997-2010 time period. Different required values for setup this model has been obtained from hydrological model and secondary literature and data sources. It has been found that annual average sediment load at Bahadurabad transit for Brahmaputra river basin is about 370.20 Mt/year for 1983-2010. Particularly, for year 1993-1996, it has been found about 379.08 Mt3/year which is close to the analysis done by Delft Hydraulics.

Sensitivity analysis for changing precipitation about -25% to 40% and temperature about 2 to 6-degree C has been performed. The result shows that BRB is almost equally sensitive to a reduction and increase in precipitation for discharge and sediment load. For -25% to 40% changes of baseline precipitation, discharge varies from -26.62% to 41.94%

of average annual discharge of base period. Similarly, average annual sediment load varies from -31.34% to 41.92% of climatic base period values.

The changes in annual average precipitation for 2010-2039, 2040-2069 and 2070-2099 from the climatic base period (1980-2009) for all three RCMs forced by eight GCMs obtained from CORDEX database have been analyzed to select specific models for doing impact analysis on sediment load considering driest, moderate wet and wettest condition. Only changes in precipitation has been considered for further climate change impact assessment as the model is found as highly sensitive for precipitation found in sensitivity analysis.

The percentage changes in average annual flow and average annual sediment load at Bahadurabad transit (SW 46.9L) from baseline period for 2020s, 2050s and 2080s are 18%, 27%, 61% and are 34%, 67%, 115% respectively. A gradual increase in average annual flow and average annual sediment load is found from 2020s to 2080s. The range of 75th and 25th percentile grows from 2020s to 2080s which indicates that uncertainty associated with the projected flow and sediment load of BRB increases as we go distant future.

The change in the quartiles of the pre-monsoonal (MAM) and monsoonal (JJAS) seasonal discharges and sediment load has been found to be increasing from 2020s towards the 2050s and 2080s, whereas, for post-monsoon (ON) and Dry (DJF) season, it has a decreasing trend. The uncertainty in percentage change in seasonal discharge and seasonal sediment load of pre-monsoon is higher than the monsoon season, but, the contribution of discharge and sediment load of pre-monsoon is very much lower than the monsoon season. So, increase in discharge and sediment load for monsoon season will have much effect on changes in total discharge and sediment load at Bahadurabad transit of BRB.

It has been found that for increase in urbanization, average monthly, seasonal and annual sediment load from BRB catchment area decreases linearly. For assuming 5% and 15% additional increase in urbanization in BRB, annual average sediment load coming from basin area at Bahadurabad transit decreases about 4.7% to 14.3%. Due to urbanization, increase in impervious area will increase overland flow contribution at Bahadurabad transit which will provide more sediment load from river. At the same time, decrease in

sediment load coming from catchment occurs as the urbanized area is very less susceptible to erosion. These two reverse condition will may provide almost same amount of average monthly, seasonal and annual sediment load at Bahdurabad transit (SW 46.9L).

6.2 Recommendations

Based on the results and the experience gained during the study, the following recommendations are made.

- The model was calibrated and validated at Bhahadurabad transit (SW 46.9L) as sediment data was available at this station only for Brahmaputra River Basin within our country. More calibration point in this model will increase the better representation of hydrological and sediment transport processes of BRB.
- As there exists numerous flow regulations in the upstream of Bangladesh constructed after 2010, it is recommended to calibrate and validate the model after including DAM and reservoirs data through Indo-Bangladesh Join River Commission, or other sources. It may give more better estimation of sediment load considering for climate change and upstream development condition.
- SMA parameters can be better estimated by measured data of soil and land use properties. Also, better calibration of surface erosion and sediment model can be done by measured regular sediment load data at Bahadurabad transit (SW46.9L).
- In the present study, land cover map was taken for at the beginning of 21st century. For better approximation of future projected flow and sediment load, land use scenarios by doing remote sensing analysis using satellite images can be incorporated in this model. It will give higher sensitivity of model due to land use changes condition.
- This model is unable to incorporate snow melt for 5% area of BRB. This incorporation may be done in future for better estimation of discharge and sediment load in dry season when rainfall is unavailable.

REFERENCES

Akbor, A. F. M. S. E., Hossain, F., Sikder, S., Shum, C. K., Tseng, S., Yi, Y., Turk, F. J., and Limaye, A., 2014. Satellite Precipitation Data-Driven Hydrological Modeling for Water Resources Management in the Ganges, Brahmaputra, and Meghna Basin. *Earth Interactions*, 18(17), 1-25.

Apitz, S. E., 2012. Conceptualizing the role of sustaining ecosystem services: sediment-Ecosystem Regional Assessment (SEcoRA). *Sci Total Environ*, 415, 9–30. doi:10.1016/j.scitotenv.2011.05.060

Alam, S., 2015. *Impact of Climate Change on Future Flow of Brahmaputra river basin using SWAT model.* M.Sc. Engineering Thesis, Department of Water Resources Engineering, Bangladesh University of Engineering and Technology (BUET).

Alam, S., Ali, M.M. and Islam, Z. 2016. Future Streamflow of Brahmaputra River Basin under Synthetic Climate Change Scenarios. *Journal of Hydrologic Engineering*, 21(11), Article ID: 05016027.

Bedient, P. B. and Huber, W. C., 1992. *Hydrology and floodplain analysis.* Addison-Wesley, New York, NY.

Bennett, T., 1988. *Development and application of a continuous soil moisture accounting algorithm for the hydrologic engineering center hydrologic modeling system (HEC-HMS)*. M.S. Thesis. Dept. of Civil and Environmental Engineering, University of California, Davis, California.

Bhattacharya, T., Aggarwal, Dr. S. P., Garg, Dr. V., 2013. Estimation of Water Balance Components of Chambal River Basin Using a Macroscale Hydrology Model. *International Journal of Scientific and Research Publications*, 3(2), 1-6, ISSN 2250-3153.

Center for Environmental and Geographic Information Services (CEGIS), 2010. *Impact of Climate Change on Morphological Processes in Different river of Bangladesh*.

Chalov, S. R., Jarsjo¨, J., Kasimov, N. S., Romanchenko, A. O., Pietron´, J., Thorslund, J., Promakhova, E. V., 2015. *Spatio-temporal variation of sediment transport in the Selenga River Basin, Mongolia and Russia*. Environ Earth Sci., 73(2), 663–680. doi:10.1007/s12665-014-3106-z

Coleman, J. M., 1969. *Brahmaputra River: channel processes and sedimentation.* Sedimentary Geology 3, 129–239.

Chowdhury, J. U., Haque, A., Datta, A. R. and Hassan, A., 2008. *Impact of Climate Change on Surface Water Flow in Bangladesh*. Tech. Rep. Classic, Institute of Water and Flood Management, BUET, Dhaka.

Chu, T. W. and Shirmohammadi, A., 2004. Evaluation of the swat model's hydrology component in the piedmont physiographic region of Maryland. *ASAE*, 47(4), 1057-1073.

CORDEX Database. (Available at: http://www.cordex.org/data-access/esgf/. Accessed on: 28/01/2017).

Cudworth, A. G., 1989. *Flood hydrology manual.* US Department of the interior, Bureau of Reclamation, Washington, DC.

Cunge, J. A., 1969. On the subject of a flood propagation computation method (Muskingum method). *Journal of Hydraulic Research*, 7(2), 205-230.

Dehvari, A., 2014. Estimation of surface runoff and sediment yield using WEPP model in Southern Ontario, Canada. *International Journal of Agriculture and Crop Sciences*, 7(11), 876-889.

Digital Elevation Model. (Available at: http://srtm.csi.cgiar.org/. Accessed on: 15/06/2016).

Engelund, F. and Hansen, E. (1967). A Monograph of Sediment Transport in Alluvial Streams. Teknisk Forlag, Copenhagen.

Feldman, A. D., 2000. *Hydrologic Modeling System HEC-HMS Technical Reference Manual.* U.S. Army Corps of Engineers, Hydrologic Engineering Center (HEC), 54, 73.

Flood Action Plan 24. Delft Hydraulics, DHI and Leeds University, 1996a. *FAP24 River Survey Project, Special Report 9, Bedform and bar dynamics in the main rivers of Bangladesh* (prepared for FPCO), Dhaka, Bangladesh, 107.

Flood Action Plan 24. Delft Hydraulics and DHI, 1996. *FAP24 River Survey Project, Special Report 13, Sediment Transport Predictors* (prepared for FPCO), Dhaka, Bangladesh, 27-30.

Flood Action Plan 24. Delft Hydraulics and DHI, 1996c. *FAP24 River Survey Project, Final Report – Annex 4: Sedimentology,* (prepared for FPCO), Dhaka, Bangladesh.

Friedlingstein, P., Andrew, R. M., Rogelj, J., Peters, G. P., Canadell, J. G., Knutti, R., Luderer, G., Raupach, M. R., Schaeffer, M., Vuuren, D. P. van & Le Quéré, C.,

2014. Persistent growth of CO2 emissions and implications for reaching climate targets. *Nature geoscience,* 7(10), 709-715.

Gain, A. K., Immerzeel, W. W., Sperna-Weiland, F. C., and Bierkens, M. F. P., 2011. *Impact of climate change on the stream flow of lower Brahmaputra: trends in high and low flows based on discharge-weighted ensemble modeling*. Hydrology and Earth System Sciences Discussions, 8(1), 365-390.

Ghosh, S. and Dutta, S., 2011. *Impact of Climate and Land Use Changes on the Flood Vulnerability of the Brahmaputra Basin.* Geospatial World Forum, 18-21 january, 2011, Hyderabad, India, 364.

Ghosh, S. and Dutta, S., 2012. Impact of climate change on flood characteristics in Brahmaputra basin using a macro-scale distributed hydrological model. *Journal of earth system science,* 121(3), 637-657.

Goswami, D. C., 1985. Brahmaputra river, Assam, India: Physiography, basin denudation, and channel aggradation. *Water Resources Research*, 21, 959–978. doi:10.1029/WR021i007p00959

Gupta, H. V., Sorooshian, S. and Yapo, P. O., (1999). Status of automatic calibration for hydrologic models: Comparison with multilevel expert calibration. *Journal of Hydrologic Eng*ineering, 4(2), 135-143.

Haifang, Y., Changxing, S., Wenwei, S., Jianbin, B. and Hui, Y., 2015. Impacts of Climate Change and Human Activities on Runoff and Sediment Load of the Xiliugou Basin in the Upper Yellow River. *Advances in Meteorology*, 2015, Article ID 481713, 12. doi:10.1155/2015/481713

Hay, L. E. and. McCabe, G. J., 2010. Hydrologic effects of climate change in the Yukon river basin. *Climatic Change*, 100(3-4), 509-523.

JRCB, 2018. About Joint Rivers Commission Bangladesh. (Available at: http://www.jrcb.gov.bd/basin_map.html. Accessed on: 11/05/2018).

Immerzeel, W., 2008. Historical trends and future predictions of climate variability in the Brahmaputra basin. *International Journal of Climatology*, 28, 243– 254.

Islam, M. R., Begum, S. F., Yamaguchi, Y. and Ogawa, K., 1999. The Ganges and Brahmaputra rivers in Bangladesh: basin denudation and sedimentation. *Hydrological Processes*, 13, 2907-2923.

Islam, Z. and Gan, T., 2015. Hydrologic Modeling of the Blue River Basin Using NEXRAD Precipitation Data with a Semi distributed and a Fully Distributed

Model. *Journal of Hydrological. Engineering*, 10.1061/(ASCE)HE.1943-5584.0001179, 04015015.

IWM and CCC, 2008. *Impact Assessment of Climate Change and Sea Level Rise on Monsoon Flooding*. Institute of Water Modelling and Climate Change Cell, Department of Environment, Ministry of Environment and Forests, Government of Bangladesh.

Jagers, H.R.A., 2003. *Modelling planform changes of braided rivers*. PhD thesis, University of Twente, The Netherlands, 313.

Jiang, Tao, Chenm, Y. D., Xu, C. Y., Chenv, X., Chen, X. and Singh, V. P., 2007. Comparison of hydrological impacts of climate change simulated by six hydrological models in the Dongjiang basin, south china. *Journal of Hydrology*, 336, 316-333. doi:10.1016/j.jhydrol.2007.01.010

Jung, H. C., Hamski, J., Durand, M., Alsdorf, D., Hossain, F., Lee, H., Hossain, A. K. M. A., Hasan, K., Khan, A. S., Hoque, A. K. M. Z., 2010. Characterization of complex fluvial systems using remote sensing of spatial and temporal water level variations in the Amazon Congo, and Brahmaputra rivers. *Earth Surf Proc Land*, 35(3), 294–304. doi:10.1002/esp.1914

Khaled, M., Islam, A. K. M. S., Islam, G. M. T., Alfieri, L., Bala, S. J. and Khan, M. J. U., 2017. Impact of High-End Climate Change on Floods and Low Flows of the Brahmaputra River. *Journal of Hydrologic Engineering,* 22(10). https://doi.org/10.1061/(ASCE)HE.1943-5584.0001567

Khoi, D. N. and Suetsugi, T., 2013. Assessment of Climate Change Impacts on Hydrology and Sediment Yield in The Be River Catchment, Vietnam. *Journal of Japan Society of Civil Engineers, Ser. B1 (Hydraulic Engineering),* 69(4), I_31-I_36, 2013.

Legates, D. R. and G. J. McCabe, G. J., 1999. Evaluating the use of goodness-of-fit measures in hydrologic and hydroclimatic model validation. *Water Resources Res.* 35(1), 233-241.

Liu, Y., 2015. Transboundary water cooperation on the Yarlung Zangbo/Brahmaputra—a legal analysis of riparian state practice. *Water Int.,* 40(2), 354–374. doi:10.1080/02508060.2015.1015319.

Merwade, V., 2012. *Terrain Processing and HMS-Model Development using HEC-GeoHMS.* Technical report. School of Civil Engineering, Purdue University.

Merwade, V., 2012. *Watershed and stream network delineation using arc hydro tools*. Technical report. School of Civil Engineering, Purdue University.

Miller, W. A. and Cunge, J. A., 1975. *Simplified equations of unsteady flow.* K. Mahmood and V. Yevjevich, eds., Unsteady flow in open channels, I, Water Resources Publications, Ft. Collins, CO.

Mirza, M. M. Q., Warrick, R. A. and Ericksen, N. J., 2003. The implications of climate change on floods of the Ganges, Brahmaputra and Meghna rivers in Bangladesh. *Clim. Change,* 57(3), 287–318.

Mahanta, P. C., Zaman, D. A. M., Newaz, S. M. S., Rahman, S. M. M., Mazumdar, T. K., Choudgury, R., Borah, P. J. and Saikia, L., 2014. *Physical Assessment of the Brahmaputra River.* Ecosystems for Life: A Bangladesh-India Initiative, IUCN, International Union for Conservation of Nature.

Moriasi, D. N., Arnold, J. G., Van Liew, M. W., Bingner, R. L., Harmel, R. D., and Veith, T. L, 2007. Model Evaluation Guidelines for Systematic Quantification of Accuracy in Watershed Simulations. *Transactions of the ASABE,* 50(3), 885−900. ISSN 0001−2351.

Nash, J. E. and Sutcliffe, J. V., 1970. River flow forecasting through conceptual models: Part 1, A discussion of principles. *J. Hydrology*, 10(3), 282-290.

Nishat, B. and Rahman, S. M.M., 2009. Water Resources Modeling of the Ganges-Brahmaputra-Meghna River Basins Using Satellite Remote Sensing Data. *Journal of The American Water Resources Association*, 45(6), 1313-1327.

Olesen, K. W., Ammentorp, H.C. and Peterson, N. H., 2001. Mega deltas and the climate change challenges, in: 11th International Symposium on River Sedimentation, Stellenbosch, South Africa, 6–9 September.

Paul, S., 2014. *Assessment of change in future flow of Brahmaputra Basin applying SWAT model using multi-member ensemble climate data.* M.Sc. (Water Resources Development) Thesis, Institute of Water and Flood Management, Bangladesh University of Engineering and Technology (BUET).

Pervez, M. S. and Henebry, G. M., 2015. Assessing the impacts of climate and land use and land cover change on the freshwater availability in the Brahmaputra river basin. *Journal of Hydrology: Regional Studies*, 3, 285–311.

Piontek, F., Müller, C., Pugh, T. A. M., Clark, D. B., Deryng, D., Elliott, J., de Jesus Colón González, F., Flörke, M., Folberth, C., Franssen, W., Frieler, K., Friend, A.

D., Gosling, S. N., Hemming, D., Khabarov, N., Kim, H., Lomas, M. R., Masaki, Y., Mengel, M., Morse, A., Neumann, K., Nishina, K., Ostberg, S., Pavlick, R., Ruane, A. C., Schewe, J., Schmid, E., Stacke, T., Tang, Q., Tessler, Z. D., Tompkins, A. M., Warszawski, L., Wisser, D. & Schellnhuber, H. J. (2013) *Multisectoral climate impact hotspots in a warming world*. Proceedings of the National Academy of Sciences, 111, 3233-3238.

Ponce, V. M. and Yevjevich, V., 1978. Muskingum-Cunge method with variable parameters. *Journal of the Hydraulics Division,* ASCE, 104(HY12), 1663-1667.

Ponce, V. M., 1986. Diffusion wave modelling of catchment dynamics. *Journal of the Hydraulics Division,* ASCE, 112(8), 716-727.

Rajib, M. A., Rahman M. M. and McBean E. A., 2011. Application of regional climate model simulation and flow data for assessing future water availability in the river jamuna. *Int. J. Environ. Sci*, 1, 884-896.

Rasul, G., 2014. Why Eastern Himalayan countries should cooperate in transboundary water resource management. *Water Policy,* 16(1), 19–38. doi:10.2166/wp.2013.190

Ray, P. A., Yang, Y. C. E., Wi, S., Khalil, A., Chatikavanij, V., Brown, C., 2015. Room for improvement: hydroclimatic challenges to poverty-reducing development of the Brahmaputra River basin. *Environ. Sci. Policy*, 54, 64–80. doi:10.1016/j.envsci.2015.06.015.

Rawls, W. J., Brakensiek, D. L. and Saxton, K. E., 1982. Estimation of soil water properties. *American Society of Agricultural Engineers,* 25(5), 1316-1320.

Renard, K. G., Foster, G. R., Weesies, G. A., McCool, D. K. and Yoder, D. C. (Coordinators). 1995. *Predicting Soil Erosion by Water: A Guide to Conservation Planning with the Revised Universal Soil Loss Equation (RUSLE).* U.S. Department of Agriculture, Agriculture Handbook No. 703.

Robert P. S. and Hilborn, D., 2015. *Universal Soil Loss Equation (USLE)*. (Available at: http://www.omafra.gov.on.ca/english/engineer/facts/12-051.htm. Accessed on: 15/01//2018)

Rossi, C. G., Dybala, T. J., Moriasi, D. N., Arnold, J. G., Amonett, C., and Marek, T., 2008. Hydrologic calibration and validation of the soil and water assessment tool for the Leon River watershed, *Soil Water Conservation,* 6, 533–541.

Rouf, T., 2015. *Flood Inundation Map of Sirajgonj District using Mathematical Model.* M.Sc. Engineering Thesis, Department of Water Resources Engineering, Bangladesh University of Engineering and Technology (BUET).

Salehin M., Chowdhury, J. U., and Islam, A. K. M. S., 2011. *Development of a water resources model as a decision support tool for national water management*. Technical report, Institute of Water and Flood Management, BUET.

Santos, I. D., Andriolo M. V., Gibertoni R. C. and Kobiyama, M., 2010. *Use of the SWAT model to evaluate the impact of different land use scenarios on discharge and sediment transport in the Apucaraninha River Watershed, southern Brazil.* Sediment Dynamics for a Changing Future (Proceedings of the ICCE symposium held at Warsaw University of Life Sciences-SGGW, Poland, 14-18 June 2010, IAHS Publication 337, 322-328.

Sarker, M. H., 2009. (unpublished). *Morphological response of the Brahmaputra-Jamuna-Padma- Lower Meghna River to the Assam earthquake of 1950*. PhD thesis, University of Nottingham, UK.

Sarker, M. H. and Thorne, C. R., 2006. *Morphological response of the Brahmaputra-Padma-Lower Meghna River system to the Assam earthquake of 1950. In: Braided Rivers: Process, Deposits, Ecology and Management* (Eds Sambrook Smith, G. H., Best, J. L., Bristow, C. S. and Petts, G.), Special Publication of the International Association of Sedimentologists, No. 36, Blackwell, Oxford, 289–310.

Sarker, M. H., Thorne, C. R., Akter, M. N., Ferdous, M. R., 2013. Morpho-dynamics of the Brahmaputra–Jamuna River, Bangladesh. *Geomorphology*, 215, 45-59.

Scharffenberg, W., 2015. *Hydrologic Modeling System HEC HMS User manual*, United States Army Corps of Engineers, Hydrologic Engineering Center (USACE_HEC), Davis, California, Version 4.1.

Shampa, 2015. *Dynamics of Bar in the Braided River Jamuna*. M.Sc. Engineering Thesis, Department of Water Resources Engineering, Bangladesh University of Engineering and Technology (BUET).

Shrestha, B., Babel, M. S., Maskey, S., Griensven, A. V., Uhlenbrook, S., Green, A. and Akkharath, I., 2013. Impact of climate change on sediment yield in the Mekong River basin: a case study of the Nam Ou basin, Lao PDR. *Hydrol. Earth Syst. Sci.,* 17, 1–20.

Singh V. P., Sharma B., Shekhar C, Ojha, P., 2004. *The Brahmaputra Basin Water Resources.* Kluwer Academic Publishers, ISBN 1-4020-1737-5.

Singh, W. R. and Jain, M. K., 2015. Continuous Hydrological Modeling using Soil Moisture Accounting Algorithm in Vamsadhara River Basin, India. *Journal of Water Resource and Hydraulic Engineering*, 4(4), 398-408.

Snyder, F. F., 1938. *Synthetic unit-graphs*. Transactions, American Geophysics Union 19:447-454.

Sorooshian, S. and Gupta, K., 1995. Model calibration, in, Computer Models of Watershed Hydrology, edited by, Singh, P., *Water Resources Publications*, Colorado, USA, 53-105.

USACE, 1944. *Hydrology, San Gabriel River and the Rio Hondo above Whittier Narrows flood control basin.* US Army Engineer District, Los Angeles, CA.

USACE, 1987. *Derivation of a rainfall-runoff model to compute n-year floods for Orange County watersheds.* US Army Engineer District, Los Angeles, CA.

van Vuuren, D.P., Edmonds, J., Kainuma, M. et al., 2011. The representative concentration pathways: an overview. *Climatic Change,* 109(5). https://doi.org/10.1007/s10584-011-0148-z

Weather data. (Available at: http://power.larc.nasa.gov. Accessed on: 31/08/2016).

Williams, J. R., 1975. *Sediment-yield Prediction with Universal Equation Using Runoff Energy Factor.* In Present and Prospective Technology for Predicting Sediment Yield and Sources: Proceedings of the Sediment Yield Workshop. USDA Sedimentation Laboratory, Oxford, Mississippi.

Wischmeier, W. H. and Smith, D. D., 1978. *Predicting rainfall erosion losses: A guide to conservation planning.* USDA, Agriculture Handbook 537. U.S. Government Printing Office, Washington, DC.

XU, C. Y., 1999. Climate change and hydrologic models: A review of existing gaps and recent research developments. *Water Resources Management,* 13, 369-382.

Yu, W. H., Alam, M., Hassan, A., Khan, A. S., Ruane, A. C., Rosenzweig, C., Major, D. C., Thurlow, J., 2010. *Climate change risks and food security in Bangladesh,* South Asia Region, Agriculture and Rural Development Unit, Sustainable Development Department, The World Bank. Earthscan Ltd., London, UK, 144.

Zhang, J. Y., Wang, G. Q., Pagano, T. C., Jin, J. L., Liu, C. S., He, R. M. and Liu, Y. L., 2013. Using hydrologic simulation to explore the impacts of climate change on

runoff in the Huaihe river basin of china. *Journal of Hydrologic Engineering,* 18(11). https://doi.org/10.1061/(ASCE)HE.1943-5584.0000581

APPENDIX

Table 1: Future monthly flow (m^3/s) at SW 46.9L for 2020s

Month	Model 1	Model 2	Model 3
Jan	193.3	279.7	261.9
Feb	125.5	51.5	48.6
Mar	2035.9	451.0	247.1
Apr	10345.7	3782.9	2539.5
May	34467.1	18645.1	12167.5
Jun	56726.4	36741.9	31158.9
Jul	73293.7	57253.7	61323.9
Aug	71951.6	65233.7	71742.1
Sep	59779.7	56736.9	63161.8
Oct	36679.8	44863.7	45933.2
Nov	12457.0	20368.2	21603.3
Dec	2391.5	4913.4	4996.3

Table 2: % Change of future monthly flow at SW 46.9L from baseline for 2020s

Month	Model 1	Model 2	Model 3
Jan	2.0	-24.6	-26.4
Feb	25.3	-23.1	-7.9
Mar	355.6	-27.9	-36.4
Apr	126.0	-12.8	1.1
May	74.7	8.2	-5.5
Jun	34.6	-1.9	-13.2
Jul	12.4	-3.3	-1.5
Aug	9.0	1.4	5.6
Sep	3.8	-3.5	4.5
Oct	-2.7	1.2	3.7
Nov	-9.6	7.5	14.4
Dec	-16.0	7.0	14.2

Table 3: Future monthly sediment load (Mt/month) at SW 46.9L for 2020s

Month	Model 1	Model 2	Model 3
Jan	0.0071	0.0114	0.0090
Feb	0.0010	0.0005	0.0008
Mar	0.1498	0.0247	0.0122
Apr	1.6235	0.5846	0.4057
May	15.1996	6.2502	2.5918
Jun	58.1704	19.1212	10.7152
Jul	125.6600	62.9411	76.1054
Aug	147.2020	118.1383	144.8226
Sep	96.7230	89.8866	116.0684
Oct	19.0694	32.2646	46.2871
Nov	1.4778	4.5820	6.1879
Dec	0.1017	0.3759	0.3510

Table 4: Change of future monthly sediment load from baseline for 2020s

Month	Model 1	Model 2	Model 3
Jan	5.8	-33.1	-50.7
Feb	-61.2	-58.8	-57.5
Mar	702.9	-9.7	-37.1
Apr	124.0	-16.1	26.6
May	173.2	-10.2	-17.1
Jun	151.1	2.1	-17.4
Jul	38.7	-8.1	4.7
Aug	16.8	-11.8	9.0
Sep	6.4	-12.4	9.9
Oct	-38.2	-7.5	24.4
Nov	-33.6	33.0	22.9
Dec	-29.8	2.4	11.1

Table 5: Future monthly flow (m^3/s) at SW 46.9L for 2050s

Month	Model 1	Model 2	Model 3
Jan	79.9	299.7	354.0
Feb	122.6	45.5	42.2
Mar	2156.7	377.1	234.5
Apr	14707.6	2950.6	2118.4
May	44444.5	19966.1	13898.4
Jun	74660.9	43072.8	36262.7
Jul	83799.3	58169.1	66076.3
Aug	77293.4	61505.5	75359.2
Sep	59216.7	55076.1	68911.8
Oct	30064.9	43533.9	48426.9
Nov	8491.0	21148.0	22269.6
Dec	1354.2	5075.2	5394.2

Table 6: % Change of future monthly flow at SW 46.9L from baseline for 2050s

Month	Model 1	Model 2	Model 3
Jan	-57.9	-19.2	-0.5
Feb	22.4	-32.0	-20.0
Mar	382.6	-39.7	-39.6
Apr	221.3	-32.0	-15.6
May	125.3	15.9	7.9
Jun	77.2	15.1	1.0
Jul	28.5	-1.8	6.1
Aug	17.1	-4.4	10.9
Sep	2.8	-6.3	14.0
Oct	-20.2	-1.8	9.4
Nov	-38.4	11.7	17.9
Dec	-52.4	10.5	23.3

Table 7: Future monthly sediment load (Mt/month) at SW 46.9L for 2050s

Month	Model 1	Model 2	Model 3
Jan	0.0050	0.0091	0.0135
Feb	0.0017	0.0002	0.0003
Mar	0.1291	0.0144	0.0158
Apr	3.7337	0.4455	0.3008
May	29.4057	9.9554	3.6374
Jun	119.6427	28.1911	17.6096
Jul	182.6479	60.9462	92.7501
Aug	155.9112	106.5425	158.0047
Sep	70.9446	80.3828	131.7789
Oct	7.3672	33.3920	41.3859
Nov	0.8538	4.9786	4.5539
Dec	0.0481	0.3389	0.4336

Table 8: Change of future monthly sediment load from baseline for 2050s

Month	Model 1	Model 2	Model 3
Jan	-25.4	-46.4	-26.0
Feb	-32.6	-78.7	-82.5
Mar	591.9	-47.6	-18.6
Apr	415.1	-36.0	-6.1
May	428.6	43.0	16.3
Jun	416.4	50.6	35.7
Jul	101.6	-11.0	27.7
Aug	23.7	-20.4	18.9
Sep	-22.0	-21.7	24.8
Oct	-76.1	-4.3	11.2
Nov	-61.6	44.5	-9.5
Dec	-66.8	-7.7	37.3

Table 9: Future monthly flow (m^3/s) at SW 46.9L for 2080s

Month	Model 1	Model 2	Model 3
Jan	78.2	254.7	370.4
Feb	210.3	25.9	32.3
Mar	1318.6	69.3	57.1
Apr	20853.4	1978.8	2223.0
May	62089.1	14140.8	14252.4
Jun	90065.1	32408.2	36720.6
Jul	95775.2	52054.9	66958.4
Aug	77402.8	61845.9	86725.2
Sep	61435.3	52090.6	75385.5
Oct	31147.9	40312.5	51066.7
Nov	7748.1	17948.1	22797.5
Dec	1103.8	3983.0	5370.7

Table 10: % Change of future monthly flow at SW 46.9L from baseline for 2080s

Month	Model 1	Model 2	Model 3
Jan	-58.7	-31.4	4.1
Feb	110.0	-61.2	-38.7
Mar	195.1	-88.9	-85.3
Apr	355.6	-54.4	-11.5
May	214.7	-17.9	10.7
Jun	113.8	-13.4	2.3
Jul	46.9	-12.1	7.5
Aug	17.3	-3.9	27.6
Sep	6.7	-11.4	24.8
Oct	-17.3	-9.1	15.3
Nov	-43.8	-5.2	20.7
Dec	-61.2	-13.3	22.7

Table 11: Future monthly sediment load (Mt/month) at SW 46.9L for 2080s

Month	Model 1	Model 2	Model 3
Jan	0.0100	0.0144	0.0124
Feb	0.0139	0.0002	0.0001
Mar	0.2024	0.0013	0.0012
Apr	7.8972	0.2308	0.1885
May	71.5453	5.0542	3.5646
Jun	159.6233	14.2895	19.6177
Jul	223.1806	55.9572	98.4982
Aug	152.1693	92.5408	208.3412
Sep	72.5886	70.2993	154.2773
Oct	12.6647	29.7604	51.8315
Nov	0.9903	4.6295	4.7200
Dec	0.0489	0.2621	0.3263

Table 12: % Change of future monthly sediment load from baseline for 2080s

Month	Model 1	Model 2	Model 3
Jan	48.3	-15.5	-31.9
Feb	447.4	-80.9	-92.2
Mar	984.9	-95.2	-93.8
Apr	989.5	-66.9	-41.2
May	1186.2	-27.4	13.9
Jun	589.0	-23.7	51.2
Jul	146.4	-18.3	35.6
Aug	20.8	-30.9	56.8
Sep	-20.1	-31.5	46.1
Oct	-58.9	-14.7	39.3
Nov	-55.5	34.4	-6.2
Dec	-66.2	-28.6	3.3

Table 13: % Change of future average annual flow from climatic base period

Time period	RCP 8.5 Model	Average Annual Flow (m^3/s)	% Change in Discharge
2020s	Model 1	30037.3	16.2
	Model 2	25776.8	-0.3
	Model 3	26265.3	1.6
2050s	Model 1	33032.6	27.8
	Model 2	25935.0	0.3
	Model 3	28279.0	9.4
2080s	Model 1	37435.7	44.8
	Model 2	23092.7	-10.7
	Model 3	30163.3	16.7

Table 14: % Change of future average annual sediment load from climatic base period

Time period	RCP 8.5 Model	Annual Average Sediment Load (Mt/year)	% Change in Sediment Load
2020s	Model 1	465.4	25.7
	Model 2	334.2	-9.7
	Model 3	403.6	9.0
2050s	Model 1	570.7	54.2
	Model 2	325.2	-12.2
	Model 3	450.5	21.7
2080s	Model 1	700.9	89.3
	Model 2	273.0	-26.2
	Model 3	541.4	46.2

Table 15: Future seasonal flow (m^3/s) at SW 46.9L for 2020s, 2050s and 2080s

Season	RCP 8.5 Model	2020s	2050s	2080s
MAM	Model 1	15616.3	20436.3	28087.1
	Model 2	7626.3	7764.6	5396.3
	Model 3	4984.7	5417.1	5510.8
JJAS	Model 1	65437.8	73742.6	81169.6
	Model 2	53991.5	54455.9	49599.9
	Model 3	56846.7	61652.5	66447.4
ON	Model 1	24568.4	19277.9	19448.0
	Model 2	32615.9	32341.0	29130.3
	Model 3	33768.2	35348.3	36932.1
DJF	Model 1	903.4	518.9	464.1
	Model 2	1748.2	1806.8	1421.2
	Model 3	1768.9	1930.1	1924.5

Table 16: % Change of future seasonal flow from climatic base period

Season	RCP 8.5 Model	2020s	2050s	2080s
MAM	Model 1	89.3	147.7	240.4
	Model 2	3.1	5.0	-27.1
	Model 3	-5.2	3.0	4.8
JJAS	Model 1	13.3	27.7	40.6
	Model 2	-1.7	-0.9	-9.7
	Model 3	0.4	8.9	17.3
ON	Model 1	-4.5	-25.1	-24.4
	Model 2	3.1	2.2	-7.9
	Model 3	6.9	11.9	16.9
DJF	Model 1	-13.6	-50.4	-55.6
	Model 2	4.3	7.8	-15.2
	Model 3	10.9	21.0	20.7

Table 17: Future seasonal sediment load (Mt/month) at SW 46.9L for 2020s, 2050s and 2080s

Season	RCP 8.5 Models	2020s	2050s	2080s
MAM	Model 1	5.66	11.09	26.55
	Model 2	2.29	3.47	1.76
	Model 3	1.00	1.32	1.25
JJAS	Model 1	106.94	132.29	151.89
	Model 2	72.52	69.02	58.27
	Model 3	86.93	100.04	120.18
ON	Model 1	10.27	4.11	6.83
	Model 2	18.42	19.19	17.19
	Model 3	26.24	22.97	28.28
DJF	Model 1	0.04	0.02	0.02
	Model 2	0.13	0.12	0.09
	Model 3	0.12	0.15	0.11